

Investigating barriers to vaccinia virus recombination using combinations of  
light and electron microscopy

by

Quinten Joseph Kieser

A thesis submitted in partial fulfillment of the requirements for the degree of

Master of Science

in

Virology

Department of Medical Microbiology and Immunology  
University of Alberta

© Quinten Joseph Kieser, 2019

## Abstract

While DNA viruses typically replicate in the nucleus of the host cell, poxvirus replication occurs exclusively within cytoplasmic structures known as viral factories. Viral factories are the sites of various processes of the vaccinia virus (VACV) life cycle including replication, morphogenesis and recombination. Recombination is catalyzed by the viral polymerase and, as such, can be detected early in infection alongside DNA replication. However, previous work in our lab showed that recombination between two co-infecting particles is significantly delayed compared to recombination events that occur within a single virus. These delays were attributed to a physical barrier that restricts genetic exchange, a prerequisite for intergenomic recombination, until late in infection. These barriers may arise due to multiple characteristics of the viral life cycle. First, it has been shown that each infecting particle gives rise to its own viral factory. Even after the apparent fusion of these individual factories, the genetic content of a single factory remained distinct. Second, each factory is enwrapped with membranes derived from the ER early during infection. It stands to reason that these membranes could persist late into infection and prevent the DNA from two closely apposed factories from mixing. Here I describe the use of light and electron microscopy to investigate the sub-structure of viral factories and the potential constraints they impose on inter-genomic recombination. Initially, we labelled calreticulin, a marker of the endoplasmic reticulum (ER) from which the membranes that enclose viral factories are thought to be derived, and observed staining patterns that suggest that viral factories are surrounded and potentially separated by membrane structures. These observations translated well to initial electron microscopy experiments that showed

membrane structures existed, at least to a limited extent, around the periphery of viral factories. Further studies used correlative light and electron microscopy to investigate the membrane ultrastructure associated with recent collision events. Under this system, cell structures, including ER-like membranes and mitochondria, could be observed at the junction of two recently collided factories. However, investigation of the 3D-ultrastructure of a recent collision event showed that these structures existed in only a limited capacity throughout the z-dimension and in a way that would not meaningfully restrict genetic mixing and recombination between closely apposed viruses. Altogether, these studies show that the membrane structures present at the periphery of viral factories early in infection likely play little role in restricting genetic mixing of factories that collide late during infection.

## Preface

I performed all experiments presented throughout this thesis independently. The exception to this is the serial sectioning and subsequent processing performed for the SEM experiments (Fig. 5.4-8). SEM serial sectioning and processing was performed by Woo Jung Cho.

Special thanks to Mira Shenouda for aiding during the super-resolution microscopy experiments (Fig. 3.1-3.4).

## Acknowledgements

First and foremost, I would like to thank my supervisor, Dr. David Evans, for taking me on both as an undergraduate project and Master's student. Your wisdom and kindness were fundamental to my success and it is thanks to you that I was able to tackle this project. I would also like to thank Dr. David Marchant and Dr. Nicolas Touret for serving on my graduate committee. Your guidance was critical in developing the skills necessary to complete my degree.

I would also like to thank the Hitt, Shmulevitz, Ingham and Moore labs for the discussion they generated in lab meetings. It is thanks to these labs that I was able to obtain a learn about topics that expanded beyond the scope of my project and communication within the larger group was an incredible avenue for growth. Thanks to Drs Bernard Moss, Jacomine Locker and Stuart Isaacs for supplying reagents used during my thesis.

My time in the Evans lab was enjoyable due to the presence of such great personalities. It is here that I would like to thank current and past members of the Evans lab. Special thanks to Dr. Ryan Noyce and Dr. James Lin for both their incredible intellectual and emotional support during my project. Thanks to Drs. Les Nagata, Chad Irwin and Sid Biswas for your guidance and Nicole Favis and Megan Desaulniers for their outstanding technical support. To my fellow graduate students Brittany Umer, Mira Shenouda and Greg Vallee, I would like to thank you for your support and friendship.

Last, I would like to thank my family for all their support during my Master's degree. It is thanks to your unconditional love that I was able to get where I am today

# Contents

List of Tables .....	ix
List of Figures .....	x
List of Abbreviations .....	xii
Chapter 1 - Introduction .....	1
1.1 History of Poxviruses and Variola .....	1
1.2 Poxviral Life Cycle.....	2
1.2.1 Viral Attachment and Entry .....	2
1.2.2 Early Gene Expression.....	3
1.2.3 DNA Replication .....	3
1.2.4 Viral Morphogenesis and Egress.....	10
1.3 Genetic Recombination .....	12
1.3.1 Proteins Involved in Recombination .....	15
1.3.2 Timing of Inter-Genomic and Intra-Genomic Recombination .....	20
1.4 Goals of the Thesis Project.....	23
Chapter 2 - Materials and Methods.....	25
2.1 Cell Lines, Viruses and Culturing .....	25
2.1.1 Cell Lines and Viruses.....	25
2.1.2 General Cell Culture .....	25
2.1.3 Bulk Virus Preparation .....	26
2.2 Microscopy.....	27
2.2.1 Fixed Cell Microscopy .....	27
2.2.2 Live Cell Microscopy.....	29
2.2.3 EdU Labelling.....	32
2.2.4 Transmission Electron Microscopy .....	34
2.2.5 Scanning Electron Microscopy .....	37
Chapter 3 – Developing a timeline of the viral life cycle .....	41
3.1 Introduction .....	41
3.2 Results.....	42
3.2.1 Super-resolution microscopy as a means to study the viral life cycle .....	42
3.2.2 Determining viral early, intermediate and late expression kinetics .....	42
3.2.3 Characterizing VACV morphogenesis.....	44

3.2.4 Treatment with rifampicin inhibits viral morphogenesis.....	50
3.2.5 E8 is a late viral protein incorporated into the virion core .....	51
3.3 Discussion.....	54
Chapter 4 – Tracking viral DNA replication using EdU .....	60
4.1 Introduction .....	60
4.2 Results.....	60
4.2.1 EdU labelling is diminished following inhibition of DNA replication .....	60
4.2.2 Optimizing EdU labelling.....	61
4.2.3 DNA replication is reduced late in infection .....	64
4.2.4 Active DNA replication occurs at sites of inter-genomic recombination.....	67
4.3 Discussion.....	69
Chapter 5 – Investigating barriers to genetic mixing using CLEM .....	73
5.1 Introduction .....	73
5.2 Results.....	74
5.2.1 ER membranes are present within and around viral factories .....	74
5.2.2 ER membranes partition genetic content of viral factories.....	76
5.2.3 Cellular structures persist following factory collision events .....	78
5.2.4 Structures persist to an extent throughout the entirety of the viral factory .....	82
5.3 Discussion.....	87
Chapter 6 – Conclusions and Future Directions.....	93
6.1 Investigating hallmarks of the VACV life cycle .....	93
6.1.1 Investigating the role of the viral E8 protein during infection.....	93
6.1.2 Intergenic recombination occurs following expression of late viral genes and occurs alongside viral morphogenesis .....	94
6.2 DNA replication is reduced late during infection at the times we would expect to observe intergenic recombination .....	96
6.3 Membranes structures can be observed at the periphery of viral factories early during infection.....	99
6.4 Tracking persistence of membrane structures following factory collision events .....	101
6.5 The structures observed at factory collision sites are not organized in a way that could sufficiently restrict recombination.....	103

6.6 Future Directions .....	105
6.6.1 Role of membrane structures in early factory fusion events .....	105
6.6.2 Role of microtubules in VACV factory mobility.....	106
6.6.3 Competition between co-infecting virions .....	110
6.7 Concluding Remarks.....	111
References .....	112

## List of Tables

Table 2.1 Components for click-chemistry reaction	33
Table 2.2 Antibodies used during the project	40

# List of Figures

## Chapter 1

Figure 1.1. Schematic of the VACV replication cycle.	5
Figure 1.2. Representation of the proteins involved in DNA replication	7
Figure 1.3. Mechanism of the SSA pathway of homologous recombination	14
Figure 1.4. Mechanism used to investigate the timing of inter-genomic and intra-genomic recombination	21

## Chapter 2

Figure 2.2. Protocol for quantifying the morphogenic forms of vaccinia virus	30
--	----

## Chapter 3

Figure 3.1. Comparison of conventional and super-resolution microscopy	43
Figure 3.2. Expression of early and late viral proteins	45
Figure 3.3. Expression of intermediate and late viral proteins	46
Figure 3.4. Visualization of the morphogenic forms of VACV	48
Figure 3.5. Quantification of morphogenic forms and total virion counts	49
Figure 3.6. Treatment with rifampicin inhibits morphogenesis	52
Figure 3.7. Morphogenic forms can be visualized shortly after the removal of rifampicin	53
Figure 3.8. Localization and expression patterns of the viral E8 protein	55

## Chapter 4

Figure 4.1. EdU labels actively replicating DNA	62
Figure 4.2. Optimizing the EdU labelling protocol	63
Figure 4.3. Visualizing EdU incorporation throughout infection	65
Figure 4.4. DNA replication is most robust early during infection	66
Figure 4.5. DNA replication occurs at sites of inter-genomic recombination	68

## Chapter 5

Figure 5.1. ER structures are present within and around viral factories	75
Figure 5.2. ER membranes are present at the periphery of viral factories	77
Figure 5.3. Cellular structures can be observed at sites of factory collision	79
Figure 5.4. Correlative light and scanning electron microscopy	81
Figure 5.5. ER-like membrane structures persist within the viral factory following collision	83
Figure 5.6. 3D-ultrastructure of a factory collision event	85

Figure 5.7. Additional cellular structures can be observed within the viral factory	86
Figure 5.8. No internal structures are observed in a factory that has not undergone an observable collision event	88

## Chapter 6

Figure 6.1. Microtubules can be observed within the viral factory	107
---	-----

## List of Abbreviations

3'-OH	3'-hydroxyl group
AraC	Cytosine arabinoside
AT	Array tomography
ATCC	American type culture collection
ATR	Ataxia telangiectasia and Rad3-related protein
CB	Cacodylate buffer
CLEM	Correlative light and electron microscopy
CRT	Calreticulin
Cy5	Cyanine 5
DAPI	4',6-diamidino-2-phenylindole
dCMP	Deoxycytidine monophosphate
DNA	Deoxyribonucleic acid
dNTP	Deoxynucleoside triphosphate
DSB	Double-stranded break
EdU	5-ethynyl-2'-deoxyuridine
EFC	Entry fusion complex
eGFP	Enhanced green fluorescent protein
EM	Electron Microscopy
ER	Endoplasmic reticulum
EV	Extracellular Virion
Fen-1	Flap endonuclease 1
FISH	Fluorescence in situ hybridization
FITC	Fluorescein isothiocyanate
FM	Fluorescence Microscopy
GAGs	Glycosaminoglycans
GFP	Green fluorescent protein

GPT	Guanine phosphoribosyltransferase
hpi	Hours post-infection
IV	Immature Virion
LM	Light Microscopy
mCh	Monomeric cherry fluorescent protein
MEM	Minimum essential media
MOI	Multiplicity of infection
MQW	Milli-Q Water
mRNA	Messenger ribonucleic acid
MT	Microtubules
MV	Mature Virion
MVA	Modified vaccinia Ankara
NA	Numerical aperture
OsO <sub>4</sub>	Osmium tetroxide
PBS	Phosphate-buffered saline
PBS-T	PBS supplemented with 0.1% Tween-20
PCNA	Proliferating cell nuclear antigen
pE/L	Poxvirus early/late promoter
PFC	Potassium ferrocyanide
PFU	Plaque forming unit
RNA	Ribonucleic acid
RNAi	RNA interference
RPA2	Replication protein A2
RT	Room temperature
SIM	Structured-illumination microscopy
siRNA	Small interfering RNA
SSA	Singel-stranded annealing

SSB	Single-stranded DNA binding protein
TCH	Thiocarbohydride
TGN	Trans-Golgi network
UDG	Uracil DNA glycosylase
VACV	Vaccinia Virus
VARV	Variola Virus
VETF	Virus early transcription factor
VMAPs	Viral membrane assembly proteins
WHO	World health organization
WR	Western reserve
WV	Wrapped Virion
YFP	Yellow fluorescent protein

# Chapter 1 - Introduction

## 1.1 History of Poxviruses and Variola

Poxviruses consist of a large family of viruses harbouring a large (130-380kb) genome<sup>1</sup>. The genomes are contained within a relatively large protein capsid measuring approximately 350 x 270nm<sup>2</sup>. Unusual among many DNA viruses is the fact that, following infection, poxviruses replicate exclusively within the cytoplasm of the host cell. During replication, poxviruses shift through multiple different forms in a process known as morphogenesis. The final two forms, MV and EV, represent the two infectious forms of poxviruses. While poxviruses represent health burdens for both humans and animals<sup>1</sup>, VARV remains the most nefarious member of the family Poxviridae. VARV, the causative agent of smallpox, exists as two clinical forms: Variola major and minor<sup>3</sup>. Of the two, Variola major was associated with a more severe manifestation of the disease. Over the course of the 20<sup>th</sup> century, smallpox is assumed to be the cause of approximately 300 million deaths<sup>4</sup>.

Humans act as the only natural hosts for VARV and this, in essence, acted as a prerequisite for its eventual eradication<sup>5</sup>. Earliest preventative techniques used a live virus in a process known as variolation to confer immunity to a susceptible individual, albeit at a mortality of 1-2%<sup>1</sup>. It wasn't until later, thanks to the work by Edward Jenner, that VACV would be used in the first ever vaccine to confer immunity to smallpox<sup>1,4</sup>. VACV proved to be effective as a preventative measure and smallpox was declared eradicated by the WHO in 1979<sup>4</sup>. Due to its known clinical efficacy and safety, VACV is being explored as a potential oncolytic virus<sup>6</sup>.

## 1.2 Poxviral Life Cycle

### 1.2.1 Viral Attachment and Entry

The mechanisms surrounding VACV binding and entry into the host cell remain elusive due to the presence of two distinct infectious forms (MV and EV). Relative to MV, EV contain an additional membrane that contains at least 6 unique proteins<sup>7,8</sup>. As such, there are no common epitopes present on both infectious forms and each form requires different attachment factors to mediate binding to the host cell<sup>7,9</sup>. Glycosaminoglycans (GAGs), along with other cellular molecules, serve as the attachment factors for MV<sup>7,8</sup>. Of the four viral proteins observed to play a role in host cell binding, three are dedicated to interacting with GAGs: D8 interacts with chondroitin sulfate<sup>10</sup> while A27 and H3 mediate the interaction with heparan sulfate proteoglycans<sup>11-13</sup>. The final binding protein, A26, interacts with laminin present in the extracellular matrix<sup>14</sup>. After adsorption to the host cell, fusion with the plasma membrane is carried out by a total of 11 proteins collectively known as the entry fusion complex (EFC) to deliver the viral core into the cytoplasm of the host cell<sup>7,15</sup>. While no attachment factor has been identified for EV, it is believed that interaction with GAGs disrupts the outermost membrane of the EV particle and expose the fusion machinery present in the MV<sup>7</sup>.

Alternatively, both EV and MV may enter the host cell by macropinocytosis<sup>7,16,17</sup>. In this model, the phosphatidylserine (PS) present in the viral membrane mimics apoptotic bodies and promotes the uptake of MV via macropinocytosis<sup>16</sup>. EV macropinocytosis occurs independently of PS. The acidic environment of the endosomes is thought to promote the activity of the EFC<sup>7</sup>.

Furthermore, increased acidity is thought to disrupt the outer membrane of EV to expose the EFC machinery present in the MV<sup>7</sup>. The envelope F13 protein has been shown to sensitize the particle to acid-induced dissolution of the outer membrane<sup>18</sup>. Endocytosis is an advantageous route for the virus to gain entry into the cell as it does not result in the deposition of any viral proteins onto the surface of the host cell and reduces the risk of recognition by the host immune system.

### 1.2.2 Early Gene Expression

Early gene expression begins immediately after complete internalization of the infectious particle<sup>19,20</sup>. All machinery required for transcription of early genes is packaged within the virion itself<sup>20,21</sup>. This machinery includes a nine-subunit RNA polymerase, the vaccinia virus early transcription factor (VETF), which is a heterodimer of the viral A6 and D7 proteins, and mRNA modifying proteins such as the mRNA capping enzyme, poly(A) polymerase and 2'-O-methyltransferase<sup>21</sup>. Approximately 100 early transcripts, which corresponds roughly to 50% of the total gene products of VACV<sup>21</sup>, are produced within the virion core<sup>20</sup>. These transcripts are extruded into the host cytoplasm for translation by host machinery<sup>22</sup> via pores in the capsid in an ATP-dependent manner<sup>20,23</sup>. The products of early gene transcription are required for release of the genome from the viral capsid<sup>24</sup>. The release of the viral genome acts as a prerequisite for the onset of DNA replication.

### 1.2.3 DNA Replication

DNA replication can be detected within the first 2 hours of infection<sup>25</sup>. DNA replication occurs within cytoplasmic structures known as viral factories or virosomes.

Viral factories arise from a single infecting virion and the number of viral factories within a given cell is proportional to the number of infecting particles<sup>26,27</sup>. Individual factories may coalesce over the course of infection<sup>28</sup>. While factories were originally reported to be composed of unbound DNA, more recent reports show that the factories are surrounded by membranes derived from the ER<sup>29</sup>. Wrapping of the viral factories takes approximately 45 minutes and complete wrapping of the viral factory corresponds to more robust DNA replication<sup>29</sup>. This led to the hypothesis that membranes play a role in VACV replication<sup>20,29</sup>. Late during infection (~6hpi) the integrity of these membranes are compromised<sup>29</sup>. While viral factories are the sites of DNA replication, other hallmarks of the VACV replication cycle including transcription, translation and progeny assembly occur within these cytoplasmic structures<sup>25</sup>. Figure 1.1 highlights the general hallmarks of the VACV life cycle.

#### 1.2.3.1 Genome Organization

The VACV genome is organized as a large polynucleotide chain connected at the terminal ends<sup>30,31</sup>. The terminal ends house DNA hairpins that potentiate a self-priming model and it is within these terminal ends that DNA replication is thought to initiate<sup>32</sup>. Specifically, single stranded nicks in the termini generate free 3'OH groups from which DNA synthesis can be initiated<sup>33</sup>. A potential initiation site may lie within the conserved region between the hairpin loops and the inverted repeats<sup>34</sup>. The self-complementarity of the genome allows the strands to fold back as replication continues to the other hairpin structure<sup>25</sup>. As such, replication occurs in a rolling circle mechanism and results in the formation of head-to-tail concatemers that must be resolved by the A22 Holliday Junction Resolvase<sup>35,36</sup>.

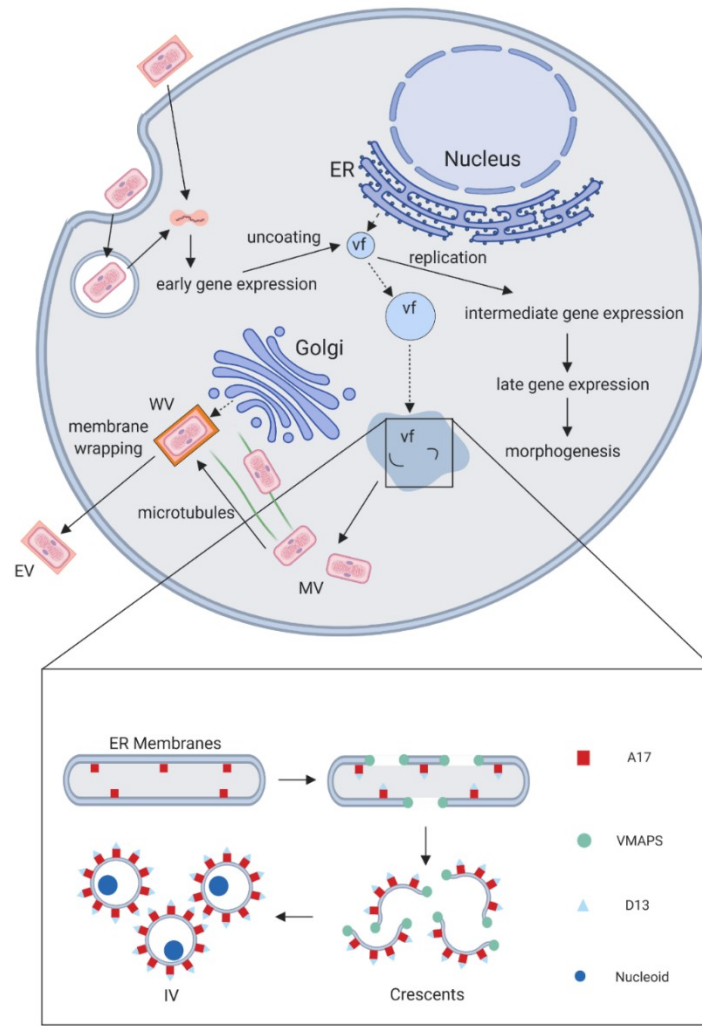


**Figure 1.1. Schematic of the VACV replication cycle.** Infection begins when either MV or EV enter the cell by either direct fusion with the plasma membrane or endocytosis. Following internalization, early gene expression begins, resulting in uncoating and subsequent replication of the viral genome in cytoplasmic viral factories (vf). Viral factories are surrounded by membranes derived from the endoplasmic reticulum (ER). Intermediate gene expression occurs concurrently with DNA replication and primes the transcription of late genes. Late genes encode for structural proteins involved in virus assembly and are expressed after the bulk of DNA replication occurs. Additionally, the transition from DNA replication to virus assembly is also characterized by reduced integrity in the ER membrane surrounding the viral factories. Assembly (inset) begins with the incorporation of the viral A17 protein into the luminal membrane of the ER. VMAPS are responsible for either the scission of the ER membrane or stabilization of naturally occurring breaks in the ER membrane to generate short membrane segments. The reduced integrity of the ER membrane also permits the D13 scaffolding protein to associate with A17 and give rise to membrane crescents, the first observable step of assembly. These membrane crescents aggregate to form immature virions. The genome is incorporated prior to sealing of the immature virion. Next, IV undergo a proteolytic maturation process, carried out by I7, to give rise to MV, the first infectious form of VACV. A fraction of MV migrate to the TGN via microtubules, where they obtain two additional membrane layers and form WV, the second infectious form of VACV. Unlike MV, WV migrate, via microtubules, to the cell surface and fuse with the plasma membrane, losing the outermost envelope layer during the process, to exit the cell prior to lysis.

### 1.2.3.2 Proteins Involved in DNA Replication

DNA synthesis is catalyzed by the 117-kDa DNA polymerase encoded by the VACV E9L gene<sup>37-39</sup>. The VACV E9 polymerase catalyzes both primer and template-dependent DNA synthesis<sup>40</sup>. Additionally, the DNA polymerase contains 3'-to-5' exonuclease activity<sup>40,41</sup>. The polymerase can use this exonuclease activity to repair double-stranded DNA breaks by initiating a single stranded annealing reaction. This process bridges both recombination and replication in VACV<sup>42-44</sup>. The role of the E9 polymerase, and other viral proteins involved in replication, is highlighted in figure 1.2.

VACV DNA replication is a concerted effort between at least 7 viral proteins<sup>25</sup>. One protein involved in replication includes the D5 helicase-primase<sup>45</sup>. The 90kDa D5 protein has been shown to synthesize oligoribonucleotides without a stringent template specificity, suggesting a role for D5 in discontinuous lagging strand synthesis<sup>46,47</sup>. Compounded with the finding that either a cellular or viral ligase, encoded by VACV A50R, is required for efficient DNA replication provides significant weighting to the possibility of semi-discontinuous DNA synthesis<sup>48</sup>. While ligases play a role in DNA replication and remediation of DNA damage, the deletion of viral ligases still results in DNA replication<sup>49,50</sup>, albeit with the caveat of a reduced host range<sup>51</sup>. However, further examination of ligase deletion mutants revealed that host ligases, Lig1 specifically, were recruited to the viral factories and complemented any deficiencies in viral ligases<sup>48</sup>. Infection of cells with low levels of Lig1, such as quiescent cells, with DNA ligase mutants resulted in severely impaired DNA replication and suggests that the ligase plays a role in expediting replication in resting cells. The uracil DNA glycosylase (UDG), encoded by VACV D4R, functions in DNA repair by removing

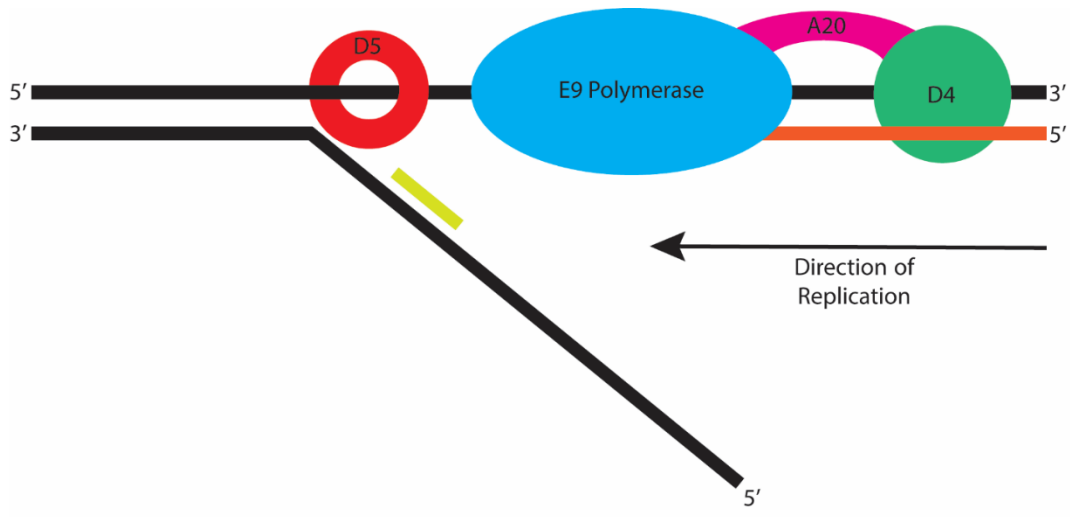


**Figure 1.2. Representation of the proteins involved in DNA replication.** VACV D5 functions as the helicase-primase during replication and unwinds the dsDNA to permit replication. D5 synthesizes the initial primer required for leading strand replication as well as primers (yellow) on the lagging strand for its replication. E9 is the DNA polymerase and, as such, is responsible for synthesis of new strands (orange). VACV A20 and D4 form the processivity factor for the E9 polymerase. D4 also functions as an UDG and removes uracil erroneously introduced into the genome.

uracil erroneously introduced into the genome<sup>52,53</sup>. H5 is another protein that, in addition to its role in DNA replication, has been suggested to play a role in transcription<sup>54</sup> and morphogenesis<sup>55</sup>. More recently, H5 was shown to associate with the E9 polymerase holoenzyme and is essential for DNA replication<sup>56</sup>. A20, in combination with D4, acts as a processivity factor to the viral DNA polymerase<sup>57</sup>. Furthermore, A20 forms a complex with D4, D5 and H5 and may function as a multi-subunit replication-repair complex<sup>58</sup>.

Multiple proteins involved in the uncoating process also play a role in DNA replication: B1R, I3L, H5R and E8R. H5, as described previously, has been shown to associate with the DNA polymerase and is essential for replication<sup>56</sup>. B1 is a protein kinase that, among other substrates, is responsible for the phosphorylation of the H5 protein<sup>59</sup>. I3L encodes a 34kDa single-stranded DNA binding protein that associates with parental DNA released from virion cores and plays a role in organizing early factories<sup>60-62</sup>. Recent investigations show that I3 is essential for DNA replication and I3 itself acts as the primary replicative SSB<sup>63</sup>. I3 also plays a critical role in DNA recombination and will be discussed in a later section.

#### 1.2.3.3 E8 and Factory Formation

The viral E8 protein was originally investigated for its potential role in mediating wrapping of the viral factory<sup>29</sup>. In this study, E8 was selected as a potential mediator of membrane wrapping due to the presence of putative membrane binding domains as well as an early gene promoter. Additionally, it was shown by microscopy that E8 localized to the periphery of viral factories, in addition to the ER, early in infection. Subsequent studies on E8 revealed that the protein was incorporated into

the virion core and was regulated by the F10 kinase<sup>64</sup>. The DNA-binding capacity of E8 is modulated by F10 and phosphorylation of E8 late during infection results in a reduction in DNA binding capacity that occurs concurrently with factory collapse and progeny assembly. However, another study contested the role of E8 and claimed that E8 was involved in early transcription rather than factory establishment<sup>65</sup>. First, it was shown that E8 is expressed late, rather than early, in infection due to the fact that E8 expression is suppressed following the inhibition of viral DNA replication. Second, DNA replication and morphogenesis occurred normally in E8 mutants at the non-permissive temperature. However, progeny infectivity was significantly reduced due to a severe reduction in early gene transcription. Altogether, the mechanism by which the viral factories obtain their ER membranes remains a mystery.

#### 1.2.3.4 Role of Host Proteins in Viral Replication

While poxviruses are considered to encode most, if not all, machinery required for replication, a more recent study shows that host machinery does may play a role in viral replication<sup>66</sup>. The study noted that after infection of the host cell, but before uncoating of the genome, VACV activates cytoplasmic ATR. ATR is a serine/threonine kinase that plays an important role in DNA damage repair<sup>67</sup>. Surprisingly, inhibition of ATR suppressed expression of late viral proteins and reduced viral replication<sup>66</sup>. Furthermore, RPA2 and PCNA, a SSB that functions in recruiting ATR to ssDNA<sup>68</sup> and a sliding clamp protein<sup>69</sup>, respectively, are recruited to sites of viral DNA replication and RNAi-mediated depletion of either results in reduced viral replication<sup>66</sup>. However, analysis of the crystal structure of E9 suggested that the C-terminal domain, where PCNA typically binds, is unlikely to interact with PCNA<sup>70</sup>. Furthermore, the

aforementioned work<sup>66</sup> and earlier work in our lab failed to observe PCNA itself within the viral factory. Overall, this study contradicts the popular opinion that all machinery required for VACV DNA replication is encoded by the virus itself and more work is required to determine the extent to which host proteins impact VACV replication.

#### 1.2.3.5 DNA Replication and Intermediate/Late Gene Expression

DNA replication serves as a requirement for intermediate and late gene transcription<sup>71</sup>. More specifically, intermediate transcription factors are transcribed from early promoters, late transcription factors are transcribed from intermediate promoters and early transcription factors are transcribed from late genes. As replication commences, intermediate transcription factors gain access to the genome and transcribe the transcription factors required for late gene synthesis<sup>72</sup>. Sequential expression of transcription factors allows for tight regulation of the VACV replication cycle.

#### 1.2.4 Viral Morphogenesis and Egress

The proteins required for morphogenesis are encoded by late viral genes and, as such, are transcribed late in infection after DNA replication has ceased<sup>73</sup>. Morphogenesis begins in the viral factories with the production of membrane crescents (Fig 1.1 - Inset). The formation of membrane crescents is dependent on the function of eight viral proteins: three structural proteins (D13, A14 and A17) as well as five regulatory proteins collectively referred to as VMAPS<sup>74</sup>. While the membranes used in early morphogenesis were originally believed to be synthesized *de novo*<sup>75</sup>, recent reports show that these membranes are in fact derived from the ER<sup>76</sup>. These

conclusions stem from investigation of VMAP mutants and show continuity between the spicule-coated crescent membranes and the ER<sup>77,78</sup>. The model postulates that ER membranes are first modified by the insertion of A17<sup>76</sup>. The VMAPS then co-ordinate to either rupture the ER membranes or stabilize naturally occurring breaks in the membrane and associate with the free ends of the membrane structures. Ruptures in the membrane allow the D13 scaffolding protein to interact with A17 and give rise to viral crescents. Multiple independent crescents aggregate to give rise to the spherical immature virion (IV)<sup>79,80</sup>. The viral genome and core proteins are incorporated into the IV prior to sealing<sup>80-82</sup>.

IV then undergo a proteolytic maturation step catalyzed by the I7 protease to produce the brick-shaped MV<sup>83</sup>. I7 cleaves the N-terminal region of A17 which results in the dissociation of the D13 scaffold. However, dissociation of D13 alone is not sufficient for maturation of the viral particles and other proteins play a role in the maturation process<sup>74</sup>. A5 represents another protein that is involved in the maturation process. A5 is incorporated into the virion core and is necessary for the transition of IV to MV. A5 will be discussed later as a marker for all intracellular virions. MV represent the more prominent of the two infectious forms of VACV and are released from the host following cell lysis<sup>73</sup>. However, a small fraction of MV are transported away from the viral factory via microtubules to obtain two additional membranes from either endosomes<sup>84</sup> or the trans-Golgi network<sup>85</sup>. These virions with additional membranes are referred to as wrapped virions (WV). After obtaining additional membranes, the WV are transported to the cell periphery by microtubules where they fuse with the host plasma membrane and are released as EV, the second infectious form of VACV.

During the fusion event, the outermost membrane of the WV is lost<sup>86,87</sup>. Even with the loss of the second additional membrane, WV and EV house a number of unique proteins when compared to MV<sup>7,8</sup>. These proteins are primarily responsible for mediating transport and dissemination of the WV/EV. For example, B5 is a 42-kDa glycoprotein present in both additional membranes of WV and is involved in WV formation<sup>88</sup>, actin-tail formation<sup>89</sup>, repulsion of superinfecting particles<sup>90</sup> and GAG-dependent dissolution of the envelope during EV entry<sup>91</sup>.

While both particles play a role in infection, EV are believed to be primarily responsible for virus dissemination within the host due to a number of advantages<sup>73</sup>. First, neutralizing antibodies against EV are more protective when compared to neutralizing antibodies against MV<sup>92</sup>. Furthermore, EV are more resistant to both neutralization by antibody<sup>93</sup> as well as complement<sup>94</sup> compared to MV. Lastly, strains that are incapable of producing EV are avirulent in mouse models<sup>95,96</sup>.

### 1.3 Genetic Recombination

DNA damage, whether it be from reactive oxygen species, double-stranded breaks (DSB), oxidation or various other sources, remains a potential threat to the viability of an organism<sup>97</sup>. As such, multiple mechanisms have evolved to combat the deleterious consequences associated with DNA damage. Homologous recombination represents one potential mechanism that can be used to facilitate DNA damage repair and it is particularly important in the context of DSB<sup>98</sup>. Recombination is the process by which there is an exchange between either the same piece of DNA (known as intramolecular recombination), or a separate piece of DNA (known as intermolecular

recombination). The exchange is usually guided by sequence homology resulting in a high-fidelity repair or tolerance mechanism. However, recombination can occur between two sequences of DNA lacking homology in a process known as illegitimate recombination<sup>99</sup>. It should be noted that the mechanism and machinery that drive both processes differ. Regardless, both forms of recombination play a critical role in DNA damage tolerance and repair as well as DNA replication.

The benefits of recombination extend into the field of virology as well. While recombination has been studied for VACV, the full details surrounding the process are not completely understood. Initial studies observed recombination with multiple members of the family Poxviridae, including variola, cowpox and vaccinia virus<sup>100,101</sup>. One of these studies noted the formation of hybrid viruses following coinfection with both variola major and cowpox<sup>101</sup>. This study highlights the ability of poxviruses to recombine with genetically distinct viruses and reveals the biological relevance of recombination as a mediator of viral evolution. In fact, genomic analysis of the Dryvax vaccine revealed it was comprised of a collection of quasispecies that harboured evidence of both intra- and inter-genomic recombination<sup>102</sup>. Even more, sequence analysis from variola suggest that recombination played a role in the evolution of this devastating pathogen<sup>103</sup>. Odd, however, is the fact that despite the high frequency of recombination experienced during infection very few recombinants are formed between co-infecting particles<sup>104</sup>.

Recombination in poxviruses most likely proceeds via a single-strand annealing (SSA) process<sup>43,105</sup>, the mechanism of which is highlighted in figure 1.3. In summary, DNA is resected from the DSB to generate ssDNA ends containing complementary

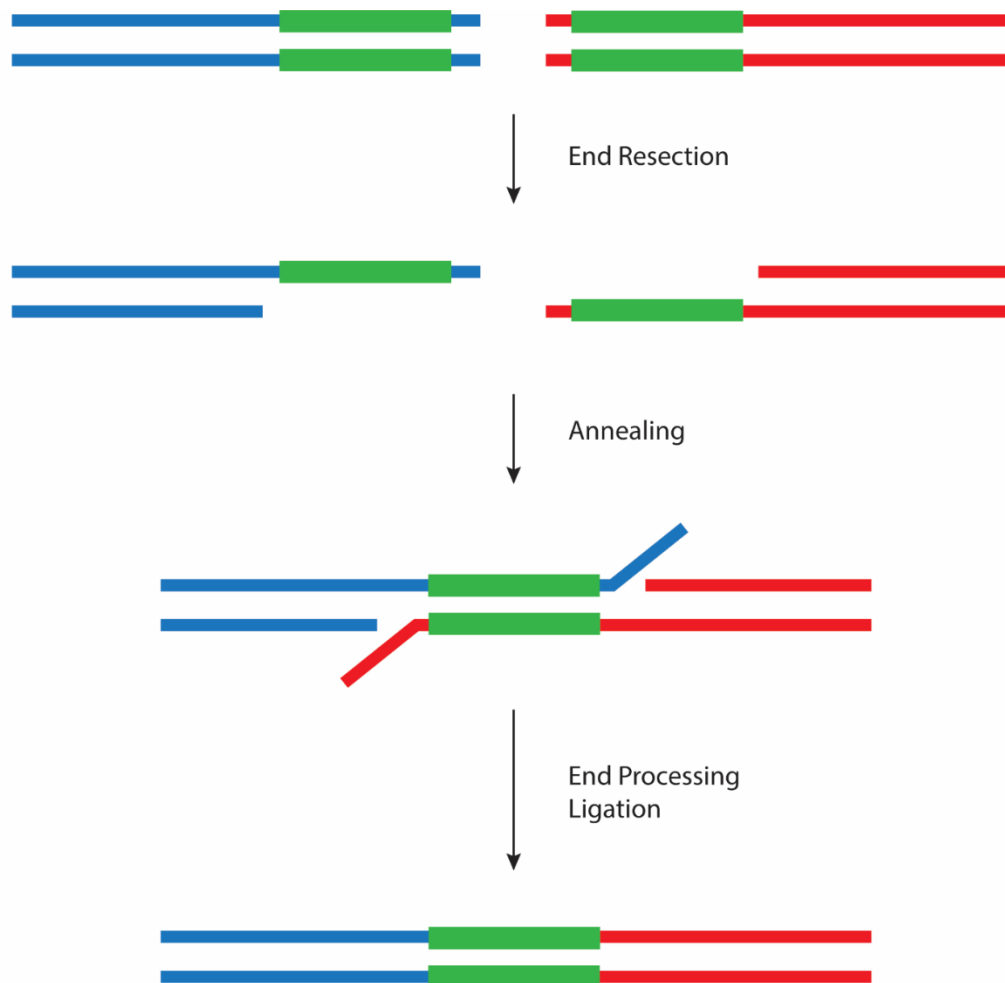


**Figure 1.3. Mechanism of the SSA pathway of homologous recombination.** First, DNA ends of the DSB are resected to generate 3' tails. Next, homologous sequences (green) present on the 3' tails anneal. Lastly, the non-homologous portions of the 3' tail are processed, and the final product is ligated together to form the final recombinant molecule.

sequences<sup>106,107</sup>. End resection occurs using 5'-to-3' exonuclease activity to generate 3' tails which are subsequently coated by an SSB. Following end resection, complementary DNA sequences present on the 3' tails anneal, and the DNA tails must be processed before ligation of the final joint molecule product. Out of the possible mechanisms of recombination, SSA is the only mechanism that requires 3'-to-5' exonuclease activity. Given that recombination is dependent on the function of a 3'-to-5' exonuclease<sup>41</sup>, SSA represents the most likely mechanism for VACV recombination.

### 1.3.1 Proteins Involved in Recombination

Due to the cytoplasmic nature of VACV replication, the proteins involved in recombination are encoded by the virus itself. Furthermore, DNA replication and recombination are intrinsically linked in VACV. It is no surprise then that proteins that are involved in DNA replication, including the E9 polymerase and the I3 SSB, are responsible for mediating recombination. Additionally, the FEN1-like nuclease, G5, has been shown to be involved in recombination. This section will outline the functions of these various proteins and the roles they play in recombination.

#### 1.3.1.1 E9 DNA Polymerase

DNA polymerases are critical in the process of recombination, particularly in the repair of DNA following a DSB. The VACV polymerase, as described previously, is encoded by the E9L gene<sup>40</sup>. In addition to the traditional polymerase function, E9 also contains 3'-to-5' exonuclease activity<sup>41</sup>. The exonuclease activity of E9 is particularly important since it is one of the few viral proteins with known exonuclease activity. Exonucleases traditionally play an intricate part of the recombination process and are

involved in resection of DSB to facilitate strand invasion and subsequent genetic exchange<sup>108</sup>. As such, the exonuclease activity of the DNA polymerase was investigated for its potential role in VACV recombination.

The first evidence for E9 and its role in recombination was provided when purified E9 was shown to facilitate strand transfer reactions<sup>42</sup>. These strand transfer reactions were dependent on sequence homology. Additional studies revealed that E9 could catalyze the formation of joint DNA molecules from linear DNA substrates<sup>43</sup>. The formation of these joint molecules was dependent on sequence homology (>12bp) and the 3'-to-5' exonuclease activity of the DNA polymerase, as noted by the retention of only the 5'-<sup>32</sup>P label. While supporting the hypothesis that E9 played a role in recombination, these studies failed to provide concrete proof of the direct role of the polymerase and its exonuclease function as mediators of genetic exchange. Attempts to investigate the E9 exonuclease activity were made difficult by the fact that the exonuclease function of E9 is essential for virus viability. To circumvent this limitation, the dCMP analog cidofovir was used to investigate the role of E9 proofreading activity in recombination<sup>41</sup>. Previous work from our lab shows that E9 can incorporate cidofovir during replication opposite to dGMP and that incorporation hinders primer extension<sup>109</sup>. More importantly, cidofovir present in the second-to-last position prevents the functioning of the E9 proofreading activity. The mechanism by which cidofovir inhibits replication suggests that any mutants resistant to the anti-viral agent would have to either avoid incorporating the agent into the growing genome or facilitate the removal of the drug following incorporation. Using this approach, two E9 mutants resistant to cidofovir were identified and sequenced<sup>41</sup>. One mutation mapped

to the polymerase domain while the other mutation mapped to the exonuclease domain. Substitution of the exonuclease mutant allele, but not the polymerase mutant allele, resulted in cidofovir resistance. This study also showed that the exonuclease activity was sensitive to the dNTP microenvironment. Specifically, reductions in dNTP pools favoured a switch from the polymerase to exonuclease activity of E9. Overall, the study shows that the DNA polymerase, and its exonuclease activity, play an important role in recombination.

#### 1.3.1.2 I3 Single-Strand DNA Binding Protein

The importance of SSBs in DNA replication, recombination and repair cannot be understated. The importance of these proteins is so universal that they have been found across all domains of life<sup>110,111</sup>. SSBs, unsurprisingly, have a high affinity for single-stranded DNA. Binding of ssDNA by SSBs prevents the formation of DNA secondary structures and protects ssDNA from the activity of nucleases<sup>110</sup>. Both of these functions maintain DNA in the functional single-stranded form. Lastly, SSBs regulate protein interactions. For example, increased phosphorylation of RPA, the primary SSB in eukaryotes, during mitosis results in reduced affinity to proteins involved in DNA replication and repair<sup>112</sup>.

The 34-kDa SSB is encoded by the I3L gene in VACV<sup>62</sup>. Initial work with I3 showed that the protein is expressed during both early and intermediate times post-infection<sup>62</sup>. Additionally, it was shown that I3 was phosphorylated on serine residues and, given the importance of SSBs in DNA replication and the fact that purified DNA polymerase could not pass through barriers of DNA secondary structure, it was postulated that I3 acted as the replicative SSB. It wasn't until later that the importance

of I3 in DNA replication would be revealed. Progress of I3 characterization was hampered by the lack of a readily available ts mutant allele of I3 and the fact that I3 is essential for virus viability. As such, earlier work used siRNA-mediated knockdown of I3 and observed drastically reduced replication (~4-fold reduction)<sup>113</sup>. However, knockdown of I3 was incomplete (8-10% residual I3) and production of late viral proteins, which are absent following inhibition of DNA replication, occurred. More recent studies using  $\Delta$ I3 mutants and a complementary cell line provided definitive proof for the role of I3 as the replicative SSB<sup>63</sup>. The absence of I3 results in a severe reduction of DNA replication in all non-complementing cell lines and, in some cell lines, prevents the expression of late viral proteins.

Along with its role in DNA replication, I3 is involved with recombination. Work elucidating the role of E9 in recombination noted that the presence of I3 enhanced the formation of joint molecules due, in part, to increased joint molecule stability<sup>43</sup>. Subsequent work noted that siRNA-mediated knockdown of I3 corresponded to reduced levels of replication and recombination<sup>41</sup>. While inconclusive in the exact mechanism by which I3 mediates recombination, this study showed that recombination is mediated to an extent by I3. Even more interesting is the fact that I3 associates with the small subunit of the viral ribonucleotide reductase<sup>114</sup>. Given that recombination is coupled to the dNTP micro-environment<sup>41</sup>, this suggests a scenario in which the dNTP synthesis complex is recruited to sites of replication and collapse of this replication complex, perhaps due to the presence of a DSB, produces a dNTP microenvironment that favours recombination over replication. If one considers the finding that I3 is phosphorylated<sup>62</sup>, that phosphorylation does not impact either the

multimerization or DNA binding capacities of I3 and that phosphorylation can regulate protein interactions among SSBs may indicate a role of kinases in regulating the protein interactions of I3. It is possible then that a viral kinase, such as the F10 late viral kinase, may play a role in the collapse of both replication and recombination complexes as the virus shifts away from DNA replication toward progeny assembly.

#### 1.3.1.3 G5 Fen1-like Nuclease

Nucleases are involved in a wide range of cellular processes including DNA replication, homologous recombination, Okazaki fragment maturation and DNA repair<sup>115</sup>. Various DNA intermediate structures are formed during these processes and nucleases recognize and bind to these structures specifically independent of the DNA sequence. One such nuclease is the FEN1 metallo nuclease that binds to single-stranded DNA flaps and has been shown to be involved in DNA replication, recombination and repair<sup>116,117</sup>. In the context of recombination, FEN1 mediates the resection of heterologous DNA at the ends of DNA breaks to permit recombination<sup>118</sup>.

The role of the VACV G5 as a FEN1 homolog was first suggested by computational analysis<sup>119</sup>. Prior to this study, little was known about the role of G5, however, it was shown to be essential for virus viability and is produced early during infection<sup>120</sup>. Unusually, study of ts mutants suggested that G5 was involved in viral morphogenesis despite the predicted nuclease activity. Due to the importance of nucleases in various replicative processes, including recombination, and the finding that multiple ts mutants of G5 exhibited anomalous phenotypes, the role of G5 during VACV infection was reinvestigated using deletion mutants<sup>121</sup>. Deletion mutants exhibited a phenotype more consistent with the hypothesis that G5 contains nuclease

activity. Specifically, both DNA replication and recombination were impaired in the mutant virus. Overall, these studies show that G5 plays an important role in recombination and replication during viral replication.

### 1.3.2 Timing of Inter-Genomic and Intra-Genomic Recombination

A seemingly contradictory observation lies in the fact that few recombinants are formed between co-infecting particles despite a high frequency of recombination<sup>104</sup>. Even stranger is the observation that the low number of recombinants produced during co-infection exhibit a high proportion of recombination events even after a single round of infection. This suggests that there is some barrier to genetic mixing, a prerequisite for recombination, of two co-infecting particles.

A collection of recombinant viruses were used to investigate the kinetics of inter- and intra-genomic recombination in an attempt to elucidate the intricacies surrounding the recombination process<sup>122</sup> (Fig. 1.4.). One of the recombinant viruses contained overlapping fragments of the mCh fluorophore conjugated to the lambda phage cro protein DNA binding domain separated by a GPT cassette in an effort to investigate intra-genomic recombination. Recombination results in the excision of the GPT cassette and the formation of the fully functional mCh protein expressed under a poxvirus early/late promoter. In this scenario, recombination is marked by the appearance of the mCh signal and was observed at approximately 3h post factory formation, a time that corresponds to active DNA replication. Another experiment used a combination of two separate recombinant viruses to investigate inter-genomic recombination. The first virus contained a truncated mCh gene but a functional

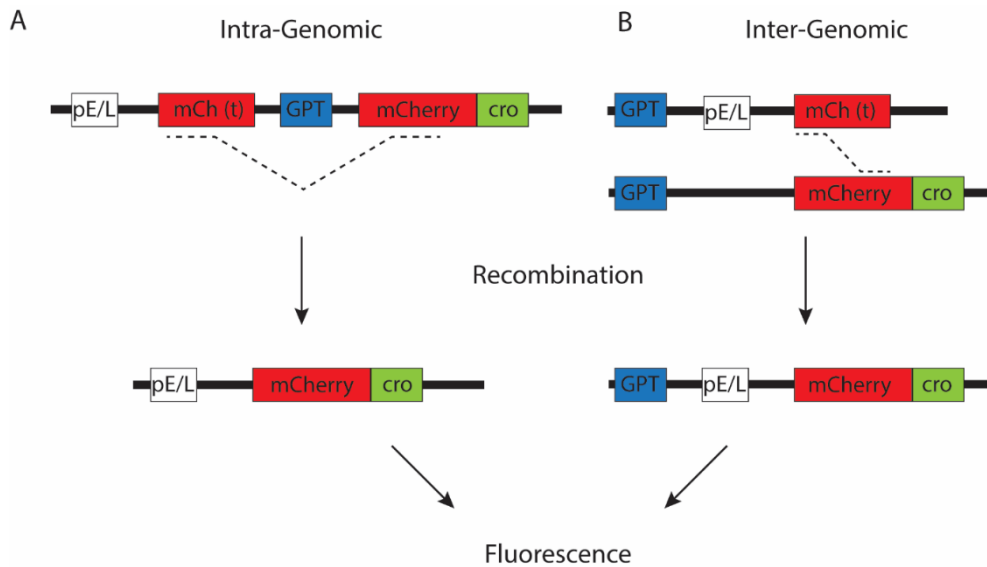


**Figure 1.4. Mechanism used to investigate the timing of inter-genomic and intra-genomic recombination.** (A) The recombinant virus used to investigate intra-genomic recombination harboured a truncated mCherry fluorescent protein expressed under a poxvirus early/late promoter (pE/L). Only after recombination would the fully functional mCherry protein conjugated to cro protein DNA-binding domain be expressed. (B) The two recombinant viruses used to investigate inter-genomic recombination. The first virus expressed a truncated mCherry protein under a functional poxvirus early/late promoter. The other virus contained the full mCherry protein conjugated to the cro DNA binding domain but lacked a promoter. Only following recombination between the two viruses would mCherry fluorescence be observed. In both viruses, recombination was noted by the observation of mCherry fluorescence.

poxvirus early/late promoter. The other virus contained a fully functional mCh gene but lacked a poxvirus promoter. Therefore, a fully functional mCh gene could only be expressed following inter-genomic recombination between the two viruses and was observed at roughly 5h following factory formation. This observation was surprising considering that the recombination event between the two co-infecting particles took place after the expression of late viral proteins, a time during the viral replication cycle that is characterized by reduced DNA replication in favour of progeny assembly. Given that replication and recombination are linked<sup>42</sup>, this may explain the observation of reduced recombinant virus production following co-infection of two genetically distinct viruses.

The study also demonstrates that recombination between viral and plasmid DNA occurs concurrently with intra-genomic recombination and suggests that there is a physical barrier, rather than an enzymatic limitation, preventing genetic mixing of two co-infecting particles and subsequent recombination events<sup>122</sup>. This physical barrier is likely reflective of the fact that each infecting VACV particle gives rise to an individual viral factory<sup>26,123</sup> and the genetic content of these individual factories remain distinct even after apparent fusion<sup>28</sup>. ER membranes are the most likely candidate for these physical barriers considering that viral factories are surrounded by ER membranes during formation<sup>29</sup> and that late factories exhibit internal ER membrane structures that could theoretically prevent genetic mixing<sup>122</sup>. Earlier work shows that the ER membranes surrounding the viral factories collapse late during infection during the transition from DNA replication to progeny production<sup>29</sup>. The late collapse of the ER membrane results in a delayed mixing of genetic content between two viral factories

and may explain the significantly delayed recombination between two co-infecting particles.

#### 1.4 Goals of the Thesis Project

The primary objective of this thesis project is to investigate the persistence of ER membranes at the periphery of the viral factory and the potential restraint they impose on genetic mixing and inter-genomic recombination. Considerable work has been performed in this line of questioning. First, the genetic content of the viral factory has been shown to be enclosed by membranes derived from the ER<sup>29</sup>. These ER membranes are likely responsible for the separation of genetic material even after the apparent fusion of viral factories<sup>28</sup>. These membrane boundaries have been shown to lose integrity late during infection and this loss of membrane integrity may allow genetic mixing of co-infecting particles to occur<sup>29</sup>. This study will expand upon previous work in our lab that showed large internal membrane structures within aggregates of viral factories late in infection<sup>122</sup>. Specifically, I used correlative microscopy to show that membrane structures persist following the collision of viral factories. These membrane structures persist late into the viral replication cycle and can be observed, to an extent, throughout the 3D-ultrastructure of an infected cell.

My thesis will also investigate the seemingly contradictory finding that inter-genomic recombination occurs late in viral infection after the expression of late viral proteins<sup>122</sup>. This is particularly odd given that DNA replication is limited late in infection<sup>29</sup> and that replication and recombination are linked<sup>42</sup>. To investigate further, I used a thymidine analog to investigate DNA replication at various time points post-

infection. In consensus with earlier findings, DNA replication was highest early during infection and significantly reduced late during infection. By correlating between live and fixed-cell microscopy, I was able to show that DNA replication does in fact occur at sites of inter-genomic recombination despite the overall reduced replication rates late in infection.

Lastly, the timing of viral morphogenesis will be tracked in regards to the viral life cycle. Intergenomic recombination occurs following late gene expression<sup>122</sup> and late genes are responsible for, in addition to other functions, viral morphogenesis. Morphogenesis relies on the capture of membranes derived from the ER<sup>78</sup>. It is plausible that capture of membranes destined for progeny production results in the collapse of the bounding membranes of the viral factories. As the infection progresses, more extensive capture of ER membranes is required to facilitate progeny production and the integrity of the factory enclosing membranes is significantly reduced. Overall, ER membrane capture for morphogenesis may act as the trigger for inter-genomic recombination.

## Chapter 2 - Materials and Methods

### 2.1 Cell Lines, Viruses and Culturing

#### 2.1.1 Cell Lines and Viruses

BSC-40 cells were purchased from the American type culture collection (ATCC) and BSC-40-eGFP-cro cells were generated as described<sup>28</sup>. VACV-WR was originally purchased from the ATCC and the recombinant VACV-pE/L-mCherry(t) and VACV-pmCherry-cro were generated from the Western Reserve strain as described<sup>122</sup>. VACV-A5-YFP was generously provided from Dr. B. Moss<sup>27</sup>.

#### 2.1.2 General Cell Culture

Both BSC-40 and BSC-40-eGFP-cro cells were cultured in MEM supplemented with 1% sodium pyruvate, antibiotics/antimycotics, L-glutamine, non-essential amino acids (NEAA) and 5% FetalGro<sup>®</sup> (RMBIO). For cell passaging, cells were first washed with PBS, incubated with pre-warmed 0.25% Trypsin-EDTA and incubated at 37°C until the cells were fully detached. To deactivate the Trypsin, 20mL of media was added to the passaged cells.

To determine cell counts for experiments that require a specific cell confluency, cells were first detached from the plate using 0.25% Trypsin-EDTA. A 10 $\mu$ L portion of the cell suspension was transferred to a small microcentrifuge tube and 10 $\mu$ L of Trypan Blue was added directly to the cell suspension. The mixture was then transferred to a Countess slide and total cell counts were determined using a Countess automated cell counter.

### 2.1.3 Bulk Virus Preparation

Virus stocks were generated by infecting 35 150mm plates of BSC-40 cells with virus at a MOI of 0.03. Cells were harvested 48 hours later using cell scrapers, collected into large centrifuge bottles and centrifuged at 2000xg for 10 minutes. Pellets were resuspended in cold 10mM Tris pH 9.0 supplemented with 2mM MgCl<sub>2</sub> and 50U/mL benzonase. Cells were then disrupted by dounce homogenization. After homogenization, the inoculum was centrifuged at 1500xg for 10 min and the supernatant was transferred to a separate tube and stored on ice. The pellet was resuspended in 10mM Tris pH 9.0 supplemented with 2mM MgCl<sub>2</sub> and 50U/mL benzonase and subjected to an additional round of dounce homogenization. After centrifugation, supernatants from the homogenized samples were pooled and incubated at 37°C for 30 minutes to digest any contaminating DNA. Virus was underlaid with 36% sucrose in 10mM Tris pH 9.0 and centrifuged at 26,500xg for 90 minutes in a JS 13.1 swinging bucket rotor. Sucrose was aspirated following centrifugation and the virus pellet was resuspended in Tris pH 8.0.

To determine virus titres, 10-fold serial dilutions of the virus stock were prepared in serum-free media. BSC-40 cells were infected in triplicate in 12-well plates by inoculating with virus for 1h at 37°C before replacing the inoculum with media supplemented with 1% carboxymethyl cellulose (CMC). The cells were incubated at 37°C for 48 hours before adding a solution containing 0.13% crystal violet, 5% ethanol and 30% formaldehyde to both fix and stain the cells. Afterwards, the crystal violet solution was removed, and viral plaques were counted to determine the original viral titre.

## 2.2 Microscopy

### 2.2.1 Fixed Cell Microscopy

Circular glass coverslips (1.5mm thickness) were sterilized by washing with 95% ethanol before flame drying. Afterwards, the coverslips were placed into a 24-well plate so that each well contained a single coverslip and cells were cultured directly on the coverslips. Cells were incubated at 37°C overnight until a final confluency of 50-70% was reached. Cells were synchronously infected by incubating the cells on ice for 15 minutes before adding virus at a MOI of 5 in cold serum-free media supplemented with 10mM HEPES buffer for 1 hour at 4°C. Afterwards, the cells were washed once with cold PBS and then incubated in fresh, pre-warmed media to the desired time point. If the experiment called for treatment with rifampicin, rifampicin was added to a final concentration of 200µg/mL in the fresh media added back to the cells after inoculation.

Cells were fixed at the designated timepoint by washing once with PBS and subsequently adding 4% pre-warmed paraformaldehyde (prepared the same day) for at least 30 minutes at 4°C. Aldehyde free radicals were quenched by adding 0.1M glycine in PBS supplemented with 0.1% Triton X-100 for 20 minutes at room temperature. Cells were then washed three times with PBS-T. Cells were blocked in 3% BSA in PBS-T for 30 minutes at room temperature. Cells were then incubated with primary antibody for either 90 minutes at room temperature or overnight at 4°C. The cells were washed three times PBS-T before incubating in secondary antibody for 45 minutes at room temperature in the dark. Cells were mounted in ProLong™ Gold Antifade mountant and sealed with nail polish.

Fixed cell images were captured using either a wide-field DeltaVision (Olympus IX-71 Base) microscope equipped with a 60X/1.42 numerical aperture (NA) oil objective lens, an Olympus IX-81 spinning disc confocal microscope using a 40X/1.3 NA oil objective lens or a DeltaVision OMX super-resolution microscope with a 60X/1.42 NA oil objective lens. Fixed cell images were processed using softWoRx processing software (Version 6.5.1) for both DeltaVision microscopes and Volocity (Version 6.3) for the Olympus microscope.

#### 2.2.1.1 Antiserum Pre-adsorption

An antiserum pre-adsorption protocol was performed in an effort to reduce background staining of the E8 antibody. First, BSC-40 cells were cultured in a 60mm dish. After reaching 100% confluency, cells were scrapped into 6mL of cold PBS and two volumes (12mL) of cold acetone (-20°C) were added. The cells were incubated on ice at 4°C for 30 minutes before centrifugation at 3900xg for 10 minutes. The pellet was resuspended in fresh, -20°C acetone and incubated on ice for 10 minutes at 4°C. The solution was pelleted by centrifugation at 3900xg for 10 minutes before collecting the supernatant and allowing the pellet to air-dry. The pellet was then transferred to the E8 antibody solution and incubated overnight on a rotator to provide constant mixing. The following day, the sample was centrifuged at 14,000rpm for 2 minutes to pellet cellular debris and the supernatant was transferred to a separate tube. This new solution was then used during primary antibody labelling.

#### 2.2.1.2 Particle Count Analysis

Data for particle counts were collected using the imaging software Volocity. Each image was split into three additional images: two marker images, one showing

D13 and A5 and the other showing B5 and A5, used to mark IV and IEV, respectively, and another image showing only A5 for counting. Regions of interest (ROI) were used to mark specific morphogenic forms on the marker images (ex. ROI's were used to surround IV in the D13 and A5 marker image). The ROI's were then transferred to the A5 only image for counting. Virion counts were performed in the A5 image to prevent miscounting due to the presence of B5 or D13. The ROI's generated from a single marker image could be used to count either IV or WV but not both. Therefore, separate ROI's need to be generated from both marker images to obtain count data for both IV and WV. The number of MV were calculated by subtracting the number of IV and WV from the total virion count. The data were collected from a total of ten cells per time point over a course of three separate experiments. A walkthrough of the particle count protocol is depicted in figure 2.1.

### 2.2.2 Live Cell Microscopy

BSC-40-GFP-cro cells were cultured in FluoroDish™ 35mm dishes for non-correlative experiments or gridded Ibidi®/MatTek dishes for correlative experiments and incubated at 37°C overnight. The following day, cells were synchronously infected by incubating the cells on ice for 30 minutes before inoculating with virus at a MOI of 5 for 1 hour at 4°C. After the inoculation, the cells were washed twice with cold PBS before adding back fresh Fluorobrite™ media supplemented with 5% Fetalgro® (RMBIO), and 10mM of both HEPES and non-essential amino acids. Cells were incubated at 37°C for 3h before sealing the dish with Parafilm® prior to imaging.

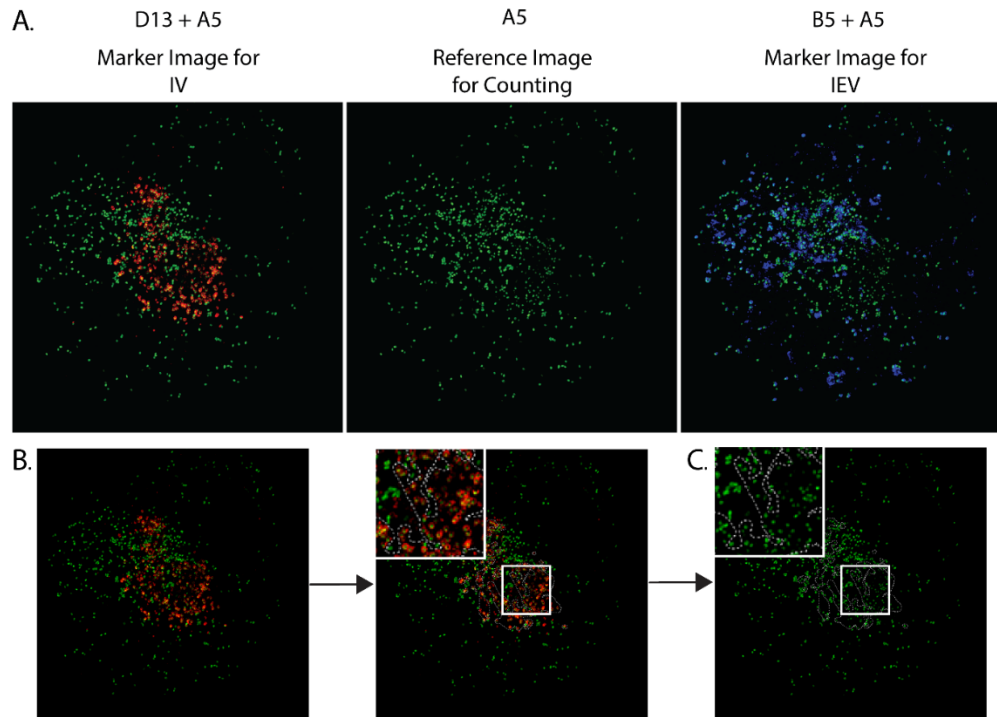


**Figure 2.1. Protocol for quantifying the morphogenic forms of vaccinia virus.**

Data analysis was performed using the image processing software Volocity. (A) The three images used throughout the quantification process. The A5+D13 and A5+B5 act as marker images to quantify IV and IEV, respectively, while the A5 image is used to count virions. (B) First, regions of interest (ROIs; dotted lines) are created around the virions of interest (D13 positive virions in this scenario). (C) The region of interest generated on the marker images are then transferred to the reference image and the virions within the ROI can be counted. The process is then repeated using the other marker image (A5+B5 for this example) to quantify the number of IEV. The number of MV is calculated by subtracting the number of IV and WV from the total virion count.

All live-cell images were captured using an Olympus IX-81 spinning disc confocal microscope using the FITC and RFP filter sets. During imaging, a series of Z-stacks were registered to image the entirety of the cell. These Z-stacks extended above and below the top and bottom of the cell to accommodate any drift that occurred during imaging. In the occurrence of extreme drift, the Z-stacks could be realigned during the intervals between imaging. Images were captured every 4-10 minutes depending on the needs of the experiment.

#### 2.2.2.1 Correlative Live and Fixed Cell Fluorescence Microscopy

BSC-40-GFP-cro cells were cultured in Ibidi® gridded 35mm dishes to permit correlation between the two imaging modalities. The following day, cells were synchronously infected as described in section 2.2.2 with minor deviations. Namely, cells were co-infected with two separate viruses (VACV-mCherry-cro and VACV-pE/L-mCherry(t)) each at a MOI of 2.5 for a total MOI of 5. After adding back warm media, cells were incubated at 37°C for 90 minutes before wrapping the dish in Parafilm® and imaging the cells.

During imaging, the quadrant of the 35mm dish that was imaged was recorded to facilitate correlation after fixation. Cells were imaged, using the FITC and Red confocal filters, every ten minutes until 6hpi, at which point EdU was added to the dish at a final concentration of 10 $\mu$ M. After adding EdU, the cells were imaged every five minutes until mCherry expression was first observed, at which point the cells were fixed by washing once with PBS and incubating with 4% PFA overnight at 4°C. The following day, aldehyde free radicals were quenched with 0.1M glycine in PBS supplemented with 0.1% Triton X-100. After washing three times with PBS-T, cells were blocked with

4% BSA constituted in PBS-T before washing an additional three times with PBS-T. Afterwards, the cells were incubated in the click chemistry reaction as outlined in table 2.1 before washing three times with PBS-T. Both viral and cellular DNA were labelled with DAPI for 45 minutes at room temperature. The bottom of the 35mm dish was transferred to a glass slide and mounted on ProLong™ Antifade Mounting Media (ThermoFisher) before sealing the sample with nail polish. Individual cells from the live-cell portion of the experiment were relocated using the grid as a reference and imaged using the DAPI and Cy5 channels of an Olympus IX-81 spinning disc confocal microscope. Images were processed using Volocity and image sequences were generated in FIJI<sup>124</sup>. Images were realigned in Adobe Illustrator by overlaying the two images.

### 2.2.3 EdU Labelling

Cells were cultured and infected with virus as described in section 2.2.1. fixed-cell microscopy and 2.2.2 live-cell microscopy. The protocols for both imaging modalities follow similar protocols with minor deviations. For fixed cell imaging, EdU was pulsed for 15 minutes at the designated time by adding two times working stock of EdU, constituted in fresh media, directly to the cells (EdU Final Concentration: 10 $\mu$ M). After the 15-minute incubation, cells were washed once with PBS before adding either fresh media to continue the infection or PFA to fix the cells. For live cell imaging, EdU was added to a final concentration of 10 $\mu$ M at 6 hpi and fixed with 4% PFA after observing the mCherry signal produced by the recombinant viruses outlined in figure 1.4.

Table 2.1. Components for click-chemistry reaction

Components	Reaction for one coverslip	Reaction for five coverslips
100mM Tris Buffer	258 $\mu$ L	1290 $\mu$ L
100mM CuSO <sub>4</sub>	12 $\mu$ L	60 $\mu$ L
Alexa Fluor® Azide	0.75 $\mu$ L	3.75 $\mu$ L
100mM Sodium Ascorbate	30 $\mu$ L	150 $\mu$ L
Total Volume	300 $\mu$ L	1500 $\mu$ L

After fixation, both modalities continue with similar sample processing as outlined in section 2.2.1. However, after blocking the cells with 3% BSA in PBS-T, cells were treated with the click chemistry reaction (Reaction components outlined in Table 2.1) for 30 minutes at room temperature in the dark. Afterwards, cells were washed three times with PBS-T and continued to primary antibody staining and subsequent steps as outlined in section fixed cell microscopy.

#### 2.2.4 Transmission Electron Microscopy

BSC-40 cells were cultured in glass-bottom, 35mm dishes overnight to a final confluency of approximately 90%. The following day, cells were synchronously infected with VACV-WR at a MOI of 5 in cold, serum-free media supplemented with 10mM HEPES buffer for 1 hour at 4°C. Following the incubation, cells were washed twice with cold 1X PBS before adding fresh media. The infected cells were then cultured at 37°C to the desired timepoint.

Cells were fixed by adding an equivalent volume of warm, 2X fixative directly to the culture dish (Final concentration: 2% glutaraldehyde, 0.1M sucrose, 2mM calcium chloride in 0.1M CB). Cells were fixed for five minutes at RT, followed by 1 hour at 4°C and finally 1 hour at room temperature before washing with 0.1M CB for five minutes a total of three times. Cells were post-fixed with 1% osmium tetroxide ( $\text{OsO}_4$ ) and 1.5% potassium ferrocyanide ( $\text{K}_4\text{Fe}(\text{CN})_6$ ) in 0.1M CB for 15 minutes before washing with 0.1M CB for three minutes a total of three times. Next, cells were washed with 0.1M sodium acetate buffer (pH 5.2) for 2 minutes a total of three times. Cell were then stained with 1% uranyl acetate in 0.1M sodium acetate buffer (pH 5.2) for fifteen

minutes at room temperature in the dark before washing three times with 0.1M sodium acetate (pH 5.2) for two minutes a total of three times. To prepare for the dehydration step of sample preparation, cells were washed once with Milli-Q® Water (MQW) for two minutes to remove the sodium acetate buffer. Sample dehydration was performed by treating the cells with increasing concentrations of ethanol (10%, 30%, 50%, 70%, 80%, 90%, 95%) for three minutes at RT each before treating with 100% ethanol for three minutes a total of three times. Resin infiltration was performed by incubating the cells in a 2:1 100% ethanol:Spurr's Resin solution for 30 minutes at RT, followed by a 1:1 100% ethanol:Spurr's Resin solution for one hour at RT and lastly with a 1:2 100% ethanol:Spurr's Resin solution for two hours at RT. Next, cells were incubated in absolute Spurr's Resin overnight and refreshed with new absolute resin for one hour the following morning before incubating the sample at 65°C for 24-72 hours to polymerize the resin.

Following polymerization, the sample was incubated at room temperature for at least 30 minutes to allow the resin to harden. The sample block face was trimmed to approximately 500µm<sup>2</sup> using razor blades. Thin sections (70nm) were cut from the sample block using a Diatome diamond knife on a Leica UM7 ultramicrotome system and collected on 200 mesh copper grids.

Two chambers were prepared in 60mm dishes for the counterstaining protocol. The first chamber was optimized for uranyl acetate staining by wrapping the dish with tin foil to prevent exposure to light, placing filter paper wetted with MQW inside the dish and subsequently placing a small piece of parafilm on top of the filter paper. The second dish was optimized for lead citrate staining by placing a small piece

of parafilm in the center of the dish and placing 6-8 pellets of NaOH around the periphery of the chamber to prevent precipitation of lead citrate due to exposure to atmospheric CO<sub>2</sub>. Immediately before use, the uranyl acetate solution was centrifuged at 10,000g for 5 minutes. After centrifugation, one 20 µL aliquot of 4% uranyl acetate was placed in the first petri dish for each grid to be stained, making sure to draw from the top of the solution to avoid transfer of any precipitate. Grids were placed specimen side down on the uranyl acetate droplets for ten minutes in the dark. While the grids were incubating, the lead citrate solution was centrifuged at 10,000g for 5 minutes and one 20 µL lead citrate aliquot was loaded for each grid one minute prior to use in the dish containing NaOH pellets. Grids were washed in a wash series by dabbing 30 times each in four subsequent beakers filled with MQW and subsequently drying on filter paper for 5 seconds before loading the grids specimen side down on the lead citrate aliquots. Grids were incubated on lead citrate for 10 minutes before rewashing in the wash series and drying on filter paper. Electron micrographs were acquired using a Hitachi H-7650 transmission electron microscope.

#### 2.2.4.1 Correlative Live Cell and Transmission Electron Microscopy

BSC-40 cells were cultured at a low confluency (10,000 to 40,000 cells were seeded for infection the following day) in a gridded, 35mm dish (Ibidi®). The following day, cells were synchronously infected by inoculating with VACV-WR at a MOI of 5 in serum-free media supplemented with 10mM HEPES buffer for 1 hour at 4°C. After the inoculation, the cells were washed twice with cold PBS before adding back fresh Fluorobrite™ media supplemented with 5% Fetalgro® (RMBIO), and 10mM of both

HEPES and non-essential amino acids. Cells were incubated at 37°C for 3 hours before sealing the dish with Parafilm® prior to imaging.

For imaging, a quadrant that contained a low number of cells (maximum of five but ideally three or less) was identified and all cells within the quadrant were imaged. Cells were imaged using an Olympus IX-81 spinning-disc confocal microscope using the FITC filter sets. Z-stacks were set to image the entirety of the cell. Each Z-stack was set to 50nm to ease correlation between the two imaging modalities. Cells were fixed immediately after observing viral factory collision by adding warm fixative directly to the culture dish (Fixative final concentration: 2% glutaraldehyde, 0.1M sucrose, 2mM calcium chloride in 0.1M CB). The rest of the fixation protocol as well as the processing for EM continued as outlined in section 2.2.3 transmission electron microscopy with one minor deviation: the block face of the polymerized resin sample was trimmed to match the outline of the quadrant imaged during the live cell process. After loading sections on copper grids, the sample was imaged using a Hitachi H-7650 transmission electron microscope.

### 2.2.5 Scanning Electron Microscopy

BSC-40 cells were cultured at a low confluency in gridded 35mm MatTek dishes overnight. Cells were then synchronously infected using the same protocol in section 2.2.4.1. Cells were incubated at 37°C for three hours prior to imaging. During imaging, a quadrant that contained one or two cells was imaged. Similar to CLEM in the previous section, the entirety of the cell was imaged at 50nm intervals so that individual Z-stacks could be aligned with the corresponding section following EM processing. Cells were

fixed after observing a collision event by adding pre-warmed fixative directly to the culture dish and incubating at RT for 5 minutes and subsequently at 4°C overnight. Cells were then washed with 0.1M CB for three minutes a total of three times before post-fixation with 1% potassium ferrocyanide and 1% osmium tetroxide in 0.1M CB for three minutes on ice. The sample was then washed three times with MQW for three minutes a total of three times before treating with 1% thiocarbohydrazide (TCH) for three minutes at RT. After washing an additional three times with MQW for three minutes each wash, cells were retreated with 1% osmium tetroxide for three minutes at RT. Cells were washed an additional three times with MQW before *en bloc* staining with 1% UA at 4°C overnight in the dark. After washing three times with MQW, cells were stained with lead aspartate for three minutes at room temperature. Subsequently, cells were washed with MQW for three minutes a final time. Next, cells were dehydrated in an ice-cold, graded ethanol series (10, 30, 50, 70, 80, 90, 95%) for three minutes each before treatment with 100% ethanol three times for three minutes each treatment. Resin infiltration was performed by treating cells with a 2:1 ethanol:Durcupan resin solution for 30 minutes, followed by a 1:1 ethanol:Durcupan solution for one hour, and then a 1:2 ethanol:Durcupan solution for two hours. Lastly, cells were incubated in 100% Durcupan resin overnight before polymerization for 48 hours at 70°C.

After polymerization, the sample block face was trimmed to approximately 500 $\mu\text{m}^2$  and sectioned using a Leica UM7 ultramicrotome. Serial sections were collected onto a silicon wafer. Serial sections were imaged using a Hitachi S-4800 field emission gun scanning electron microscope.

#### 2.2.5.1 3D-Reconstruction

Combinations of FIJI<sup>124</sup> and IMOD<sup>125</sup> were used to generate the correlative images. First, an image sequence was created for the serial EM images. Next, the serial images were registered using the TrakEM2 plug-in for FIJI. After registration, the realigned images were transferred to IMOD to generate the 3D model. Separate contours were generated for each area of interest. In this scenario, a contour was created for the membrane structure found within the viral factory, the periphery of the viral factory, MT and mitochondria. These individual contours were used to generate the 3D-model.

Primary Antibodies				
Protein Detected	Origin	Source	Catalog Number	Dilution
VACV D13	Rabbit	Dr. Bernard Moss		1:1000
VACV I3 (10D11)	Mouse	ProSci		1:10000
VACV B5	Mouse	Dr. Stuart Isaacs		1:10000
VACV E8	Rabbit	Dr. Jacomine Locker		1:500
Calreticulin	Rabbit	Abcam	ab2907	1:200
B-Tubulin	Mouse	Sigma-Aldrich	T5293	1:250
Secondary Antibodies				
GAM AF 488	Goat	Invitrogen	A11029	1:2000
GAM AF 555	Goat	Invitrogen	A21127	1:2000
GAM Cy5	Goat	Invitrogen	A10524	1:2000
GAR AF 488	Goat	Invitrogen	A11008	1:2000
GAR AF 555	Goat	Invitrogen	A21428	1:2000
GAR Cy5	Goat	Invitrogen	A10523	1:2000

## Chapter 3 – Developing a timeline of the viral life cycle

### 3.1 Introduction

VACV gene expression is regulated in a temporal fashion. In short, early genes are expressed immediately after the complete internalization of the infecting particle. Early genes drive both the uncoating and subsequent replication of the viral genome. Replication promotes the transcription of intermediate genes which, in turn, result in the expression of late viral proteins. Previous work in our lab investigated the kinetics of both intra- and inter-genomic recombination in regard to the viral life cycle<sup>122</sup>. While intragenic recombination occurred early during infection, intergenic recombination could only be detected late during infection following the expression of late viral proteins. The delay in recombination between two co-infecting particles suggests that there is some barrier that limits recombination. As such, it is important to investigate the hallmarks of infection in order to develop a more complete understanding of the potential barriers to infection and what processes could promote inter-genomic recombination events. The remainder of this chapter will discuss the techniques used to track the hallmarks of infection as well as their relation to the kinetics of recombination.

## 3.2 Results

### 3.2.1 Super-resolution microscopy as a means to study the viral life cycle

While fluorescence microscopy represents a potential tool to hallmarks of the viral life cycle, a few complications arise when one considers the size of viral particles. VACV virions measure approximately  $350 \times 270\text{nm}^2$ , which lies close to the resolution ( $\sim 200\text{nm}$ ) associated with traditional fluorescence microscopy<sup>126</sup>. As such, sub-viral structures may lie beyond this limit of resolution. To circumvent this, I made use of a technique known as structured-illumination microscopy (SIM) that increases the limits of resolution by approximately two-fold when compared to traditional fluorescence microscopy. This technique allowed us to resolve the intricacies of sub-viral structures (Fig. 3.1). When comparing the two imaging modalities, it becomes clear the details surrounding the localization of proteins within the virion are only fully realized with SIM. Due to the advantages surrounding super-resolution microscopy, the technique was used for the remainder of the chapter, unless otherwise stated.

### 3.2.2 Determining viral early, intermediate and late expression kinetics

First, multiple viruses containing fluorescently tagged proteins were used to establish the hallmarks of infection. Two such viruses included the VACV-I1L-mCh virus, in which the viral I1 protein is conjugated to a mCh fluorophore, and the VACV-A5L-YFP virus, which has the viral A5 protein conjugated to a YFP fluorophore. The I1 protein is a telomeric DNA binding protein that plays a role in progeny morphogenesis and is expressed under an intermediate promoter<sup>127,128</sup>. Conversely, the A5 protein, which is also involved in morphogenesis<sup>129</sup>, is expressed late during infection. By using a

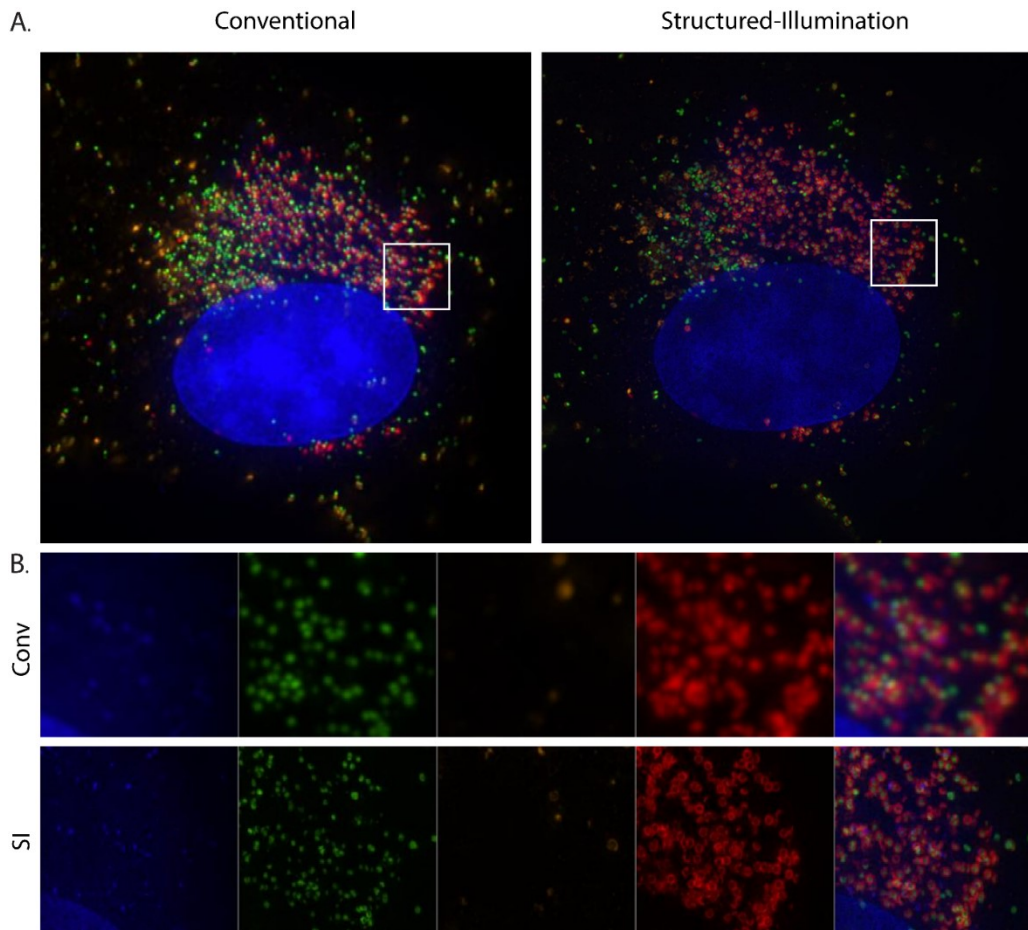


**Figure 3.1. Comparison of conventional and super-resolution microscopy.** BSC40 cells were infected with VACV-A5L-YFP, fixed at 8hpi and stained with antibodies against B5 and D13. (A) A single cell infected with virus imaged using either conventional (left) or super-resolution (right) microscopy. (B) Increased magnification of the regions highlighted in (A). Of particular note is the clear ring structure observed under super-resolution microscopy compared to conventional microscopy.

combination of these two viruses, as well as antibodies to the early I3 protein and late D13 protein, we could track early, intermediate, and late viral gene expression. Using this approach, I was able to detect I3 expression as early as 3hpi (Fig. 3.2). I3 appeared alongside the first detectable traces of viral factories, as signified by cytoplasmic DNA, and was localized within the viral factories. I3 remained associated with the viral factories up until at least 10hpi. While I3 was localized diffusely throughout the viral factories early during infection, the protein adopted a more punctate appearance late during infection. The intermediate I1 protein was detected at 4hpi, just shortly after expression of the early I3 protein (Fig. 3.3). Similar to I3, I1 localized to viral factories for the duration of the infection. However, unlike I3, I1 maintained a diffuse pattern of staining for the duration of the time course. The late viral protein, D13, exhibited slightly different kinetics between the separate experiments. One experiment exhibited D13 staining as early as 4hpi (Fig. 3.3) while the other experiment had D13, as well as the late A5 protein, first appear at 5hpi (Fig. 3.2). It is possible that variability in the induction of infection could account for the variations in expression kinetics between the two experiments. Regardless, late expression was never observed prior to the expression of early or intermediate genes suggesting that late genes are expressed shortly after the production of intermediate proteins.

### 3.2.3 Characterizing VACV morphogenesis

Late viral proteins are responsible for, among other functions, the assembly of progeny virions in a process known as morphogenesis. Morphogenesis encompasses the process that results in the production of the two infectious forms of VACV. To develop an understanding of the hallmarks of infection in relation to inter-genomic

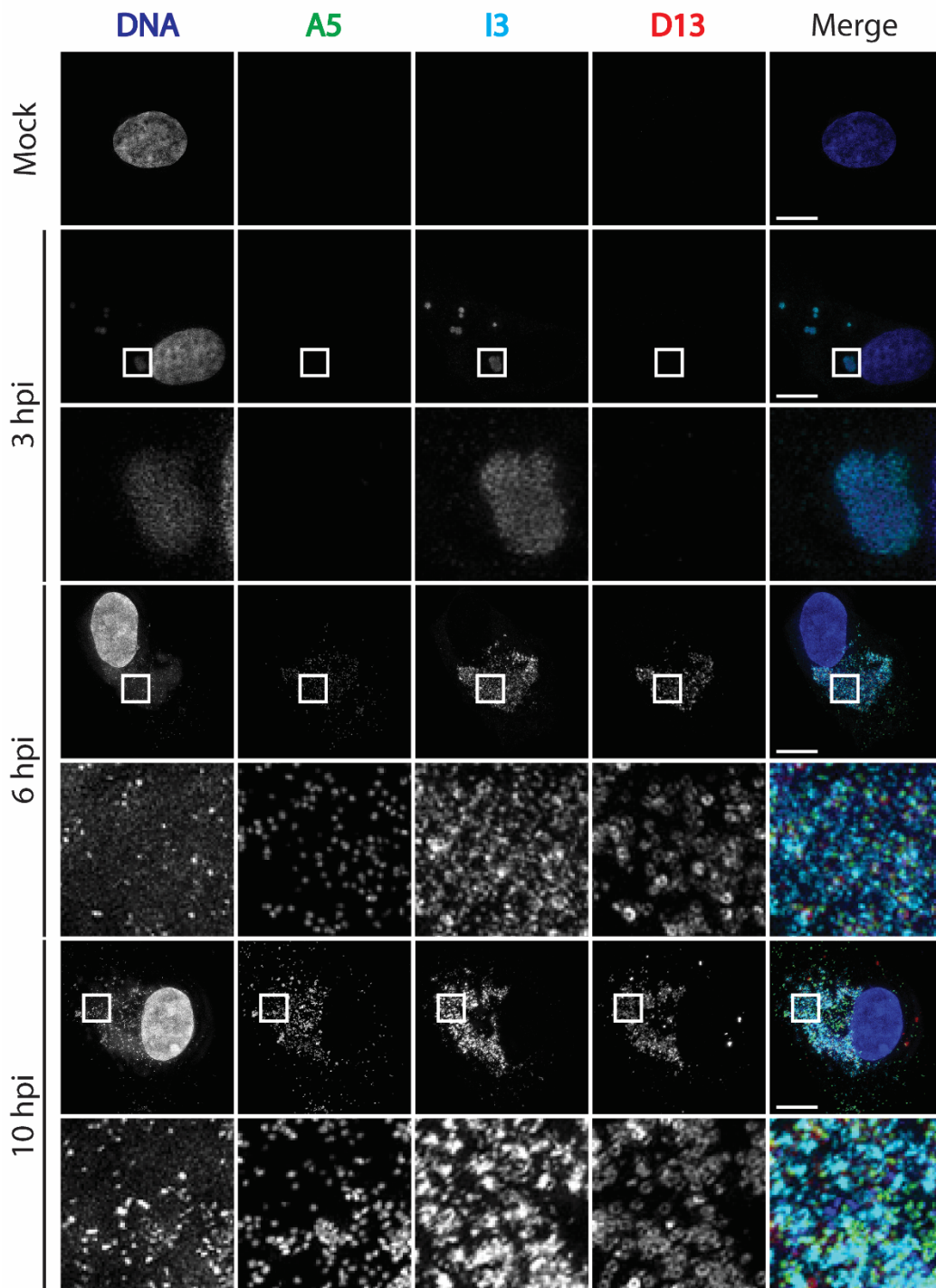


**Figure 3.2. Expression of early and late viral proteins.** Cells were infected with VACV-A5L-YFP, fixed at the designated times and labelled with antibodies against D13 and I3. Early gene expression (I3) was detected at 3hpi and first appeared at the same time factories could first be observed. Late viral proteins (A5 and D13) could be observed at 6hpi.

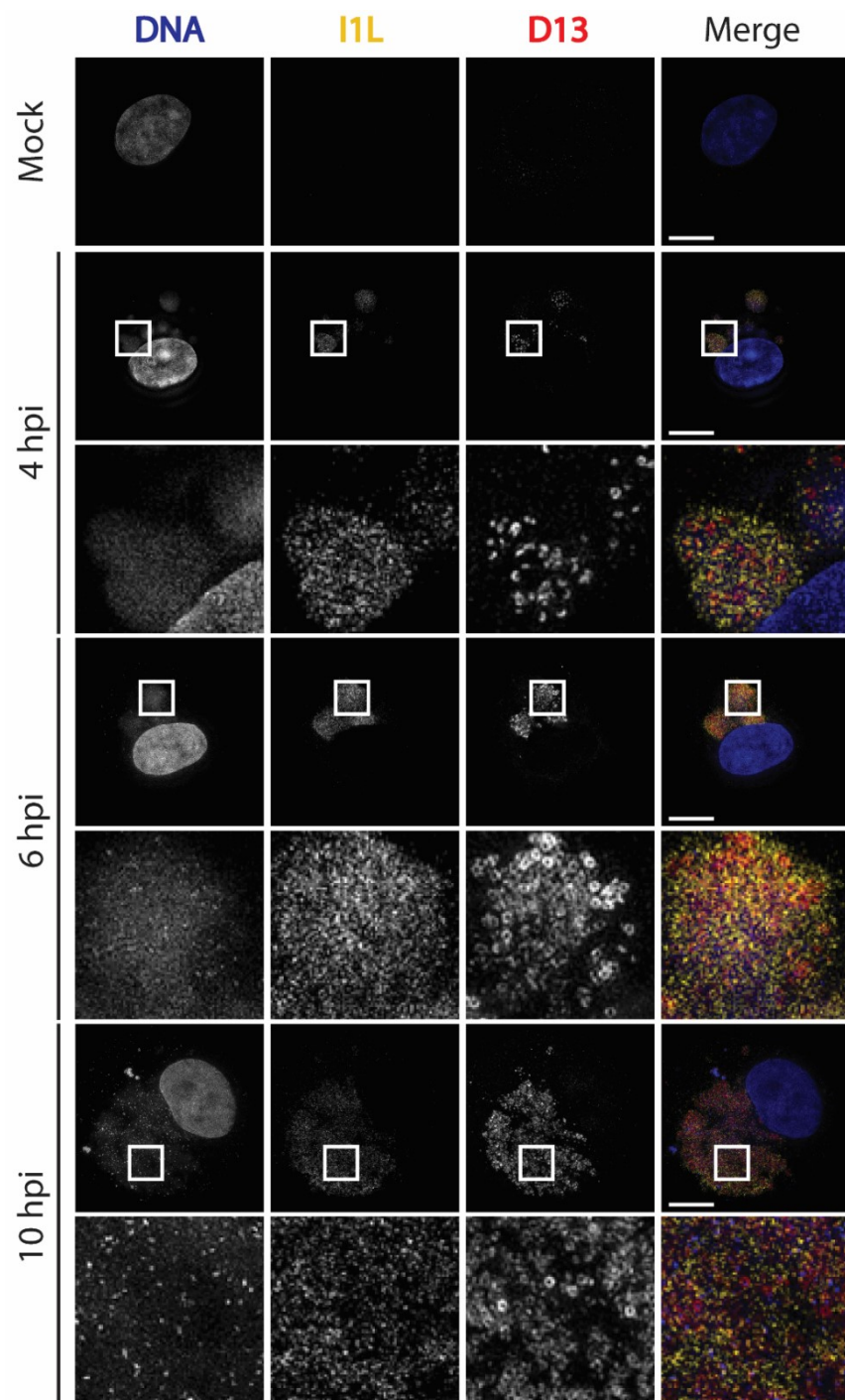


**Figure 3.3. Expression of intermediate and late viral proteins.** BSC40 cells were infected with VACV-I1L-mCh, fixed at the designated times and labelled with DAPI and antibodies against D13. Both intermediate (I1) and late (D13) could be detected at 4hpi. Both I3 and D13 localized within viral factories for the duration of the infection.

recombination, we first looked at the timing of morphogenesis. To do this, I labelled three separate viral proteins: D13, A5 and B5. A5 is a viral protein that is incorporated into the virion core structure early in morphogenesis and is present in all morphogenic forms of VACV<sup>129</sup>. D13 is a scaffolding protein found on both viral crescents and immature virions<sup>74</sup>. The D13 scaffold is lost during maturation of IV into MV and, as a result, acts as a marker of IV. In contrast, B5 is an envelope protein that is present only on virions that obtained additional envelope membranes and acts as a marker of WV<sup>87-90</sup>. By simultaneously labelling these three proteins, we were able to differentiate each morphogenic form within an infected cell at various time points during infection (Fig. 3.4). Each morphogenic form exhibited a unique phenotype. IV first appeared primarily at 5hpi and were localized exclusively within the viral factory (Fig. 3.4). MV were also first observed at 5hpi but localized within the cytoplasm of the host cell rather than in the viral factory. Later during infection, MV formed large aggregates within the cytoplasm of the host cell. Lastly, WV were first observed at 5hpi and were localized toward the periphery of the cell near the plasma membrane. B5 staining that was not associated with any viral particles was observed near, but not within, the viral factories and likely represents B5 protein present within the trans-Golgi network. The increased resolution associated with SIM allowed us to investigate the sub-viral localizations of each of the three labelled proteins. In agreement with their role as a scaffolding and envelope protein, D13 and B5, respectively, exhibited ring-like that appeared to enclose the virion core.

We also quantified the proportion of each morphogenic form within a single cell using this approach (Fig. 3.5). Each form stains positive for A5 while IV and WV are

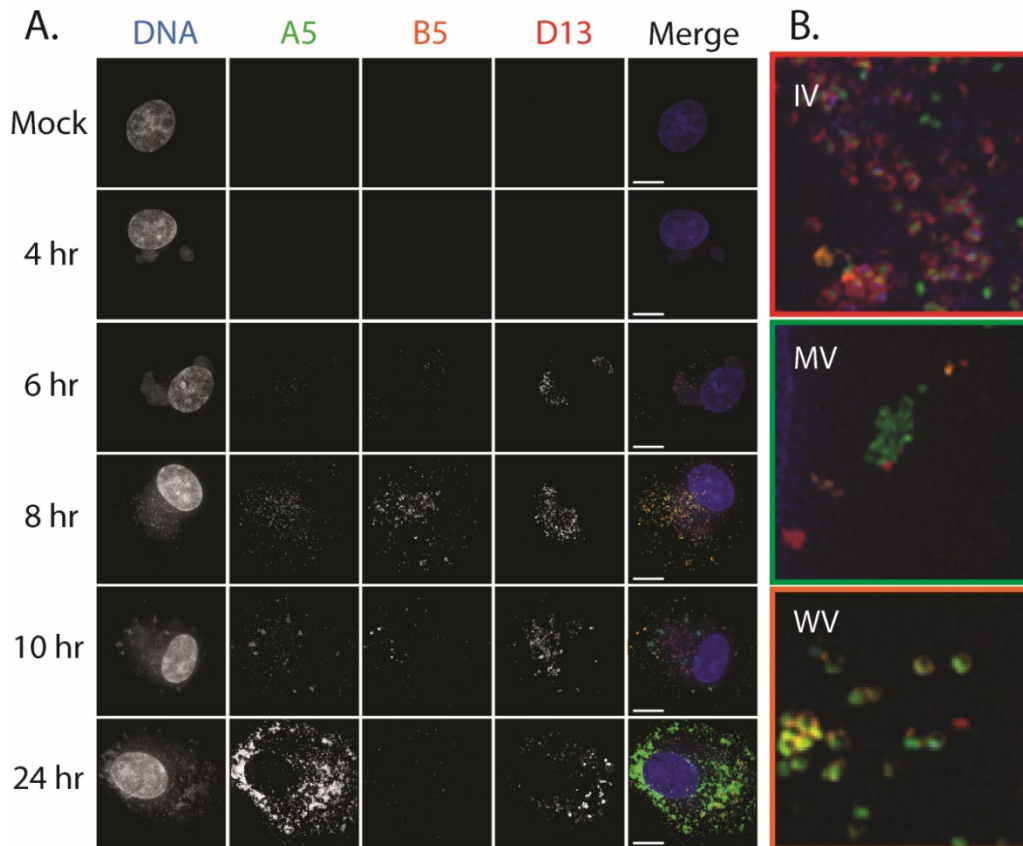


**Figure 3.4. Visualization of the morphogenic forms of VACV.** BSC40 cells were infected with VACV-A5L-YFP and fixed at various times. Viral and cellular DNA were labelled with DAPI while viral B5 and D13 were labelled with antibodies. (A) The appearance and localization of the morphogenic forms of VACV. A5 acts as a label for all forms while D13 and B5 are found exclusively on IV and WV, respectively. IV localize to viral factories at all time points. MV are present in the cytoplasm of the host cell and form aggregates later during infection. WV are also found in the cytoplasm of the host cell but favour a peripheral localization pattern. Bar=10 $\mu$ m. (B) Magnified images of each morphogenic form. The scaffolding and envelope structures of IV and WV, respectively, are clearly visualized.

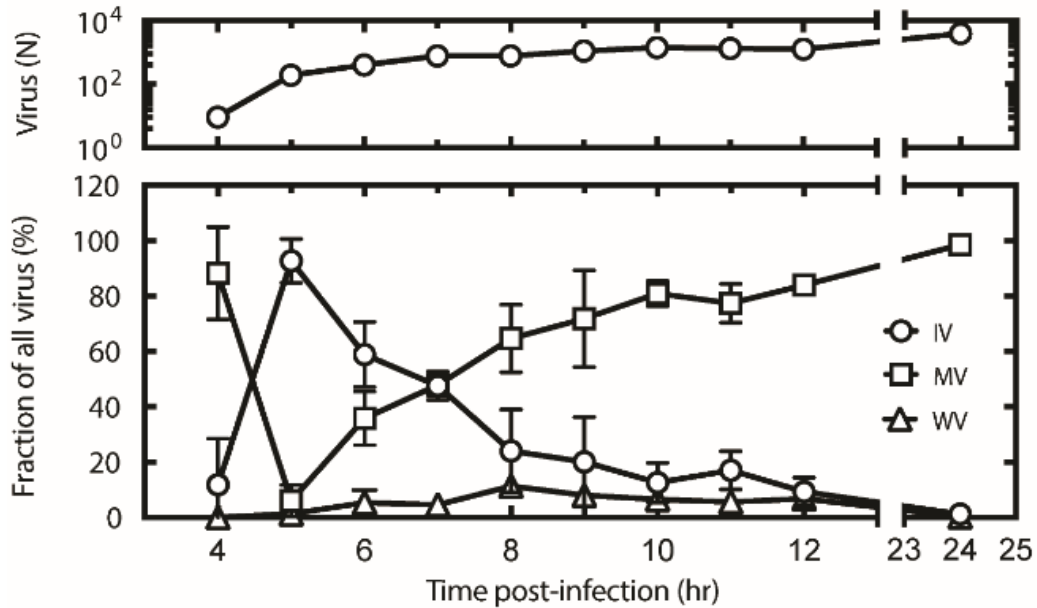


**Figure 3.5. Quantification of morphogenic forms and total virion counts.** Data were collected as described in section 2.2.1.2. Briefly, IV were characterized as virions positive for D13+A5, MV as virions exclusively positive with A5, and WV as particles positive for both A5+B5. Total viral counts were obtained by counting all A5+ virions. Counts are collected from a total of three separate experiments for a total of ten cells per time point. Error bars represent standard deviation.

additionally stained with D13 or B5, respectively. In extension, MV are characterized by the presence of A5 and the absence of both D13 and B5. This modality allows us to differentiate each population in a single cell and subsequently quantify the total population of virions and the proportion of each morphogenic form at various time points (Fig. 3.5). Populations of interest were defined by the presence or absence of D13 and B5 but count data were generated using total counts of A5 to normalize the counts between the different populations. At 4hpi, we observed a large proportion of MV (~75%) and a smaller proportion of IV (~25%). Few cells stained positive for A5 at this time point and the limited number of cells that stained positive for MV harboured few particles (<10). Therefore, the MV detected at 4hpi are likely inoculating virus rather than progeny virions. Of the cells that exhibited A5 staining at 4hpi, only a single cell also showed D13 staining. These D13+ virions all localized within the viral factory which suggests that morphogenesis had begun in this cell. IV are the predominant form present at 5hpi but the total proportion of IV dwindle as the infection progresses. Conversely, MV represent a small portion of total virions at 5hpi but gradually become the most prominent form as the infection progresses. WV compose only a small percentage of the total virions at any given point. The total proportion of WV never exceeds 10% and peaks at 8hpi.

#### 3.2.4 Treatment with rifampicin inhibits viral morphogenesis

Rifampicin is an anti-biotic agent that has a unique interaction with VACV. Specifically, rifampicin reversibly interferes with the interaction of D13 and A17<sup>130</sup>. As a result, D13 localizes to large inclusion bodies within the cytoplasm of the host cell<sup>131</sup>. This results in a perturbation of viral morphogenesis. As a result, neither IV nor the two

subsequent infectious forms are produced following the treatment of infected cells with rifampicin. As such, rifampicin can be used to test the validity of A5, B5 and D13 to act as markers of viral morphogenesis. To test this, cells were synchronously infected with VACV-A5-YFP before adding fresh media supplemented with or without rifampicin (200µg/ml). Cells were fixed at various times post-infection and labelled with both D13 and B5. Each labelled protein exhibited a vastly different phenotype following treatment with rifampicin relative to untreated samples using this approach (Fig. 3.6). D13 no longer localized to viral factories but rather to dense inclusion bodies within the host cytoplasm. These D13 inclusion bodies failed to localize alongside A5 suggesting a block in production of IV. A5 localized exclusively within the viral factories and exhibited puncta of varying sizes relative to the more uniformly sized puncta in untreated cells. B5 continued to localize to the regions near, but not within, viral factories. However, B5 no longer colocalized with A5 at the periphery of the host cell. The lack of cytoplasmic A5 and the lack of any colocalization between A5 and B5 suggest that neither MV nor WV are produced following treatment with rifampicin. However, removal of rifampicin resulted in a rapid reversion of the adverse effects caused by the antibiotic (Fig. 3.7). D13 can be visualized within the viral factories as early as 5min after the removal of rifampicin and exhibit a similar ring-like structure compared to untreated cells. Both MV and WV can be detected within 40 min following the removal of rifampicin.

### 3.2.5 E8 is a late viral protein incorporated into the virion core

Next, we investigated the role of E8 during a viral infection. E8 was initially identified for its potential role in viral factory biogenesis based on the findings that the

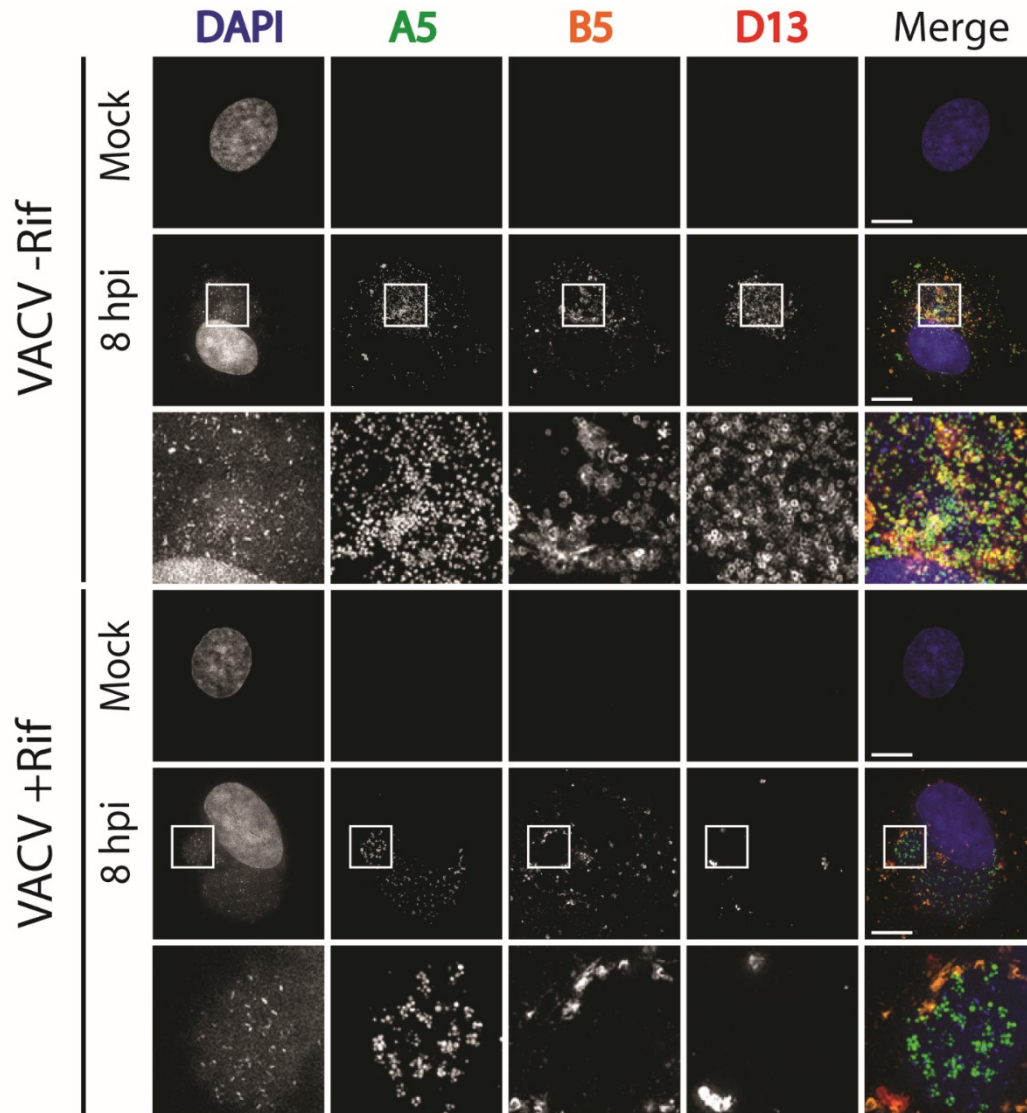


**Figure 3.6. Treatment with rifampicin inhibits morphogenesis.** BSC40 cells were infected with VACV-A5L-YFP at a MOI=5 in the presence (VACV+Rif) or absence (VACV-Rif) of rifampicin (200µg/ml) before fixing cells at 8hpi. D13 and B5 were labelled with antibodies while bulk DNA was labelled with DAPI. Viral proteins exhibit an altered localization in the presence of rifampicin. D13 no longer localizes to viral factories (-Rif) but now localizes in large inclusion bodies in the cytoplasm of the host cell. A5 exhibits an irregular shape when compared to non treated cells and B5 no longer localizes around viral cores at the periphery of the host cell. Bar=10µm.

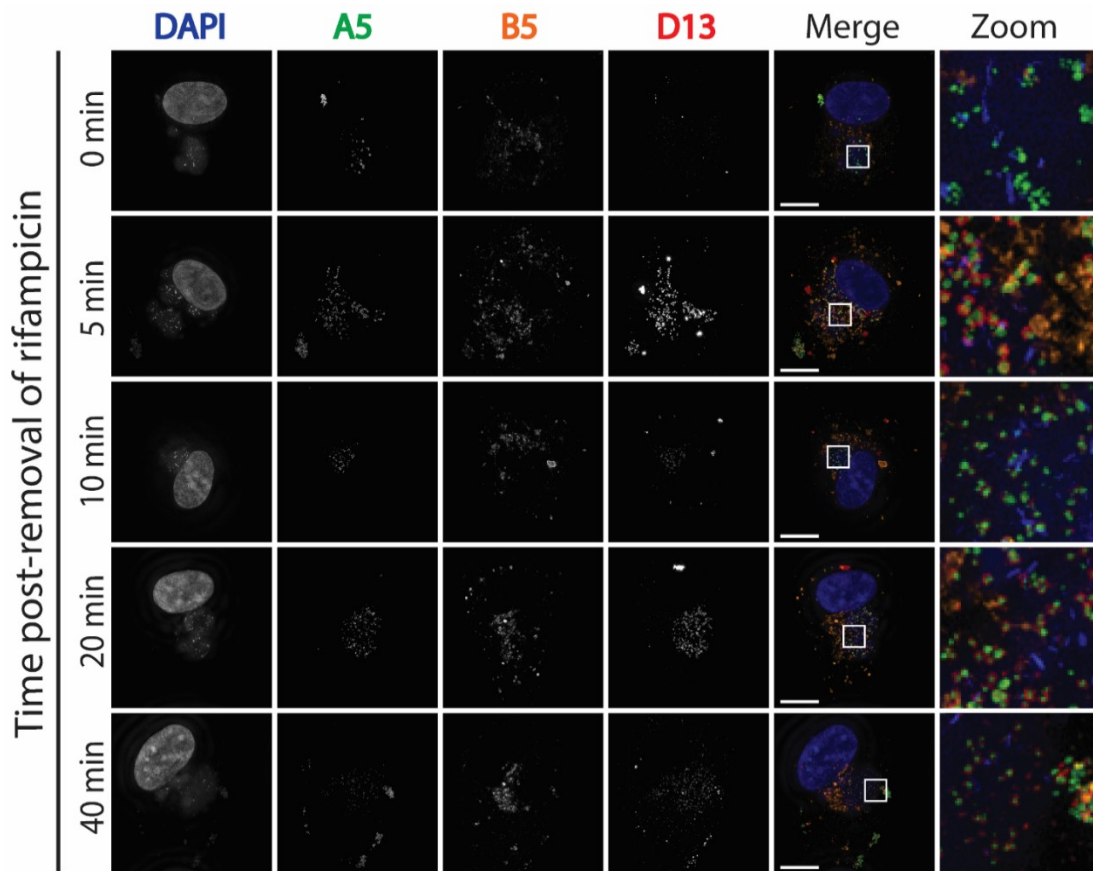


**Figure 3.7. Morphogenic forms can be visualized shortly after the removal of rifampicin.** Cells were infected with VACV-A5L-YFP in the presence of rifampicin (200 $\mu$ g/ml). At 6hpi, media was aspirated, and cells were washed once with PBS before adding back media. Cells were then fixed at the designated times after removing rifampicin and labelled with antibodies against D13 and B5. Within five minutes of removal, D13 relocalized to the viral factory and could be seen as a scaffold around virion cores. Both MV and WV could be visualized within the cytoplasm of the host cell within 40 minutes after removing rifampicin. Bar=10 $\mu$ m.

DNA sequence contained both putative transmembrane domains as well as a VACV early promoter and the protein localized to the periphery of the viral factory<sup>29</sup>. Prior to labelling, an antibody pre-adsorption protocol was used to combat high background staining of the E8 antibody. To investigate E8 localization and expression kinetics, cells were synchronously infected with VACV-A5R-YFP and fixed with either PFA or methanol at various time points before labelling with an antibody against E8. Under fixation with PFA, but not methanol, E8 localized to viral factories as early as 3hpi (Fig. 3.8A). Interestingly, E8 localized diffusely throughout the viral factory. This observation does not agree with previous work that showed E8 stained exclusively at the periphery of the viral factory. Additionally, E8 colocalized with virion core structures late during infection which supports the hypothesis that E8 is packaged into the viral core. However, even following an antibody pre-adsorption protocol, background fluorescence of the E8 antibody in mock-infected cells was exceptionally high and, in some instances, exceeded the intensity of E8 in virus-infected cells. Interestingly, when cells were fixed with methanol, rather than PFA, background staining was significantly reduced (Fig. 3.8B). Furthermore, no staining was visible in the viral factory early in infection (3hpi) and E8 staining of the viral core was much more apparent late in infection (8hpi).

### 3.3 Discussion

In VACV, intergenic recombination between two co-infecting particles is significantly delayed when compared to intragenic recombination<sup>122</sup>. This delay can be attributed to a physical barrier that limits mixing of the genetic content of two co-infecting particles. To develop a more complete understanding of the processes that

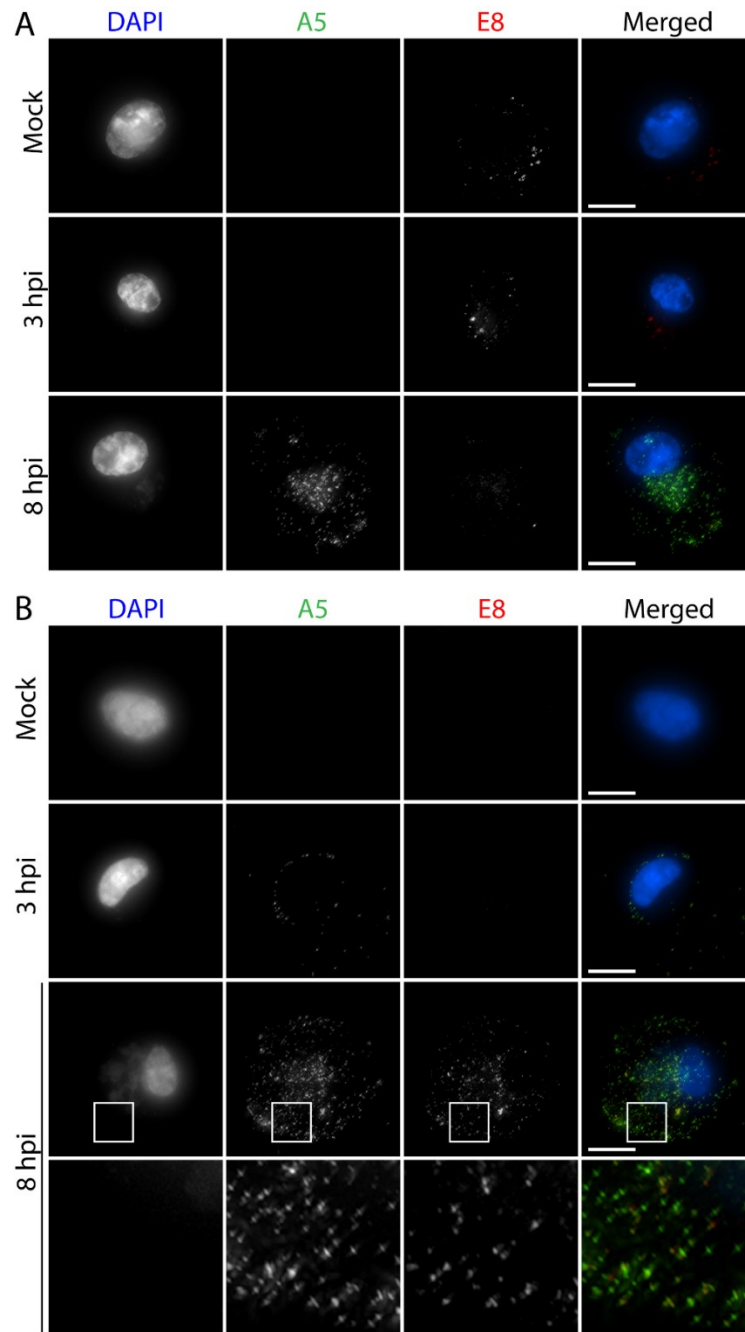


**Figure 3.8. Localization and expression patterns of the viral E8 protein.** BSC40 cells were infected with VACV-A5L-YFP at a MOI=5 and fixed with either 4% PFA (A) or 70% methanol (B) before staining with an antibody against E8. Under PFA fixation, E8 was observed at 3hpi and localized primarily in the viral factory. However, early observation of E8 was not visible at 3hpi following fixation with 70% methanol and localized along side the viral core throughout the cytoplasm of the host cell.

precede inter-genomic recombination, we investigated hallmarks of the VACV life cycle including viral early, intermediate, and late gene expression as well as viral morphogenesis using super-resolution microscopy. Super-resolution microscopy was chosen due to the improvements in resolution associated with the technique relative to traditional fluorescence microscopy. This increase in resolution allowed us to elucidate details of sub-viral structure, which was particularly important in characterizing the morphogenic forms of VACV.

First, viral early, intermediate and late gene expression was monitored using I3, I1 and A5/D13, respectively (Fig. 3.2-3.3). Under this system, early gene products were first detected at 3hpi and appeared concurrently with viral factories (Fig. 3.2). Intermediate gene expression was slightly delayed compared to early gene expression and was first detected at 4hpi (Fig. 3.3). Late gene products were first detected between 4-5hpi. While all samples were synchronously infected to limit variation in the induction of infection, it is possible that small variations exist that alter the kinetics of infection within a given sample. It is important to note that the expression pattern observed in this study (Fig. 3.2-3.3), as well as others<sup>122</sup>, precede the timing exhibited by an intergenic, but not intragenic, recombination event. Specifically, intergenic recombination events were detected at approximately 6h30min post-infection, around 1h30min after the appearance of late viral proteins. This is particularly confusing when one considers that replication, which is linked to recombination in VACV<sup>41,42</sup>, is reduced late during infection<sup>29</sup>. This may have important implications regarding the reduced frequency of hybrid viruses produced following a co-infection<sup>103,121</sup>. This line of questioning will be investigated in **Chapter 4**.

Afterwards, the kinetics of morphogenesis, which occurs following late gene expression, were characterized using a combination of three viral proteins: A5, B5 and D13. The ability of the three proteins to act as successful markers of morphogenesis was supported by the observation that treatment with rifampicin, which is known to interfere with progeny assembly, altered the phenotypes of all three marker proteins (Fig. 3.6) and removal of rifampicin quickly restored the associated phenotypes of each protein (Fig. 3.7). By using A5, B5 and D13 as markers, we were able to detect all intracellular morphogenic forms as early as 5hpi (Fig. 3.5). Interestingly, the onset of morphogenesis occurs just prior to the time when intergenic recombination was detected<sup>122</sup>. Given the similarities in timing, and the fact that the process of morphogenesis is actively occurring when recombinants are detected, it is possible that morphogenesis acts as one of the triggers that permits genetic mixing of two co-infecting particles. This is more enticing when one considers that the original membranes that bind viral factories<sup>29</sup> and the membranes involved in progeny assembly<sup>78</sup> are both derived from the ER. The potential roles of these membranes in limiting recombination and the possibility of morphogenesis acting as a trigger for inter-genomic recombination will be discussed further in **Chapter 5**.

Last, the role of E8 during a viral infection was investigated due to its potential role in factory biogenesis. E8 was supposedly expressed early during infection and incorporated into membranes derived from the ER that would eventually encompass viral factories<sup>29</sup>. This role was reflected by the fact that E8 stained at the periphery of early viral factories, presumably found in the membranes derived from the ER<sup>29</sup>. This peripheral staining pattern represented a wonderful opportunity to track the physical

barriers that were thought to limit genetic mixing and recombination<sup>122</sup>. In this regard, we attempted to track E8 staining throughout the duration of the infection to tease apart when this peripheral membrane structure, which presumably reflected the barrier to genetic mixing, collapsed. Under PFA fixation, we first observed E8 localized to viral factories at 3hpi (Fig. 3.8A). Our initial findings also suggested that E8 was expressed early during infection (compare I3 expression in Fig. 3.2 with E8 expression in 3.8A). However, unlike the previous study, which observed E8 staining exclusively at the periphery of the viral factory, we observed a diffuse E8 pattern throughout the entirety of the viral factory. This diffuse staining pattern countered the original hypothesis that E8 is embedded into the membrane surrounding a viral factory and plays a role in viral morphogenesis. Late during infection, E8 was observed to localize within viral cores as noted by colocalization between A5 and E8. This agreed with multiple previous works that showed that E8 is packaged within the virion core<sup>29,64,65</sup>. Unusual was the fact that, even after an antibody pre-adsorption protocol with acetone pelleted BSC40 cells, background staining of the E8 antibody remained high. In fact, E8 staining in mock-infected cells exceeded the staining intensity of cells infected with virus. This is particularly troubling in that legitimate signal cannot be differentiated from background fluorescence. However, the issue of exceptional background fluorescence was alleviated by fixing the samples with 70% methanol, rather than PFA (Fig. 3.8B). Under methanol fixation, E8 was no longer detected early in infection suggesting that E8 is expressed late, rather than early, during infection. Furthermore, E8 still localized to viral cores under the new fixation protocol which further reinforced the finding that E8 is incorporated into the virion core. These findings align with more

recent work on the E8 protein which showed that E8 was expressed late, rather than early, during infection<sup>65</sup>. The studies continued to show that viral factories and morphogenesis proceeded normally for E8 mutants at the non-permissive temperature. Collectively, these observations strongly opposed the original hypothesis that E8 is responsible for factory biogenesis. Further exploration showed that E8 was responsible for transcription of early viral mRNAs.

## Chapter 4 – Tracking viral DNA replication using EdU

### 4.1 Introduction

Recombination has long been known to be an important mediator of DNA damage repair, particularly in the context of double stranded DNA breaks that occur during replication<sup>108</sup>. The fitness of an organism is stabilized by limiting the introduction of mutations into a genome. Furthermore, recombination provides the genetic variability that gives rise to evolution. For VACV, recombination is catalyzed by the E9 DNA polymerase in conjunction with I3, the primary replicative SSB<sup>43</sup>. As such, DNA replication and recombination are intimately linked. It is unsurprising that recombination is detected at such a high frequency during VACV infection<sup>104</sup>. It is surprising that the recombination frequency among co-infecting virions is significantly reduced. Even more strange is that recombination between two viruses occurs after the expression of late viral proteins, a time marked by reduced replication<sup>122</sup>. Given that replication is linked to recombination, the low frequency of hybrid virus production probably reflects a balancing act between DNA replication and progeny virus production. Throughout this chapter, I will describe the use of multiple imaging techniques to investigate DNA replication both throughout the VACV life cycle as well as at sites of inter-genomic recombination.

### 4.2 Results

#### 4.2.1 EdU labelling is diminished following inhibition of DNA replication

First, I investigated whether I could label newly replicated viral DNA using EdU. EdU is a thymidine analog that is incorporated into actively replicating DNA. After

incorporation, a copper-catalyzed click-chemistry reaction could be performed to attach a fluorescent probe to the EdU molecule. To test EdU labelling of viral factories, cells were plated in the presence or absence of AraC, a DNA replication inhibitor, to determine if inhibiting DNA replication would prevent EdU incorporation. Cells were pulsed with EdU 2h prior to fixation. After fixation, the EdU molecules were conjugated to a fluorophore using a click-chemistry reaction. Afterwards, viral I3 was labelled with an antibody to identify viral factories. Under these conditions, EdU labelled both cellular and viral DNA (Fig. 4.1A). The incorporation of EdU into the host nuclei was surprising given that host DNA replication is thought to be inhibited during VACV infection<sup>132,133</sup>. Both the EdU and I3 signal localized to the same areas within the cell and shows that EdU can be used to label newly replicated viral DNA. Treatment with AraC diminished the nuclear signal of EdU (Fig. 4.1B). Furthermore, both cytoplasmic I3 and EdU signals were not present following treatment with AraC. Altogether, these observations show that EdU only labels actively replicating DNA.

#### 4.2.2 Optimizing EdU labelling

After determining that EdU could be used to effectively label actively replicating viral DNA, it was pertinent to develop an optimized procedure for EdU labelling. To do this, cells were infected with VACV and pulsed with EdU either 10, 15 or 20 minutes prior to fixation. Under this labelling schematic, EdU signal could only be detected if EdU was pulsed on cells for at least 15 minutes prior to fixation (Fig. 4.2). Given that a shorter pulse reflects more accurate results, EdU was pulsed for 15 minutes, unless stated otherwise, prior to fixation in each subsequent experiment.

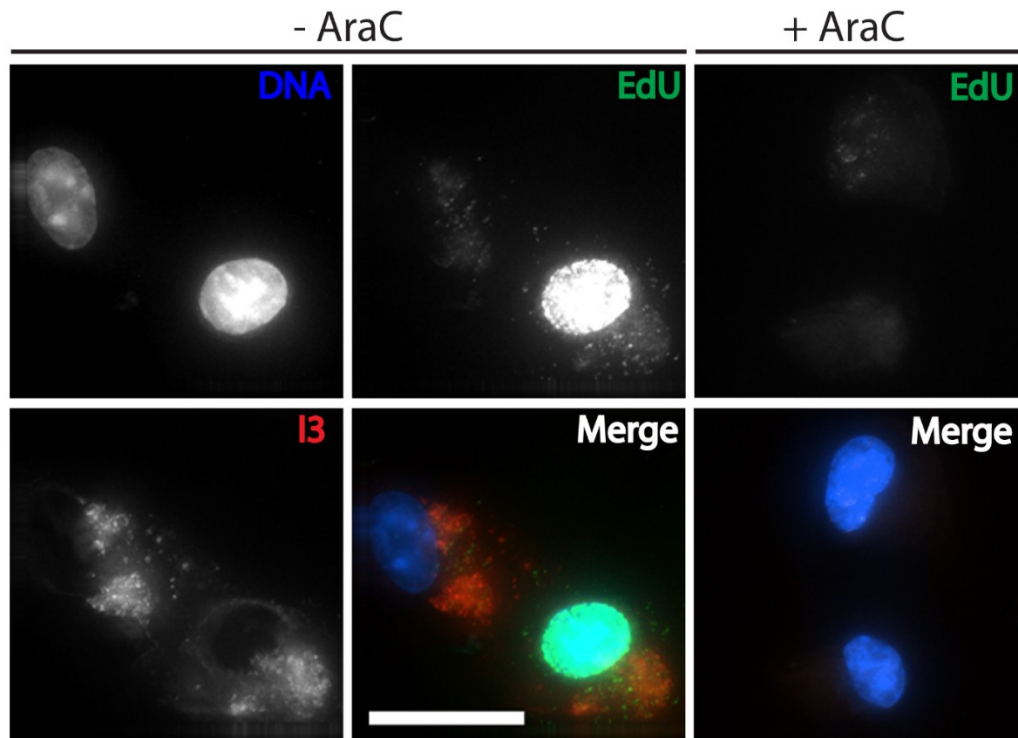


**Figure 4.1. EdU labels actively replicating DNA.** BSC40 cells were infected with VACV-WR at a MOI=5 in the presence or absence of cytosine arabinoside (AraC). Cells were pulsed with EdU beginning at 4hpi and subsequently fixed at 6hpi. DNA was labelled with DAPI, I3 was labelled with antibodies and a mCh fluorophore was conjugated to EdU using a click-chemistry reaction. In the absence of AraC, EdU can be observed within viral factories (colocalization with I3) as well as the nucleus. However, EdU staining is significantly reduced when media is supplemented with AraC.

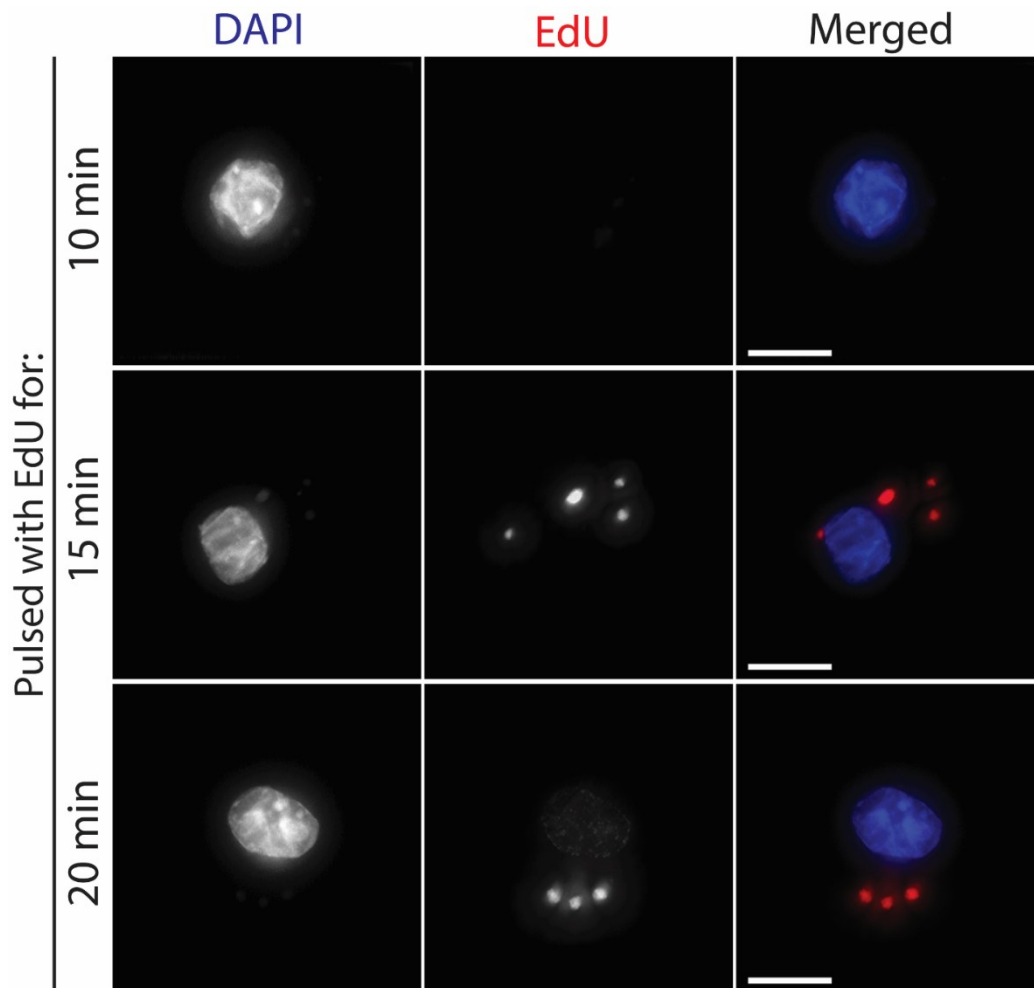


**Figure 4.2. Optimizing the EdU labelling protocol.** BSC40 cells were infected with VACV-WR and pulsed with EdU for the indicated times prior to fixation. Afterwards, a mCh fluorophore was conjugated to EdU using a copper-catalyzed click-chemistry reaction.

#### 4.2.3 DNA replication is reduced late in infection

Recombination in VACV is mediated by the viral DNA polymerase. However, recombination between two co-infecting particles occurs late in infection following the expression of post-replicative genes. Therefore, it is critical to determine if active DNA replication is reduced late during infection in a way that could limit the frequency of recombination of two co-infecting viruses. To investigate DNA replication throughout VACV, infected cells were pulsed with EdU 15 minutes prior to fixation at various time points. Using this approach, we were able to visualize DNA replication at various time points throughout the VACV replication cycle (Fig. 4.3). EdU stained most significantly at earlier time points and localized within the viral factories or host cell nucleus. Specifically, EdU staining appeared most prominently at 3-5hpi and reflects results obtained from another group<sup>29</sup>. EdU staining began to dim late during infection at 6hpi and was barely visible at both 7 and 8hpi likely due to a reduction in DNA replication.

The ratio of EdU and DAPI signal intensities was measured in an effort to quantify EdU incorporation (Fig 4.4). In agreement with the micrographs, DNA was replicated more profusely earlier in infection, peaking at 4hpi. However, the two time points that experienced the highest levels of EdU incorporation, 3 and 4hpi, also exhibited large margins of error. This is likely due to increased levels of replication resulting in a greater variance of EdU incorporation. EdU incorporation begins to drop at 5hpi and equivalent levels of EdU incorporation were observed at 6hpi. EdU incorporation is minimal at both 7 and 8hpi, reflecting reduced replication at late stages of infection.

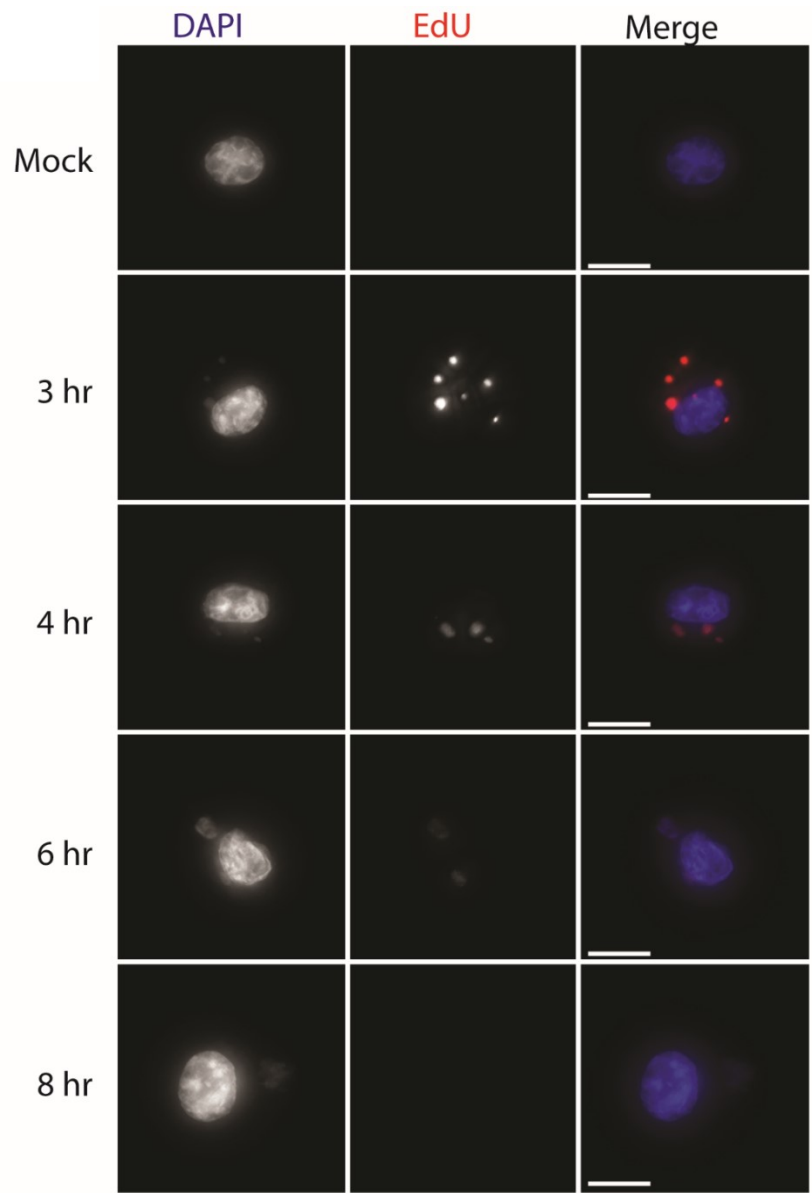


**Figure 4.3. Visualizing EdU incorporation throughout infection.** BSC40 cells were infected with VACV-WR at a MOI=5 and pulsed with EdU for 15min prior to fixation at the designated times. Bulk DNA was labelled with DAPI and EdU was labelled with a Cy5 fluorophore via a click-chemistry reaction. EdU incorporation was most noticeable early during infection and gradually decreased throughout the duration of the infection. Bar=10 $\mu$ m.

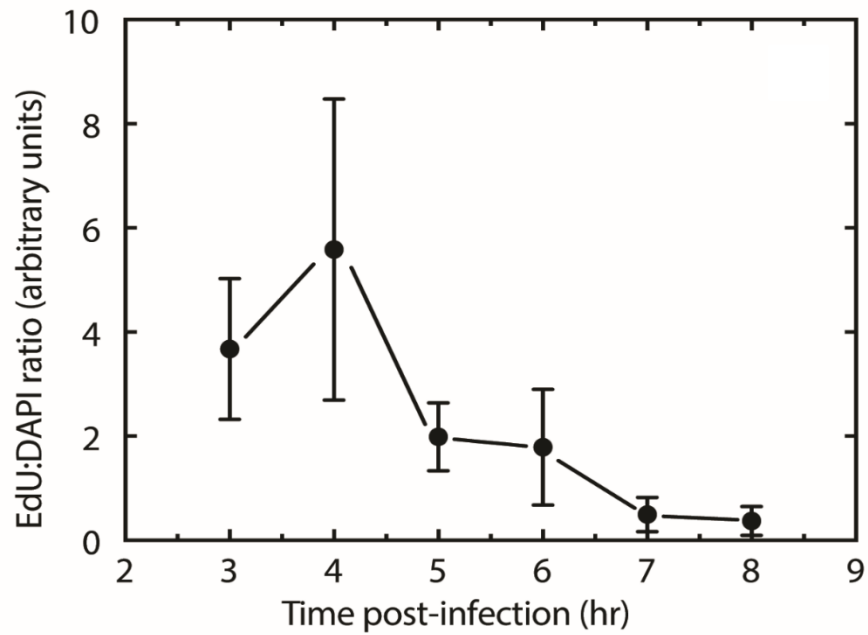


**Figure 4.4. DNA replication is most robust early during infection.** EdU intensity was normalized to DAPI fluorescence. Data were collected over a course of three separate experiments with a minimum of 13 cells per time point. Error bars represent standard deviations.

#### 4.2.4 Active DNA replication occurs at sites of inter-genomic recombination

I investigated whether active DNA replication occurred at sites of inter-genomic recombination given that recombination and replication are intrinsically linked<sup>41</sup>. To do this, I made use of a cell line and two recombinant viruses previously produced by our lab. The cell line, BSC40-eGFP-cro, stably expresses the eGFP fluorophore conjugated to the DNA-binding domain of the lambda phage cro protein. This fluorophore binds to DNA and results in a fluorescent DNA signal. Following infection with VACV, the fluorophore migrates to the viral factory where it exclusively labels viral DNA. As such, this cell line allows one to track viral DNA using live-cell microscopy. The two recombinant viruses contain overlapping but incomplete fragments of the cro DNA binding domain conjugated to a mCh fluorophore (Depicted in Fig. 1.4). Only following recombination between the two viruses is a fluorescent signal produced. The appearance of mCh fluorescence signals intergenic recombination between the two recombinant viruses. To investigate DNA replication at sites of recombination, BSC-40-eGFP-cro cells were plated on gridded dishes, to aid in relocation later, and co-infected with both recombinant viruses at a combined MOI of 5. After infection, cells were monitored using live-cell microscopy. At 6hpi, EdU was added to the cells and monitored until a mCh signal was produced. The cells were then fixed and processed for fixed-cell imaging by performing a click-chemistry reaction to attach a fluorescent probe to incorporated EdU molecules and labelling both viral and cellular DNA with DAPI (Fig. 4.5). Recombination between the two co-infecting particles was first observed at 5h20min post-infection as noted by the appearance of the mCh

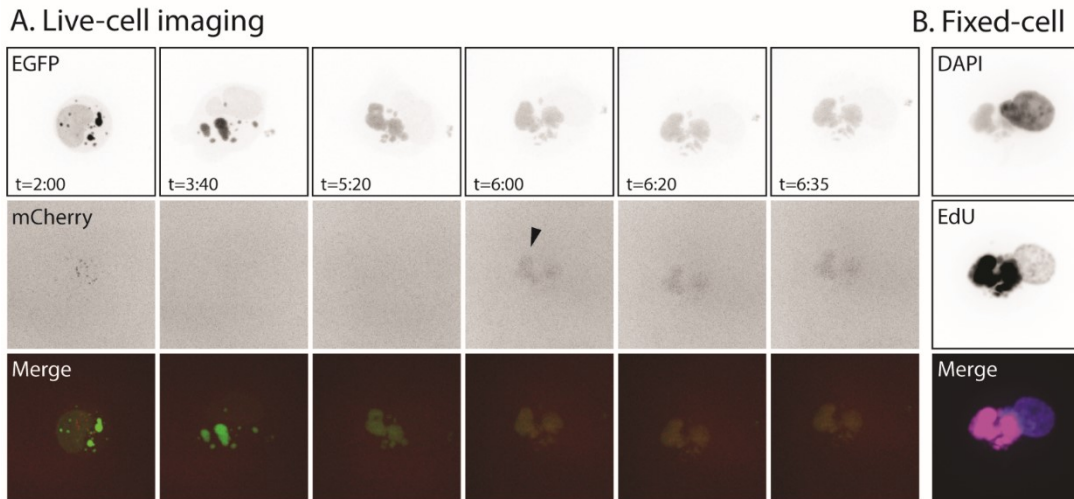


**Figure 4.5. DNA replication occurs at sites of inter-genomic recombination.** BSC40-eGFP-cro cells were infected with VACV-pE/L-mCherry(t) and VACV-pmCherry-cro at a MOI of 2.5 each for a total combined MOI of 5. Cells were pulsed with EdU at 6hpi and fixed after observing a factory collision event. Incorporated EdU molecules were stained with a click chemistry reaction and DNA stained with DAPI. (A) Time stills from the live-cell portion of the experiment. Recombination (as noted by appearance of mCherry) was first observed at 5h20min post-infection. Fluorescence associated with the recombination event was initially weak and mCh could be visualized much easier late during infection (arrow). (B) The same cell followed during the live-cell portion was reimaged after processing for fixed cell microscopy. EdU could be detected in the viral factory that initially exhibited mCh fluorescence.

fluorophore (Fig 4.5A). Therefore, cells were pulsed with mCh forty minutes after the first appearance of the recombination signal. Regardless, the viral factory stained positive for both mCherry and EdU (Fig. 4.5B). Since the sample was pulsed with EdU after the appearance of the mCh recombination signal, the positive EdU signal suggests that, despite occurring late during infection, active DNA replication occurs at sites of inter-genomic recombination.

### 4.3 Discussion

VACV recombination and replication are intrinsically linked<sup>43</sup>. Therefore, it is surprising that recombination between co-infecting viruses occurs late during infection after the bulk of DNA replication has ceased in favour of progeny morphogenesis<sup>122</sup>. The reduced replication observed late in infection may provide basis for the seemingly paradoxical observation that very few hybrid viruses are produced despite the seemingly high frequency of recombination<sup>104</sup>. We made use of multiple imaging techniques and resources in an effort to understand DNA replication during poxvirus infection and the implications it has on recombination frequency among co-infecting viruses.

First, EdU incorporation was explored as a potential technique that could be used to label actively replicating viral DNA. EdU was selected as a means to fluorescently label replicating DNA due to a few distinct advantages. First, the alkyne group present on the EdU molecule to which the fluorescent probe is attached is rare in natural biology and results in limited background fluorescence as a result. Second, the fluorescent probe is attached by a simple click-chemistry reaction rather than harsh

denaturation of DNA. However, the click-chemistry reaction may quench fluorescence, therefore, care should be taken into consideration upon experimental design. To determine if EdU could label replicating viral DNA, cells were infected with VACV-WR and pulsed with EdU for 2h prior to fixation to ensure EdU incorporation. Cells were also treated with AraC to ensure that actively replicating DNA, rather than all DNA, was exclusively labelled. Both cellular and viral DNA was labelled using this approach (Fig. 4.1). The labelling of host DNA was surprising since VACV infection has been theorized to inhibit host cell replication<sup>132,133</sup>. In this regard, DNA replication was reduced in host cells 1hpi relative to control cells. Since viral replication has not yet begun by 1hpi, it is believed that early viral factors inhibit host DNA synthesis. Given that an EdU signal was present within the host nucleus, these data agree with the finding that host replication is reduced, but not completely inhibited, following VACV infection. In the context of viral factories, the EdU label localized alongside I3 within the host cytoplasm. Viral I3 concentrates within the cytoplasmic viral factories<sup>60,62,113</sup>. Therefore, it is likely that these cytoplasmic structures represent viral factories and that EdU is able to label viral DNA. Odd, however, is the fact that the DAPI signal (DNA) does not localize to these same cytoplasmic sites. Reduced DAPI intensity is likely reflective of fluorescence quenching associated with the click-chemistry reaction. Lastly, treatment with AraC resulted in a severe reduction of the EdU signal (Fig. 4.1 – AraC+). Since EdU is only incorporated into actively replicating DNA, a reduction in EdU intensity would be expected following treatment with a DNA replication inhibitor. Overall, this experiment shows that EdU acts as an effective mean to label actively replicating viral DNA.

Next, DNA replication was examined throughout VACV infection by pulsing with

EdU just prior to cell fixation at multiple time points (Fig. 4.3). To estimate DNA replication, the intensity of the EdU signal was compared to the DAPI signal. This was done to develop an understanding of EdU incorporation relative to the total viral DNA (Fig. 4.4). DNA replication was more robust early during infection, particularly at 3 and 4hpi. These observations align closely with observations by another group<sup>132</sup>. In this study, DNA replication was robust early during infection and increased DNA replication correlated positively with the extent to which viral factories are enclosed by ER membrane. A collapse of ER membrane structure later during infection corresponded with a reduction in DNA replication. Similarly, DNA replication began to decline late during infection, beginning at 5hpi (Fig. 4.4). Replication continued to decline throughout infection and was minimal at both 7 and 8hpi. Viruses produced by inter-genomic recombination appear late during infection, primarily being produced at approximately 5.5hpi<sup>122</sup>. At this time, DNA replication has already begun to decline. Since DNA replication and recombination are connected through the VACV DNA polymerase, a reduction in DNA replication may result in the reduced frequency of recombination observed between two co-infecting viruses<sup>104,122</sup>.

Last, we investigated DNA replication at sites of active inter-genomic recombination. To do this, cells were infected with recombinant viruses that produce mCh fluorescence following successful intra-genomic recombination and pulsed with EdU at 6hpi to investigate whether active DNA replication occurs at sites of inter-genomic recombination (Fig. 4.5). Using this approach, mCh fluorescence was observed at 5h20min post-infection but cells were monitored till 6h35min post-infection due to the weak signal produced by the mCh fluorophore (Fig. 4.5A). By correlating between

the two imaging modalities (compare Fig. 4.5A and 4.5B) an EdU signal, signifying active DNA replication, could be detected within the same factory that produced a mCh recombination signal. Given that DNA replication is still active between 5 to 6hpi (Fig. 4.4) it is unsurprising to observe active DNA replication within this single factory. Interestingly, the mCh recombination signal was detected 40 minutes prior to pulsing with the EdU label. This means that this specific factory was undergoing recombination before the EdU label was added to the sample. Therefore, this experiment shows that DNA replication occurs at sites of inter-genomic recombination and that DNA replication continues even during the recombination process itself. Furthermore, the mCh recombination signal was always observed alongside EdU incorporation but EdU signals could be detected independently of mCh fluorescence. Therefore, all sites that exhibited intergenic recombination also experienced active DNA replication. While inconclusive, this supports the findings that DNA replication and recombination are linked in VACV.

Overall, EdU proved to be a useful tool in investigating DNA replication throughout a viral infection. By using EdU, the extent of DNA replication could be examined at multiple time points during infection. Similar to previous findings, replication was more robust early during infection and began to decline later during infection. Despite this, active DNA replication could be detected at sites of inter-genomic recombination. Altogether, these findings reinforce the hypothesis that DNA replication and recombination are intrinsically linked during VACV infection.

## Chapter 5 – Investigating barriers to DNA mixing using correlative microscopy

### 5.1 Introduction

An interesting hallmark of VACV infection is that each infecting particle gives rise to its own viral factory<sup>26,123</sup>. As infection progresses, individual factories appear to coalesce into a large aggregate of factories that is amorphous in shape. Interestingly, even after apparent fusion of viral factories, the genetic content of a single factory remains distinct<sup>28</sup>. This is particularly confounding considering that the DNA from two co-infecting particles must first mix before inter-genomic recombination can occur. If the genetic content of two factories are constrained in some way, should we expect to see a delay in recombination between co-infecting viruses? This question was explored in earlier work from our lab<sup>122</sup>. This study showed that even though the enzymatic activity required for recombination is active early in infection, inter-genomic recombination between two co-infecting viruses is significantly delayed relative to intra-genomic recombination within a single virus. The study posited that there is a physical barrier, rather than an enzymatic barrier given that recombination between viral and transfected plasmid DNA occurred earlier in infection, preventing efficient mixing of genomic DNA and subsequently delaying recombination between two co-infecting particles.

Membranes derived from the ER are the most likely candidate for the barrier that limits genetic exchange among adjacent factories. During development, factories are surrounded by membranes derived from the ER<sup>29</sup>. Wrapping is most complete early

in infection and could restrict movement of genetic material among viral factories. However, surrounding membranes begin to disassemble starting around 4hpi. This results in a scenario where DNA could mix efficiently late in infection and recombination between two co-infecting particles could occur. While these membranes have been observed early<sup>29</sup> and late<sup>122</sup> during infection, the fate of these membranes and the potential role they play in restricting genomic mixing has never been directly followed. In this chapter, I will describe the use of multiple imaging modalities, including fluorescence and electron microscopy and combinations thereof, to investigate ER membranes during VACV infection.

## 5.2 Results

### 5.2.1 ER membranes are present within and around viral factories

Given that ER membranes surround viral factories early during infection, I thought it appropriate to reinvestigate the presence of ER during later stages of infection. To do this, I infected BSC-40 cells with VACV-WR and stained for both calreticulin (CRT), a marker of the ER, as well as cellular and viral DNA after fixing the cells at 6 hpi (Fig. 5.1). While largely void from areas containing viral DNA, CRT was observed both within and surrounding viral factories. Internal membrane structure may reflect the apparent fusion of smaller factories into larger aggregates given that cells were infected at a high MOI (MOI=5) and fixed late during infection. If ER membranes persist even after the apparent fusion of viral factories, we would expect to see membrane structure within the viral factory. Even more interesting is the presence of CRT surrounding the periphery of the viral factories. These ER membranes appear to form partitions between adjacent factories. These ER boundaries were more

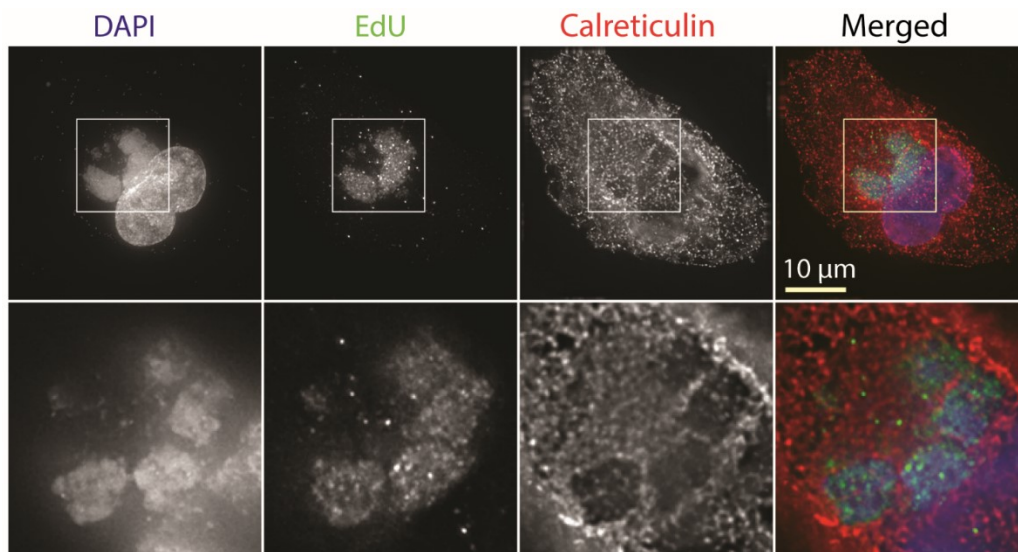


**Figure 5.1. ER structures are present within and around viral factories.** Cells were infected with VACV-WR and pulsed with EdU 15min prior to fixation at 6hpi. EdU was conjugated to a Cy5 fluorophore, DNA with DAPI and calreticulin with an antibody. The top row represents a projected image containing all z-stacks. The bottom row represents a projection of fewer z-stacks (7 x 125 $\mu$ m) to better represent the membrane structure separating the individual viral factories.

apparent when investigating a smaller z-stack of the sample and distinct ER barriers between nearby viral factories were observed (Fig 5.1 – Second Row). While inconclusive in the exact role ER membranes have during infection, these data suggest that ER is in fact present at the periphery of the viral factory and has the potential to restrain genetic mixing of adjacent factories.

### 5.2.2 ER membranes partition genetic content of viral factories

The previous experiment showed that ER membranes are present between adjacent factories. However, these experiments provide no information on the ultrastructure of the ER membranes and, thus, cannot definitively show that ER acts as a barrier between adjacent factories. As such, it is critical to investigate the ultrastructure of the viral factories. To do this, BSC-40 cells were infected with VACV-WR and processed for electron microscopy (Fig. 5.2). Cells were fixed at 3.5 and 4 hpi, respectively, because previous research indicates that factories were maximally wrapped with ER membranes at these time points<sup>29</sup>. The EM micrographs show clear membrane structure at the periphery of viral factories (Fig 5.2A). Membrane structures do not appear to surround the entirety of the viral factory. This likely reflects the observation that factories never experience complete enclosure even at times when factories experience most complete wrapping<sup>29</sup>. However, it is worth noting that membranes appear to separate the contents of adjacent factories (Fig 5.2B). In this image, ER membrane structures are quite visible at the periphery of viral factories and appear capable of forming adequate partitions among factories. Given the close proximity of the factories, it is tempting to say that these membranes persist following a factory collision event. Altogether, these results reinforce the earlier hypothesis that

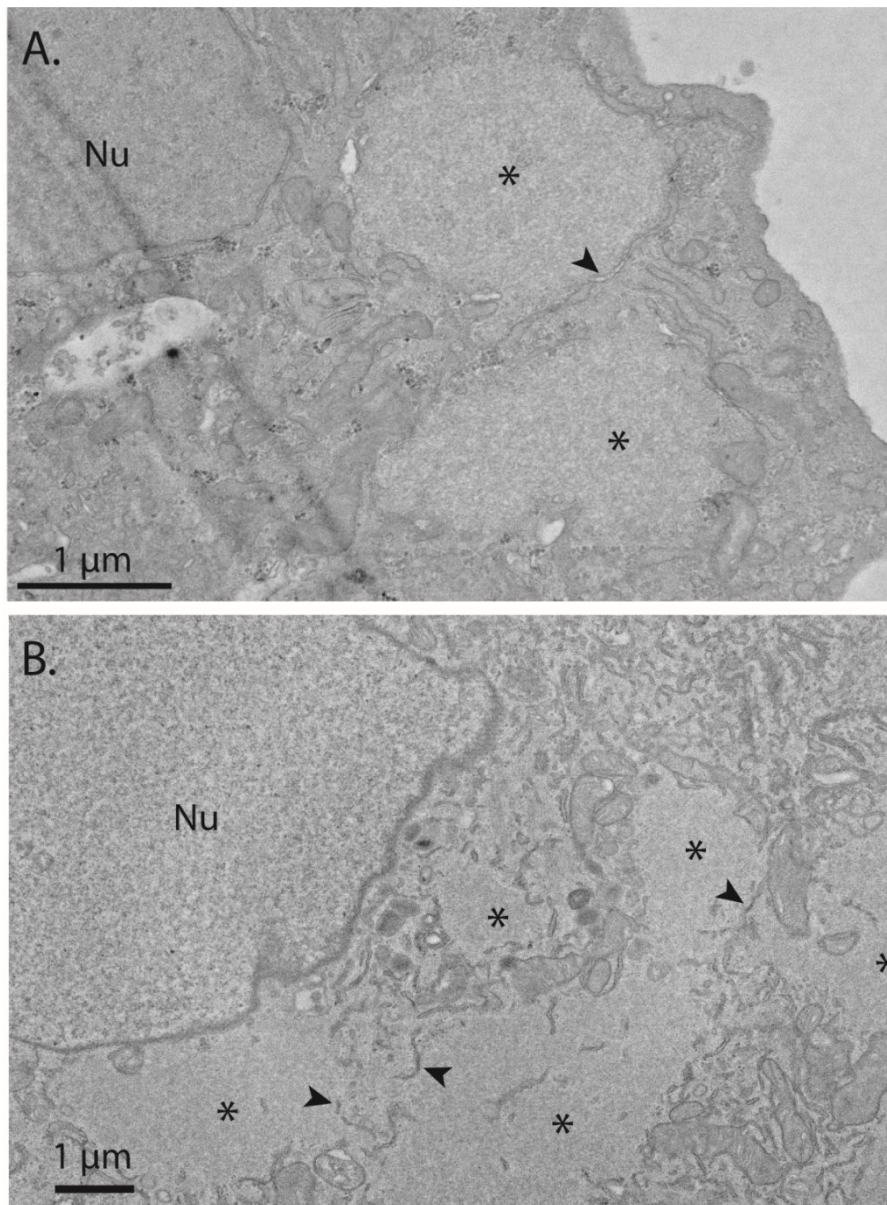


**Figure 5.2 ER membranes are present at the periphery of viral factories.** BSC40 cells were infected with VACV-WR at a MOI of 5 and fixed at 3.5 (A) or 4 (B) hpi and processed for TEM. (A) Double membrane structures, likely ER membranes, are present at the periphery of the upper viral factory. This membrane structure appears to form a barrier between the two factories. (B) Several factories have coalesced in the perinuclear region. Membrane structures are present at the periphery and within the viral factory.

suggest that each viral factory is wrapped by membranes from the ER and provides evidence that these membranes may persist following collision of adjacent factories.

### 5.2.3 Cellular structures persist following factory collision events

ER structures would need to persist following collision of two distinct viral factories to act as barriers to genetic mixing. While the previous experiment provided evidence for membrane barriers surrounding two viral factories it provided no definitive evidence that these membrane barriers remain following a collision event. To investigate this phenomenon an understanding of the kinetics of the infection would be required. However, traditional EM processing provides little information on the kinetics of the experiment. To circumvent this limitation, I used a technique known as CLEM, which uses a combination of both FM and EM to investigate the kinetics and ultrastructure of a region of interest within a single cell. This technique is invaluable in the fact that FM provides an unprecedented understanding of the kinetics of infection, in this case factory collision, and EM permits investigation of the ultrastructure of these rare events. In this experiment, BSC-40-eGFP-cro cells were infected with VACV-WR and observed with live-cell microscopy until a factory collision event occurred at 4h35min post-infection (Fig. 5.3A). After observing collision, cells were fixed and processed for EM to investigate the membrane ultrastructure (Fig 5.3B). Interestingly, the peripheral membrane structure observed early during infection is largely absent from the viral factories (Compare figure 5.2A with 5.3B). Furthermore, the earliest products of morphogenesis, including both crescents and IV, were observed within the viral factory. Stills from the live cell portion of the experiment were overlaid onto the electron micrographs to confirm the identity of the factory collision events. By doing

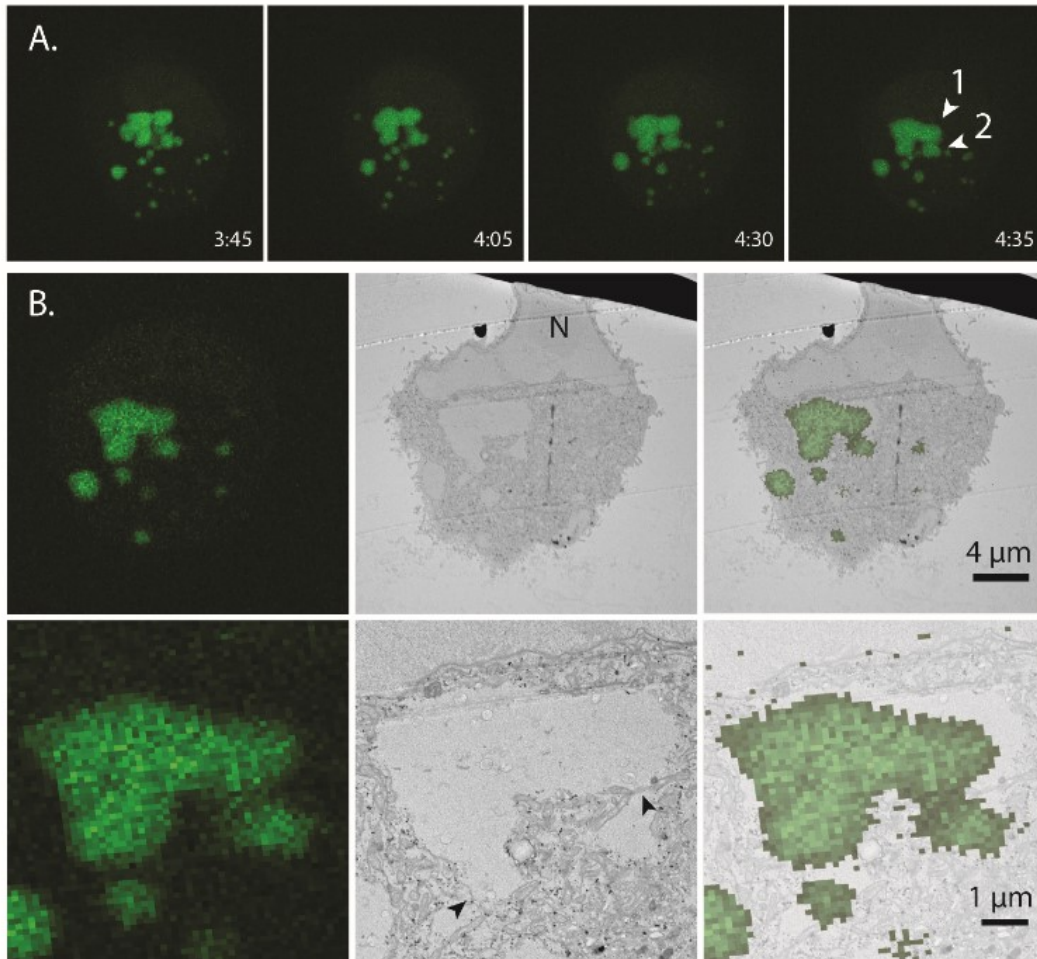


**Figure 5.3. Cellular structures can be observed at sites of factory collision.** BSC40-eGFP-cro cells were infected with VACV-WR at a MOI of 5. Infection was tracked using live-cell microscopy until collision was observed at which point cells were fixed and processed for TEM. (A) Images captured during the live-cell experiment. Cells were fixed and processed for TEM after observing the collision event at 4h35min post-infection. (B) TEM micrographs of the collision event. Cellular structures can be observed between the junction sites. One collision (upper right arrow) appears to have mitochondria separating the two factories while the lower collision event (lower left arrow) appears to have ER-like membrane structures between the two factories. Products of morphogenesis, including viral crescents and IV, can be visualized within the factories.

this, two potential collision events could be observed within this single cell. One of these potential collision events (Fig 5.3B – EM: lower left arrow) contains ER-like membrane structure between the two viral factories. Surprisingly, mitochondria appear at the junction site of the other factory collision event. Despite the differing origin, it is possible that either structure, mitochondria or ER-like membranes, could act as a barrier to genetic mixing given that they appear to partition the adjacent factories.

An additional experiment was performed using SEM, rather than TEM, for the correlative component. Similar to the first experiment, viral factory development was tracked using live-cell microscopy until collision was observed at 4h45min post-infection (Fig. 5.4A). Like the previous experiment, the membrane structure present at the periphery of the viral factories were absent (Fig.5.4B). Additionally, products of morphogenesis could be observed in the viral factory. Dissimilar to the previous experiment, however, is the lack of a clearly defined barrier between the two recently collided viral factories. It should be noted that, remnants of membrane structure are still present between the two factories. Given the fragmented appearance of the membrane structures, it is possible these membranes are actively undergoing the deconstruction process that occurs late during infection. This is more plausible when one considers that products of morphogenesis can be observed within the factory. Despite this, the genetic material of the two recently collided factories remain distinct even with the limited presence of potential barriers between the viral factories.

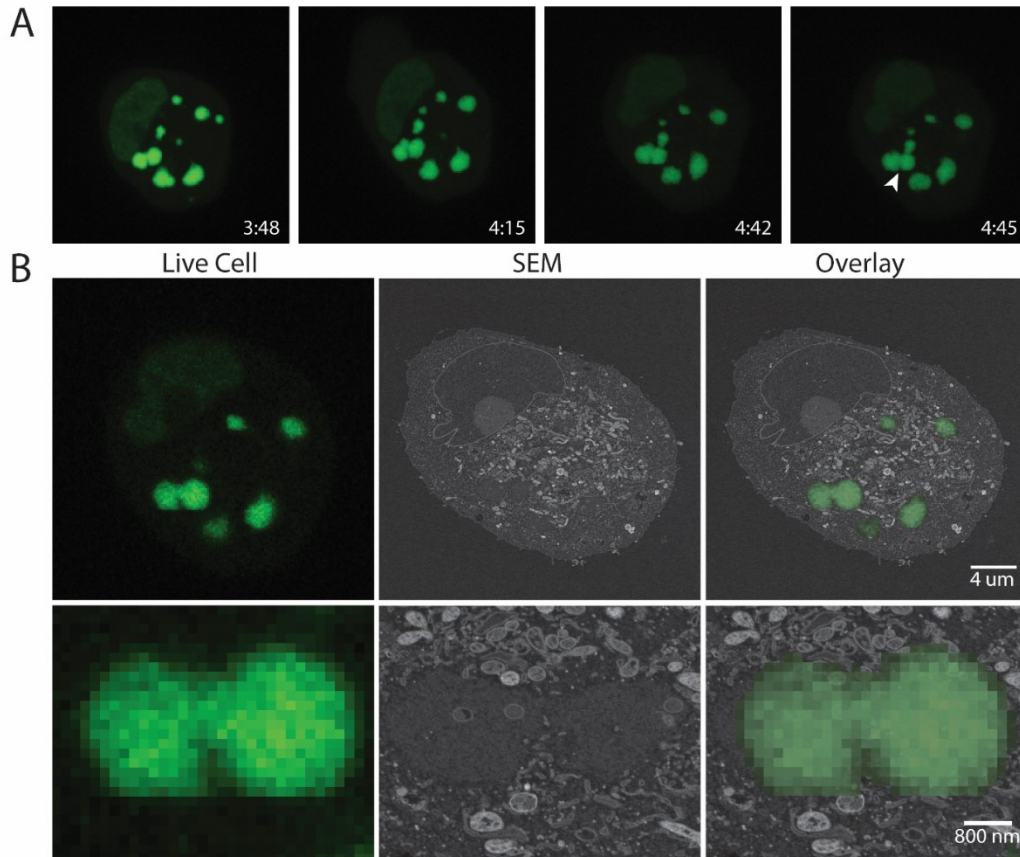


**Figure 5.4. Correlative light and scanning electron microscopy.** BSC40-eGFP-cro cells were infected with VACV-WR at a MOI of 5 and the infection was tracked using live-cell microscopy. The sample was fixed and processed for SEM after observing the factory collision event at 4h45min post-infection. (A) Images captured during the live-cell experiment. Cells were fixed and processed for SEM after observing the collision event at 4h45m post-infection. (B) SEM micrographs of the collision event. While no clear membrane structure exists at the periphery of the viral factories remnants of ER membrane are present between the two viral factories. Additionally, the genetic content of the two factories remain distinct. Furthermore, IVs are present within the viral factories signifying that viral morphogenesis has begun.

#### 5.2.4 Structures persist to an extent throughout the entirety of the viral factory

The ultrathin sections required for EM experiments translates to two-dimensional micrographs. However, an understanding of the 3D-ultrastructure would provide a more complete understanding of the role membranes and other structures play during the VACV life cycle. For this project, array tomography was used to develop an understanding of the three-dimensional ultrastructure of factory collision events. Array tomography hinges upon imaging serial sections to construct a model that displays the 3D-structure of the region of interest. By combining this technique with live-cell fluorescent microscopy, we were able to generate the 3D-ultrastructure of factory collision events. Like the previous experiments, viral factory development and collision events were observed using live-cell fluorescent microscopy (Fig. 5.5A). It should be noted that multiple collision events occurred during the experiment. Two particular collision events will be highlighted in this report. Both collision events occurred at 4h31m post-infection. Cells were processed for electron microscopy after observing the collision event at 5h43m post-infection and serial sections were imaged (Fig 5.5B). The EM micrograph highlighted in figure 5.5B represents a single micrograph from the serial sections and corresponds to the viral factories that underwent collision at 4h31min post-infection (Fig 5.5A - panel 3). Interestingly, ER-like membrane structures are visible within the interior of the viral factory but, like previous experiments, absent from the periphery of the factories. The reduced membrane structure at the periphery of the viral factory may be a remnant of the late fixation of the sample and the onset of viral morphogenesis. The identity of the individual collision

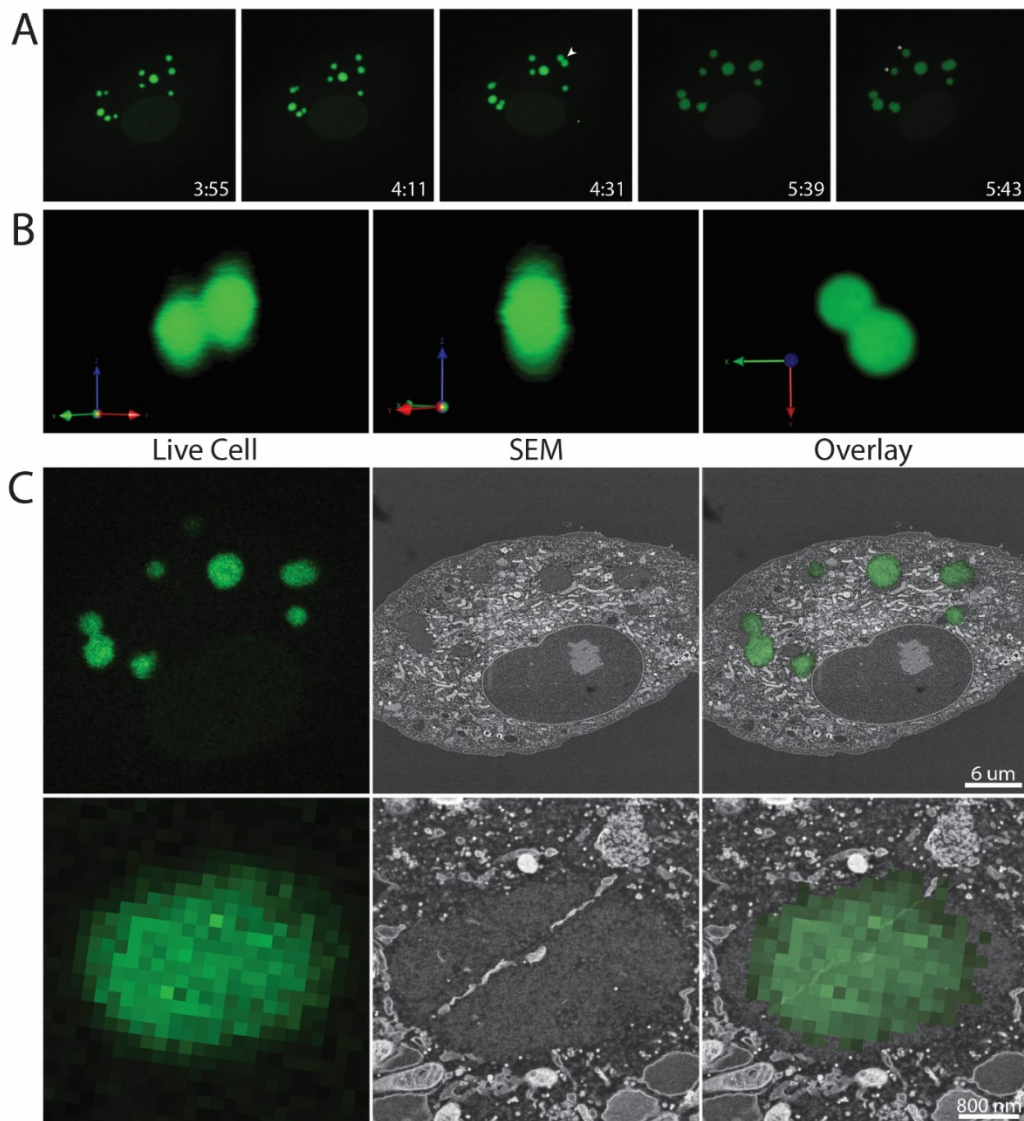


**Figure 5.5. ER-like membrane structures persist within the viral factory following collision.** BSC40-eGFP-cro cells were infected with VACV-WR at a MOI of 5 and factory kinetics were tracked using live-cell microscopy. Multiple collision events were observed. However, cells were ultimately fixed and processed for SEM after observing the collision at 5h43min post-infection. Serial sections were collected so that the entirety of the viral factory could be imaged. (A) Images from the live-cell portion of the experiment. The collision highlighted in this figure occurred at 4h31min post-infection. (B) 3D-volumes of the collision event at 4:31m post-infection in multiple orientations. (C) Electron micrographs of the factories that collided at 4h31m post-infection. ER-like membrane structures were observed to span the diameter of the viral factory. Additionally, viral crescents, the first observable product of morphogenesis, can be observed within the viral factory.

events could be determined by overlapping the fluorescent and EM images (Fig 5.5C). Images were captured from each individual section to collect serial images (Fig. 5.6A). Four serial images show that this membrane structure persists through multiple sections of the viral factory. Afterwards, a 3D model of the complete factory could be generated by aligning individual micrographs from the serial sections (Fig 5.6B). It becomes more apparent that the membrane structure within the interior of the viral factory observed in figure 5.5B were not present throughout the entirety of the viral factory. Rather, it appears as if there are multiple distinct membrane segments that run throughout the viral factory. These membrane segments may be indicative of a single large internal membrane structure undergoing deconstruction. Alternatively, the multiple membrane segments may represent multiple collision events that gave rise to the viral factory. Yet another possibility is that the internal membrane structures derive from cellular debris present in the cytoplasm of the host cell and these structures are captured during the factory collision event. This theory is particularly enticing due to the fact that peripheral membrane structure is absent late during infection.

A separate collision event from the same cell highlights a similar observation (Fig. 5.7). Like the previous experiment, serial sections were imaged to develop an understanding of the 3D-ultrastructure of the viral factory. Interestingly, consecutive sections show both ER-like membrane structure and mitochondria present within the viral factory (Fig. 5.7B). A 3D-model of the collision event shows that the internal structures only exist to a limited degree throughout the viroplasm (Fig. 5.7C). Unusually, the internal structure lies in the middle of the viral factory, away from the observed collision location (Fig. 5.7C – arrow). Therefore, it is possible that cellular

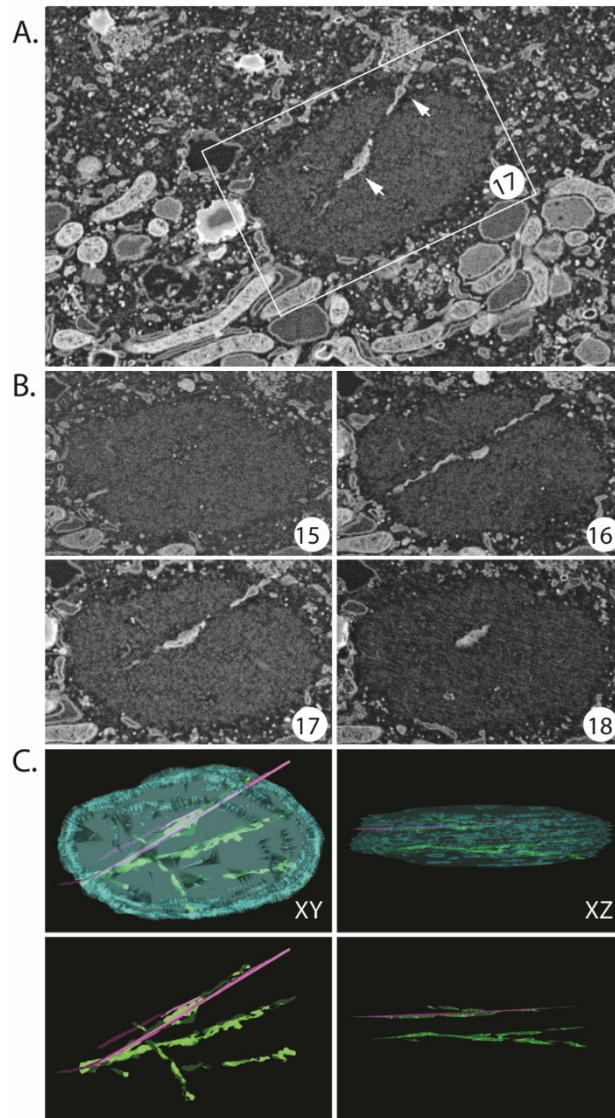


**Figure 5.6. 3D-ultrastructure of a factory collision event.** (A) A micrograph representing a single section of the 44 serial sections used to generate the 3D-model of the factory collision event. The factory collision event was observed at 4h31min post-infection, approximately 75min prior to fixation. (B) Four consecutive serial sections showing that the ER-like membranes present within the factory only exist to a limited degree in the z-dimension. Each section is 50nm thick and, thus, these four images represent 200nm of the original structure. (C) Serial sections were imaged and realigned to permit 3D-reconstruction of the viral factory. A total of 44 images were used in the reconstruction. The cyan structure represents the boundary of the viral factories and the green structure represents the ER-like membrane structures found inside the viral factories. The magenta structures represent the microtubule structures (~25nm) that can be seen in sections 15, 16 and 17. The models are shown in two separate orientations with and without the factory boundaries.

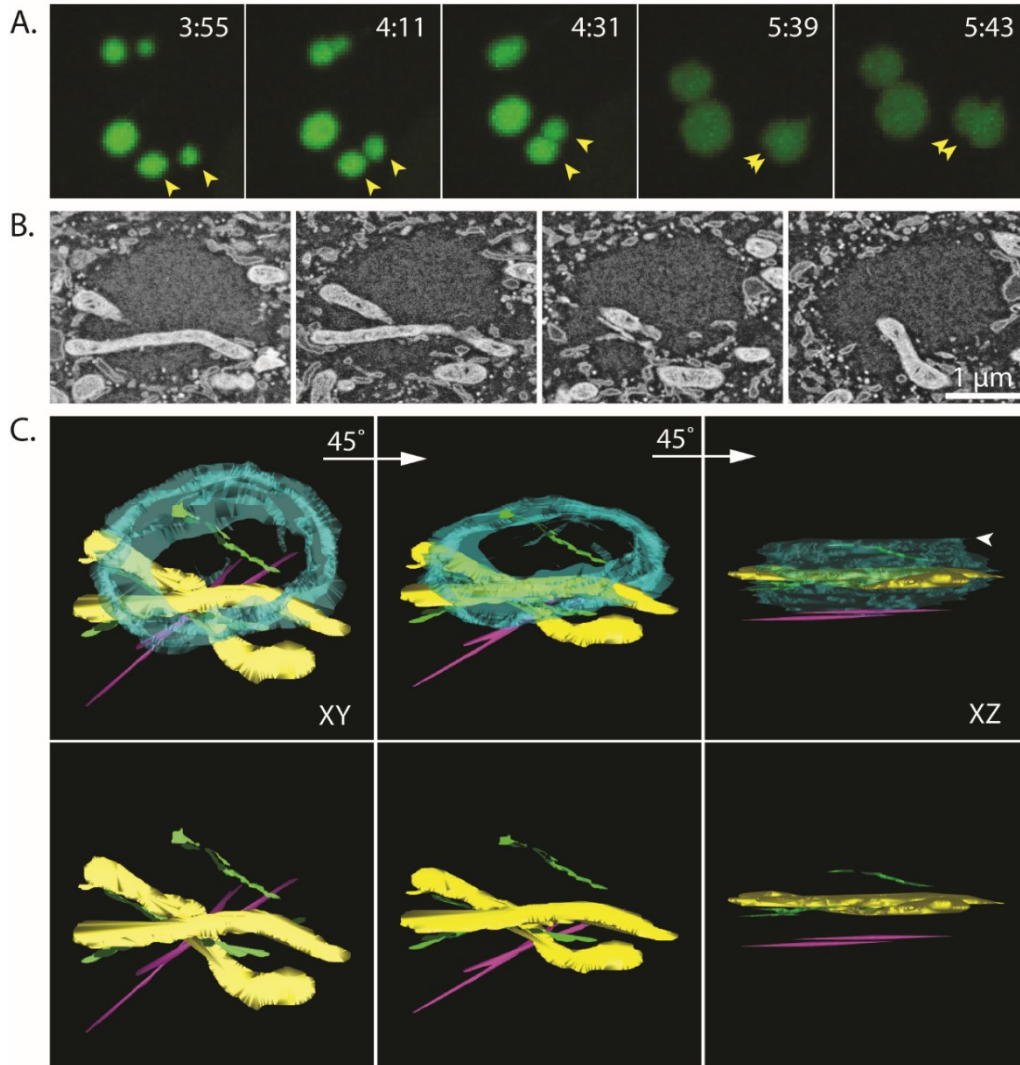


**Figure 5.7. Additional cellular structures can be observed within the viral factory.** (A) A magnified series showing a separate collision event from figure 5.5 that also occurred at 4h31min post-infection. (B) Four representative serial sections highlighting additional cellular structures, namely mitochondria, present in the viral factory. These sections show 4 of the 33 sections used to generate the model. (C) 3D-model of the collision event. Cyan represents the factory boundaries, green shows the ER-like membrane structures found within the factory, magenta highlights the microtubule structures observed in close proximity to the factory and yellow is mitochondria. The junction site between the two viral factories occurred at the top of the factory as shown in the top right image (white arrow). The model is shown from the top and front-facing orientations as well an orientation intermediate to the two.

constituents, including ER-like membranes and mitochondria, could be introduced into the factory independently of a collision event. Alternatively, a separate factory collision event could have occurred prior to the onset of live-cell imaging.

Lastly, serial images were obtained from a cell that had not undergone an apparent collision event (Fig. 5.8). It is possible that a collision event occurred before cells were monitored via live-cell imaging. However, the relatively small size of the factory suggests that no prior collision event has occurred. Unlike previous experiments, this particular factory exhibited no internal structures within the viral factory. Given that this viral factory also does not exhibit peripheral membrane structure, it seems more plausible that internal structures derive from cellular constituents and debris captured during the collision event rather than being permanent structures associated with factories.

### 5.3 Discussion

During poxvirus infection, recombination between two co-infecting particles is significantly delayed relative to recombination within a single virus. This phenomenon may arise due to two characteristics of the poxvirus life cycle: each infecting virion gives rise to its own factory<sup>26</sup> and viral factories are surrounded by ER membranes early in development<sup>29</sup>. If these peripheral membranes that bind viral factories persist late into infection, they may limit DNA mixing among factories and, in turn, delay recombination. A combination of microscopic techniques were used to investigate viral factory membrane ultrastructure during VACV infection.

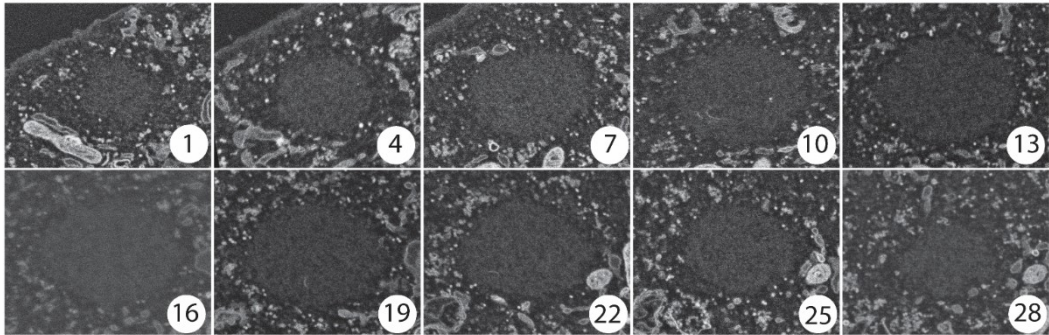


**Figure 5.8. No internal structures are observed in a factory that has not undergone an observable collision event.** Serial sections collected from one of the two factories that have not undergone an observable collision event from figure 5.5 (top panel – rightmost image, lower left asterisk). Every third section of the 30 sections that correspond to this single factory are shown.

First, fluorescence microscopy was used to investigate ER structure by staining CRT (Fig. 5.1). Cells were fixed and imaged at 6hpi, a time when DNA replication has largely ceased in favour of progeny assembly. Despite being fixed later in infection, membrane structure was clearly visible both within and around viral factories. Particularly interesting is that membrane structures appear to stain heavily at the junctions between adjacent factories. Both the strong staining at the periphery of the viral factories and the late fixation of the cell give credence to the hypothesis that membrane structures persist late in infection that may limit genetic mixing of viral factories. These observations translated well to traditional TEM micrographs (Fig 5.2). While stained earlier, TEM images showed ER structure at the periphery of two viral factories (Fig. 5.2A) and these membrane structures seemed to partition factories that have undergone a potential collision event (Fig. 5.2B). These micrographs agree with earlier observations of membrane structure that could potentially restrict recombination.

Next, two separate CLEM experiments were used to investigate membrane persistence following factory collision. Compared to the previous micrographs, both factories exhibited limited peripheral membrane structure (Fig. 5.3 and 5.4). Additionally, products of morphogenesis were observed in both factories imaged during the CLEM protocols. Given that a reduction in membrane wrapping occurs alongside the onset of morphogenesis<sup>29</sup>, it is possible that these factories have lost most, if not all, of the original binding membrane. Despite this, it is possible the limited ER-like structure observed between the junction site of two viral factories (Fig 5.3B – EM: lower left arrow) could represent residual binding membrane structure that

persisted following the collision event. Membrane structures observed between viral factories of a separate experiment could also represent the original membranes surrounding viral factories that have persisted following a collision event (Fig. 5.4B). The fragmented appearance of the membrane structure, as well as the appearance of products of morphogenesis, could reflect active deconstruction of the binding membrane structure that would in turn permit genetic mixing among viral factories. Alternatively, the structures present between adjacent factories may represent cellular debris or constituents that were trapped during the collision process. This hypothesis becomes more plausible when one considers that cellular structures besides ER membranes, namely mitochondria, are present at collision junctions and that membrane structure is largely absent from the periphery of viral factories (Fig. 5.3B – EM: upper arrow).

One final experiment used AT-CLEM to investigate the 3D-ultrastructure of the membranes following a factory collision event (Fig. 5.5). Cells were fixed late during infection at 5h43min post-infection after observing a collision event. However, multiple collision events were observed throughout the course of infection. The 2D- and 3D-ultrastructure of one of the earlier collision events (4h31min) was investigated to develop an understanding of membrane structure well after the observation of a collision event. ER-like membrane structures could be observed spanning the interior of the viral factory (Fig. 5.5B) in multiple segments (Fig.5.6B). Each individual segment spanned approximately 200nm in the z-direction but collectively the ER-like segments did not span the entirety of the viral factory. There are multiple possible origins of these internal membrane structures. First, it is possible that each membrane segment arrived

from a separate collision event. This is possible given that live-cell imaging began at 3h55m post-infection. As such, the fate of individual factories could not be tracked before this time. Alternatively, it is possible that the membrane segments once belonged to a larger membrane structure that spanned the entirety of the viral factory. Since products of morphogenesis are present, it is possible that this larger membrane structure has begun to deconstruct, and this dismantling of the membrane structure could explain the gaps between individual membrane segments. Of course, these two theories are not mutually exclusive, and the observed internal ER-like structure could arise from a combination of both. This is particularly enticing given that the membrane structures exhibit multiple orientations within the viral factory. Alternatively, internal structures could represent cellular debris present in the cytoplasm of the host cell that was captured during the collision event. This is possible when one considers that ER-like membrane structures can be observed in close proximity to viral factories. Additionally, a separate collision event from the same cell (Fig. 5.7) showed mitochondria, in addition to ER-like membranes, within the viral factory. Both mitochondria and ER-like membranes can be observed near viral factories. As such, it is possible that either of these cytoplasmic structures could be captured during the collision event. Odd, however, is the observation that ER-like membranes, but not mitochondria, were present at the observed junction between the two colliding factories (Fig. 5.7C – arrow). This is unusual since one would expect that debris captured during a collision event would appear at collision sites rather than within the viral factory. It is still possible that the mitochondria and ER-like structures situated within the center of the viral factory away from the collision sites could have arisen

from a separate collision event that occurred prior to the onset of live-cell imaging. Lastly, the serial sections of a viral factory that had undergone no apparent collision event were investigated (Fig. 5.8). This particular viral factory exhibited no internal structure. This would suggest that the internal structure observed in a factory does, in fact, result from a collision event. Since live-cell imaging began at 3h55m post-infection, it is possible that this individual viral factory had undergone collision before monitoring began. However, this possibility is less likely given the smaller size of the factory.

## Chapter 6 – Conclusions and Future Directions

### 6.1 Investigating hallmarks of the VACV life cycle

There are many mysteries that still surround the process of recombination in VACV. One such mystery details the discrepancies observed between recombination that occurs between two co-infecting particles and recombination that occurs within a single virus<sup>122</sup>. In this regard, intergenic recombination between two co-infecting particles is significantly delayed relative to intragenic recombination. Given that the enzymes that drive recombination are able to catalyze recombination events between viral and plasmid DNA early during infection, a process that is possible due to the fact that plasmid DNA is replicated within viral factories<sup>134</sup>, this delay has been attributed to a physical barrier that restricts the genetic content of two apposed viral factories from mixing<sup>122</sup>. It is hypothesized that this barrier is overcome late during infection and that deconstruction of this barrier allowed genetic mixing and, in turn, recombination, between two co-infecting viruses to occur. To develop a more complete understanding of the processes that result in the formation and subsequent destruction of this barrier, we tracked hallmarks of the VACV life cycle.

#### 6.1.1 Investigating the role of the viral E8 protein during infection

Early work on the viral E8 protein implicated a role for the protein in factory biogenesis by facilitating the interaction between viral DNA and the ER membranes that surround virosomes<sup>29</sup>. This conclusion came from the observation that E8 was supposedly expressed early in infection, contained a putative transmembrane domain and localized to the periphery of viral factories. If E8 does in fact play a role in factory

biogenesis by mediating the interaction between the ER and viral DNA, the integrity of the E8 signal around the viral factory may reflect the barrier that restricts recombination between two co-infecting viruses. As such, we investigated the localization of E8 throughout the duration of an infection (Fig. 3.8). Surprisingly, E8 did not stain at the periphery of the viral factory (Fig. 3.8A). Rather, E8 stained diffusely through the entirety of the viral factory. This observation is in stark contrast to the proposed role of E8 as an integral membrane protein that is incorporated into the membranes enclosing a viral factory<sup>29</sup>. Even more strange is the fact that only samples fixed with PFA stain positive for E8 at 3hpi. Samples fixed with 70% methanol exhibited an expression patterns that mirrored late viral protein kinetics and E8 localized primarily to virion cores rather than the viral factory (Fig. 3.8B). The differing observations between the two fixatives reflects the fact that epitopes can be altered by the fixatives themselves. For E8, PFA is likely the less efficacious fixative given that the background signal in mock-infected cells could exceed the staining intensity of virus-infected cells. Therefore, methanol fixation likely provides a more accurate representation of the true localization of the E8 protein. Given that under methanol fixation, E8 exhibited staining patterns that more closely resembled the proposed role of E8 as a late viral protein that plays a role in transcription rather than factory biogenesis<sup>65</sup>, we ceased exploration of E8 as a marker of the barrier to recombination.

#### 6.1.2 Intergenic recombination occurs following expression of late viral genes and occurs alongside viral morphogenesis

We made use of a combination of proteins (I3, I1, A5 and D13) to investigate viral early, intermediate and late gene expression (Fig. 3.2-3). Under this system, we

could observe early gene expression as early as 3hpi and early gene expression occurred simultaneously with the appearance of the cytoplasmic viral factories (Fig. 3.2). Intermediate and late gene expression were observed later during infection at 4 and 5hpi, respectively (Fig.3.2-3). While late gene expression could be observed earlier at 4hpi (Fig.3.3) a subsequent experiment that tracked morphogenesis using a combination of multiple late viral proteins (Fig. 3.4) showed that late proteins are primarily expressed at 5hpi and very rarely at 4hpi. Regardless of the discrepancy in timing, intergenic recombination is consistently observed after the expression of late viral proteins. Specifically, we observed recombination between two co-infecting viruses at 5h20m (Fig.4.5) as well as 6h30m post-infection just following expression of late viral proteins. Earlier work in our lab showed recombination between two different viruses occurring at approximately 5.5h post factory formation, which roughly corresponds to 6.5hpi<sup>122</sup>. Altogether, both experiments suggest that intergenic recombination occurs following the expression of late viral proteins. Since late viral proteins are responsible for progeny assembly, we tracked viral morphogenesis to further relate hallmarks of the viral life cycle to the timing of intergenic recombination.

To characterize viral morphogenesis, we tracked the expression and localization patterns of three late viral proteins: A5, B5 and D13. Using this approach, all three morphogenic forms were observed to appear at 5hpi (Fig. 3.5). As such, the onset of morphogenesis occurs just prior to the observation of intergenic recombination, which is observed to occur at 5h20m post-infection (Fig. 4.5) or even later in infection<sup>122</sup>. Therefore, it is enticing to suggest that morphogenesis promotes the conditions that permit recombination between two co-infecting virions. Odd,

however, is the observation that the transition into morphogenesis is accompanied by a reduction in DNA replication<sup>29</sup>. This becomes even more puzzling when one considers that the viral polymerase plays an important role in mediating recombination<sup>41</sup>. Why then, do we see recombination between two co-infecting particles occurring at a point in infection that we would otherwise expect a reduction in replication and, in extension, recombination?

## 6.2 DNA replication is reduced late during infection at the times we would expect to observe intergenomic recombination

To delve deeper into this apparent paradox, we made use of a molecule known as EdU. EdU is a thymidine analog that is incorporated into replicating DNA and, thus, can be used as a marker for DNA replication. First, we showed that EdU was capable of labelling viral factories by pulsing cells infected with VACV with EdU (Fig. 4.1). In this scenario, EdU labelling was significantly reduced following treatment with AraC, an inhibitor of DNA replication, suggesting that only actively replicating DNA is labelled. Collectively, this experiment showed that EdU acts as an effective marker of replicating viral DNA.

After determining the efficacy of EdU, infected cells were pulsed with EdU at multiple time points during infection in an effort to understand DNA replication throughout a viral life cycle (Fig. 4.3-4). DNA replication was most robust early during infection, peaking at 4hpi. However, replication was reduced beginning at 5hpi and continued to decline gradually throughout the course of infection until EdU incorporation was minimal at 7-8hpi. Inter-genomic recombination is typically detected

between 5.5-7hpi as shown by this study (Fig. 4.5) and others<sup>122</sup>, a time that is characterized by relatively low levels of DNA replication (Fig. 4.4). Since DNA replication and recombination are both catalyzed by the viral DNA polymerase<sup>41</sup>, we would expect to see active DNA replication at sites of recombination. A combination of live and fixed cell fluorescence microscopy was used to investigate whether active DNA replication that could drive recombination events was present at sites of intergenic recombination (Fig. 4.5). Under live-cell imaging, the production of recombinants, as marked by the appearance of mCh, were detected at 5h20m post-infection. Cells were subsequently incubated in the presence of EdU starting at 6hpi before fixation at 6h35m post-infection. After fixed-cell processing and correlation between the two imaging modalities, EdU staining could be detected at sites of intergenic recombination. Given that EdU was pulsed after the appearance of the mCh signal, this experiment suggests that DNA replication occurs at sites actively undergoing a recombination event. Interestingly, EdU labelling could be detected independently of a mCh recombination signal which shows that recombination between two co-infecting viruses does not necessarily occur even in the presence of active DNA replication. This could occur due to a variety of reasons. For example, the cell may have been infected by a single virus or the viral factories of the two genetically distinct viruses do not lie close enough in proximity to permit genetic exchange. Alternatively, viral factories may not have adequately overcome the barrier that restricts genetic exchange between two apposed factories. Conversely, a mCh recombination signal is never detected independently of positive EdU labelling. While inconclusive, this would suggest that DNA replication acts as a prerequisite for recombination and further reinforces the findings that reveal the

link between DNA replication and recombination. When taken together these experiments may provide an explanation for the low frequency of recombinants produced between two co-infecting viruses<sup>104</sup>. Given that recombination is mediated by the viral DNA polymerase, low levels of DNA replication should theoretically correspond to reduced levels of recombination. Inter-genomic recombination occurs at a time point that is characterized by low levels of DNA replication. As such, it is tempting to suggest that the low frequency of recombinants observed between co-infecting viruses at least partially results from a decreased capacity for viral replication late in the viral life cycle.

Even more interesting is the fact that inter-genomic recombination occurs concurrently with viral morphogenesis and is observed shortly after the appearance of the first products of morphogenesis. This raises an interesting question: does viral morphogenesis produce the conditions that allow genetic mixing and recombination between co-infecting particles? The potential answer to this question becomes more clear when one considers J. Locker's study of viral factory ultrastructure<sup>29</sup>. This work posits that individual factories are enclosed with membranes derived from the endoplasmic reticulum. Membrane enclosure is maximal (80-85%) early during infection. However, factories become less defined by these boundaries as infection progresses and assembly of progeny viruses commence. Furthermore, Locker observed a positive correlation between DNA replication and the extent to which a factory is wrapped by membranes and suggests that ER membranes play a role in viral DNA replication. If so, morphogenesis may act as the potentiator for inter-genomic recombination. The membranes used for both factory enclosure and assembly of

progeny virions are derived from the endoplasmic reticulum<sup>135</sup>. It is possible that morphogenesis results in the capture and subsequent collapse of the membrane structures that surround a viral factory. In extension, lack of the surrounding membrane structure results in the amorphous appearance of a viral factory late in infection. Considering that membranes may play a role in DNA replication<sup>29</sup>, this suggests that the onset of virion assembly would act as the trigger point that results in reduced replication late in infection. This hypothesis agrees with our findings that DNA replication begins to decline at the same time that products of morphogenesis are first observed (Compare 5hpi in Fig. 3.5 and 4.4).

### 6.3 Membranes structures can be observed at the periphery of viral factories early during infection

We should be able to visualize ER membranes surrounding viral factories if they do indeed play a pivotal role in factory formation, maintenance and replication. To investigate further, we infected cells with VACV and labelled CRT, a marker of the ER (Fig. 5.1). ER membrane structure was observed around and within a given viral factory. The internal membrane structure may arise due to multiple possibilities. First, the observed internal membrane structures could arise from cellular constituents that are present in the cytoplasm that are merely captured during factory collision events. VACV repurposes ER membranes for both factory formation<sup>29</sup> and progeny assembly<sup>78</sup>. Therefore, it is possible that remnants of ER membrane present in the cytoplasm that arose from ER restructuring are simply trapped during a factory collision event rather than deriving from a membrane structure that originally enclosed early factories.

Alternatively, it is possible that the internal membrane structures originally derived from the membranes that surrounded individual factories<sup>29</sup>. It is possible that these membranes persist following collision of individual factories, which can occur within 30 minutes of factory formation<sup>28,122</sup>. If true, this observation suggests that membrane structure is preserved even after the apparent fusion of multiple viral factories. As such, it is possible that membranes derived from the ER act as the barrier that restricts intergenic recombination. Similarly, the external membrane structure observed at the periphery of the viral factory may reflect the membrane structures that originally enclosed viral factories early during infection. Oddly, the micrographs were fixed and imaged at 6hpi, a time that corresponds to reduced (30%) wrapping of the viral factory. This may suggest that these membrane structures could persist even following the onset of morphogenesis and act as barriers to genetic mixing. This is further reinforced by the observation that these membrane structures appear to form clear partitions between adjacent viral factories and that the genetic content of a given factory is clearly distinct from neighbouring factories.

While the previous experiment suggests that membrane structures exist at the periphery of viral factories, the reduced resolution associated with fluorescence microscopy fails to reveal critical information. For example, it is unclear if the integrity of the peripheral membrane structures is sufficient to act as a barrier to recombination. As such, we used EM to further investigate the role of membrane structures in factory organization (Fig. 5.2). At 3.5hpi, we observed ER-like structures at the periphery of the viral factories (Fig. 5.2A). Odd is the fact that these membrane structures do not appear to enclose the entirety of the viral factory. These samples were fixed early in infection,

at a time when viral factories should be maximally (85%) wrapped by ER membranes<sup>29</sup>. However, the membranes do appear between the junction site of the two viral factories and could represent a potential barrier to genetic mixing. An additional image captured just later in infection (4hpi) also showed membrane structures at the periphery of viral factories. Even more, these membrane structures also appeared between the potential synapses of the multiple factories. Overall, these images suggest that membrane structures are present at the periphery of viral factories, at least early during infection, in a way that may restrict recombination.

#### 6.4 Tracking persistence of membrane structures following factory collision events

The previous experiments suggest that membrane structures are present, to a certain extent, at the periphery of viral factories. However, in order to restrain genetic mixing and recombination, these membrane structures would need to persist following collision of viral factories. To investigate membrane ultrastructure following collision, we used a technique known as CLEM. CLEM is a powerful technique in that it allows one to maintain an understanding of the kinetics of the experiment via light microscopy before obtaining ultrastructural information with EM. CLEM experiments were performed using both TEM (Fig. 5.3) and SEM (Fig. 5.4). In the first experiment, cells were fixed after observing a collision event at 4h35min post-infection (Fig. 5.3A) before processing for EM (Fig. 5.3B). Similar to the results highlighted in figure 5.2, membrane structures were present only to a limited extent around the periphery of the viral factories. However, unlike the previous experiments, products of morphogenesis,

including both viral crescents as well as IV, are present within the viroplasm. Peripheral membrane structures were observed to collapse following the onset of morphogenesis<sup>29</sup>. It is possible then that the reduced integrity of the peripheral membrane structure is a result of the onset of morphogenesis. Taken together with the observation that morphogenesis occurs just prior to the production of intergenic recombinants (Fig. 3.5) it becomes more enticing to suggest that morphogenesis is the trigger that permits intergenic recombination by causing a deconstruction of the membranes that enclose viral factories. However, deconstruction of the factory membranes may in turn cause a reduction in DNA replication, as noted by a decrease in replication observed alongside the onset of morphogenesis (Fig. 4.4), which in turn explains the reduced frequency of recombinants produced between co-infecting viruses. Given that ER-like membranes are observed between the collision sites in two separate experiments (Fig. 5.3B – lower arrow, Fig. 5.4B) it stands to reason that the membranes that originally enclose viral factories persist till late during infection and are subsequently deconstructed and repurposed during morphogenesis to permit genetic mixing and recombination.

However, the hypothesis that the original binding membrane structures act as the barrier to genetic mixing is weakened by the observation that structures other than ER-like membranes, namely mitochondria, appear to separate adjacent factories (Fig. 5.3B – upper arrow). Given that both ER-like membrane fragments and mitochondria are found in close proximity to viral factories, it is possible that the structures present at collision junction sites represent cell constituents trapped during the collision event. This observation raises multiple questions: are the barriers that restrict recombination

derived from cell constituents or the membranes that originally enclosed factories?  
Furthermore, regardless of their origin are the structures present at junctions capable of limiting genetic mixing and recombination?

## 6.5 The structures observed at factory collision sites are not organized in a way that could sufficiently restrict recombination

To investigate these questions further, we made use of a technique known as array tomography. This technique allowed us to explore the 3D-ultrastructure of a factory collision events in an effort to determine if the structures observed at the junctions of two recently collided factories could restrict recombination. Multiple collision events were observed during the live-cell portion of the experiment, but the cells were ultimately fixed after observing the collision event at 5h43min post-infection. Of the multiple collision events observed, the ultrastructural information of three factories in particular were investigated. In the first collision event, which occurred at 4h31min post-infection, ER-like membrane structures could be observed within the virosome (Fig. 5.5). By tracking the orientation of the collision of these two viral factories during the live-cell portion of the experiment (Fig. 5.5A), it becomes apparent that the internal membrane structures lie at the approximate junction site of the independent viral factories. Interestingly, the membrane structures appear to span most of the diameter of the viral factory but contain notable gaps that would compromise the structure's ability to act as a barrier. Products of morphogenesis, namely viral crescents, are present within the viral factory. Therefore, it is possible that the integrity of the membrane structure was undermined by the onset of

morphogenesis. Investigating the entire 3D-ultrastructure revealed that multiple internal membrane fragments exist within the interior of the viral factory (Fig. 5.6). Surprisingly, these internal membrane structures only exist to a limited extent throughout the z-dimension of the viral factory. For example, the internal structures highlighted in figure 5.5B and 5.6A only appear in 4 of the 44 imaged sections. The limited membrane structures could arise due to multiple possibilities. First, these membranes may represent a larger structure that is undergoing deconstruction due to the onset of morphogenesis. Second, each individual membrane structure could have arisen due to a separate collision event. Lastly, it is possible that these membrane structures represent cellular debris captured during the collision event. This last hypothesis is the most probable given that the membrane structures are largely absent from the periphery of the viral factory at the time the collision was observed (Fig. 5.3A and 5.4A). Investigation of a separate factory that was shown to have undergone a collision event, also at 4h31min post-infection, also revealed cell constituents, including both mitochondria and ER-like membranes, within the interior of the viral factory (Fig. 5.7). However, yet another viral factory that underwent no observable collision event lacked the presence of cell constituents within the virosome (Fig. 5.8). Taken together, these observations suggest that the structures observed at collision sites are cell constituents captured during collision rather than structures associated with viral factories. Furthermore, these structures only exist through a small portion of the z-dimension of the sample. As such, it is unlikely that that structures observed at the junctions of collision events, neither mitochondria nor ER-like membranes, physically prevent genetic mixing and recombination. However, it is possible that these

cytoplasmic structures impede the movement of viral factories in a way that would delay the collision events themselves. After collision, physical properties of the DNA itself, such as high viscosity, may result in limited genetic mixing that

## 6.6 Future Directions

### 6.6.1 Role of membrane structures in early factory fusion events

Micrographs of late viral factories reveal little to no membrane structure present at the periphery of viral factories (Fig. 5.3-5.8). These observations suggest that the membrane structures that exist around viral factories early during infection do not persist late into infection and, as a result, do not act as barriers to recombination. However, micrographs of cells imaged earlier in infection showed membrane staining to a certain extent around the outer edges of the viral factories (Fig.5.2). It is possible that while membrane structures play little role in limiting genetic mixing and recombination late during infection these peripheral membrane structures could prevent the exchange of genetic material between early viral factories that undergo an apparent fusion event as early as 30min within factory formation<sup>28,122</sup>.

Combinations of light and electron microscopy could be used to investigate the role of membrane structures following the earliest collision events. Similar to the CLEM experiments described throughout chapter 5, samples could be fixed after observation of early collision events that occur within the first hour of factory formation. Afterwards, these same samples could be processed for EM to investigate membrane ultrastructure. This would allow us to determine if early membrane structures contain the capacity to restrict genetic mixing and recombination. If the samples do appear to

restrict genetic mixing, one could alter the timing of fixation to investigate the persistence of these structures. For example, after observing an early collision, fixation could be delayed an additional 15min. By continuing with this approach, it would be possible to track the persistence of early membrane structures throughout the duration of an infection. By relating the persistence of the membrane structures to hallmarks of the viral life cycle, it may be possible to deduce information on which processes permit genetic mixing between two co-infecting viruses.

#### 6.6.2 Role of microtubules in VACV factory mobility

Cytoskeletal structures were observed within the interior and tangential to viral factories (Fig. 5.6B and 5.7 – magenta structures). These structures likely represent microtubules given that they measure 25nm in diameter. Could it be that microtubules play an important role in factory organization and mobility or do these structures also represent cellular debris captured during a collision event? While microtubule structures could be observed within factories under EM, the method itself represents a particularly poor medium for developing an understanding of localization and kinetics of a structure of interest. As such, we used fluorescence microscopy to investigate the localization of microtubules in relation to viral factories during an infection (Fig. 6.1). While microtubule staining was particularly punctate, microtubule structures could be observed within the interior of viral factories. Cells were infected at a low MOI (0.5) so that each cell, in theory, was infected with a single virion. Therefore, the microtubules observed within factories likely represent structures that are associated with viral factories independently of a collision event.

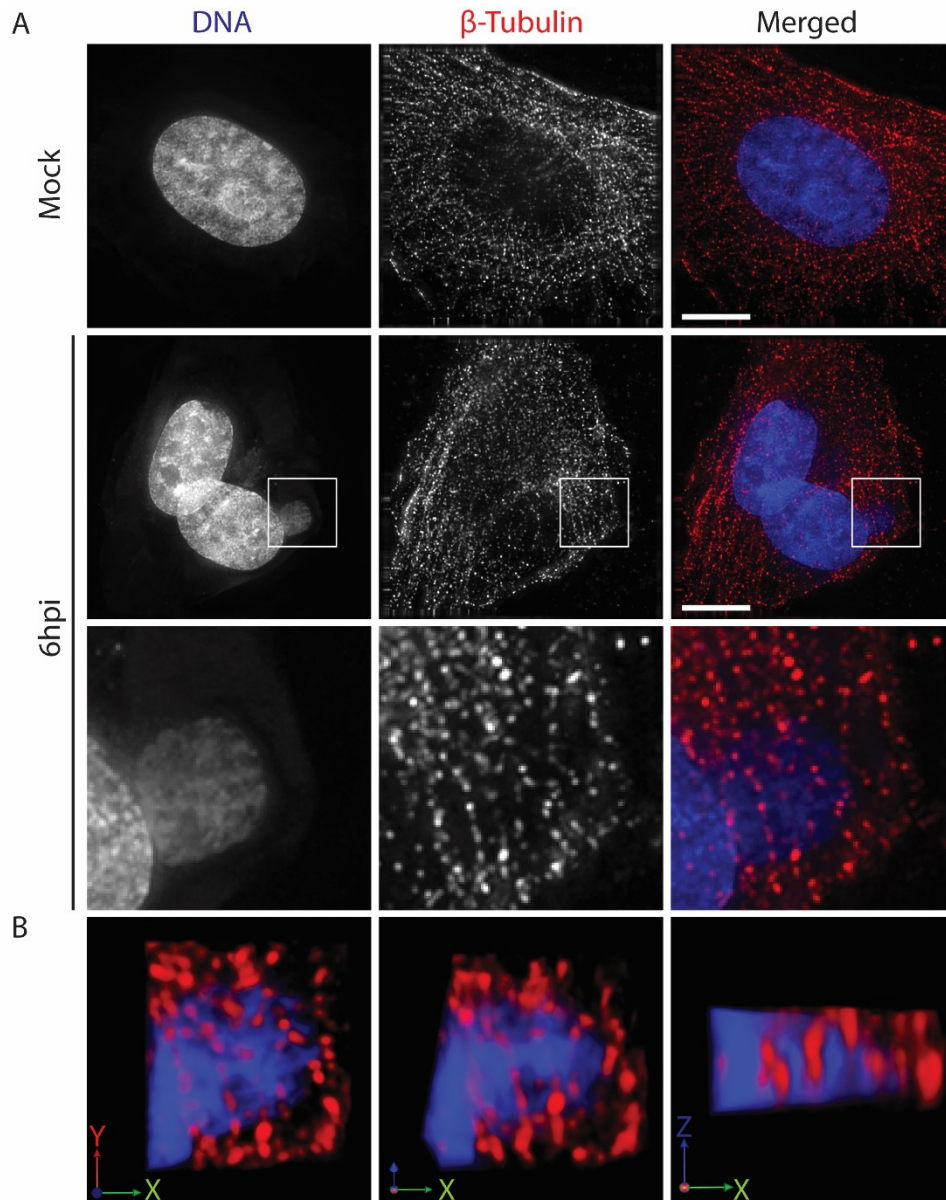


**Figure 6.1. Microtubules can be observed within the viral factory.** BSC40 cells were non-synchronously infected with VACV-WR at a MOI=0.5 and fixed at 6hpi. Bulk DNA was labelled with DAPI and microtubules were labelled with an antibody. (A) Microtubule staining within the viral factory. Only z-stacks that corresponded to the viral factory were projected to reduce the obscurity of the image. (B) 3D-volume of the area highlighted in part A. The image highlights the XY orientation (left) and the two subsequent 45° rotations transitioning into the XZ dimension (right).

Microtubules play an extended role during VACV infection. Following internalization, the viral cores are transported to sites of disassembly via microtubules<sup>136,137</sup>. It is possible that after internalization and transport of cores to sites of disassembly the released viral genome uses MT as a scaffold during growth of viral factories. Development of viral factories on the MT cytoskeleton would provide a number of benefits. First, MT localization would allow viral factories to migrate within the host cell cytoplasm potentially using the MT-associated motor proteins, such as dynein. This transportation could promote the collision and eventual fusion of small factories. Additionally, MTs are involved with the transport of a subset of MVs to the TGN where they obtain additional membranes and form WV<sup>86,138</sup>. Development of viral factories on MT may provide a convenient structure that allows MV to easily migrate to the TGN to obtain these additional membranes. As such, it would be interesting to track the development of viral factories in relation to MT under a live-cell setting. Additionally, it would be interesting to track the localization of the viral proteins that have been shown to harbour the ability to bind to MT to tease apart their role in MT binding and migration. These proteins include A10<sup>139</sup>, L4<sup>139</sup> and A51<sup>140</sup>.

MT also play an important role in mediating movement of viral factories. Early factories migrate in a microtubule-dependent fashion and exhibit microtubule-motor-dependent movement kinetics<sup>141</sup>. While movement of early factories frequently resulted in collision and apparent fusion of small factories, these movements appeared to lack a directional bias and factories remained in the periphery of the host cell. It isn't until later during infection, once the viral factories grow in size, that viral factories begin accumulating in the perinuclear region. However, unlike smaller viral factories, large

factory movement is independent of MT-motor movement but rather relies on MT-dependent cell contractility events to drive migration of factories to the perinuclear region. The tendency for small factories to remain at the periphery while large factories travel to the perinuclear region raises an interesting question. Does the MT-mediated contractility event that causes large factories to drift to the perinuclear region serve as a method of separating viral factories until late during infection? If true, these motility events may act as an additional means of delaying inter-genic recombination by regulating the spatial organization of viral factories. It stands to reason that separation of viral factories would prevent genetic mixing and recombination. In extension, MT-dependent contraction may act as a method of preserving the fitness of a given virus. Factories begin translocation late during infection. It is possible that these late factories are well into the process of DNA replication and are beginning the process of morphogenesis. This would ensure the replication of the parental strains while providing an opportunity later during infection for recombination events to produce potentially beneficial recombinants. As such, it would be interesting to determine if perturbation of the contraction events that cause factories to centralize within a cell would impact the frequency at which recombinant viruses are produced. In this regard, the viral F11 protein would represent a potential target protein. F11 perturbs RhoA-mDia signalling that subsequently results in alterations to microtubule dynamics<sup>142</sup>. Furthermore, MVA, which lack a functional F11 protein, do not exhibit the same cell contraction events that result in factory localization in the perinuclear region<sup>141</sup>. However, introduction of a functional F11 protein in MVA results in restoration of MT-

dependent motility<sup>143</sup>. Therefore, production of *F11L* knockouts would allow us to investigate the role contraction events play in restricting recombination.

### 6.6.3 Competition between co-infecting virions

The late timing of intergenic recombination events raises an interesting question. Are the events that promote factory collision and genetic mixing temporally regulated in an effort to produce parental progeny prior to the onset of intergenic recombination? If true, this system would promote the production of the presumably fit parental strain prior to generation of genetically diverse recombinants. This system, in turn, introduces another question. If infection is regulated in a way that promotes production of parental strains prior to the onset of recombination, would we expect to see co-infecting viruses in competition for the resources of a single cell? Interviral competition among co-infecting viruses in a given cell would ensure that only the most evolutionary fit viruses are replicated at the expense of less fit viruses. For the competition studies, it would be pertinent to compare a virus that is capable in replication, preferably VACV-WR, to a virus deficient in replication, such as *F4L* deleted viruses<sup>144</sup>. Multiple methods could be used to track interviral competition. First, the two competing viruses could be conjugated to separate fluorophores. This system has been used before and it was shown that factories are presumably labelled exclusively with the fluorophore encoded by the virus and that these fluorescent signals do not appear to be freely diffusible<sup>122</sup>. Alternatively, one could correlate between live and fixed cell microscopy, as described in chapter 4, and identify the separate viruses using FISH. Live-cell microscopy would provide a beneficial medium in which one could track factory development throughout the duration of the infection. It would also be

interesting to apply EdU as a means of determining DNA replication between the two competing viruses. We could compare the intensity of the EdU signal in cells infected with each virus alone to cells co-infected with each virus to determine the effects of interviral competition.

## 6.7 Concluding Remarks

Many mysteries surround the process of recombination in VACV. It is known that recombination is driven by exonuclease activity of the viral DNA polymerase<sup>41</sup>. However, despite the ability to mediate recombination early during infection, recombination between two co-infecting viruses is significantly delayed and occurs at a reduced frequency relative to intraviral recombination<sup>122</sup>. This delay was attributed to the fact that the genetic content of an individual viral factory remains distinct even after an apparent fusion event<sup>28</sup>. Membranes derived from the ER represented the most logical barrier to genetic mixing given that they are present at the periphery of viral factories early during infection and appear to compartmentalize the viral factory late during infection<sup>29,122</sup>. In this study, we used a combination of light and electron microscopy to investigate factory ultrastructure in an effort to discern the barriers of recombination. We found that while cellular structures can be observed both at the junction sites of two recently collided viral factories and within the factory itself, these structures likely represent cellular constituents present in the cytoplasm that were captured during factory collision. These structures do not exist throughout the z-dimension in a meaningful capacity to restrict genetic exchange among factories. Therefore, it is likely that the barriers to recombination arise due to spatial organization of the viral factories or biophysical properties of the DNA itself.

## References

1. Pauli G, Blümel J, Burger R, et al. Orthopox Viruses: Infections in Humans. *Transfus Med Hemother*. 2010;37(6):351-364. doi:10.1159/000322101
2. Cyrklaff M, Risco C, Fernández JJ, et al. Cryo-electron tomography of vaccinia virus. *Proc Natl Acad Sci U S A*. 2005;102(8):2772-2777. doi:10.1073/pnas.0409825102
3. Lofquist JM, Weimert NA, Hayney MS. Smallpox: a review of clinical disease and vaccination. *Am J Health Syst Pharm*. 2003;60(8):749-756; quiz 757-758. <http://www.ncbi.nlm.nih.gov/pubmed/12749161>. Accessed June 16, 2019.
4. D.A. H. The eradication of smallpox – An overview of the past, present, and future. *Vaccine*. 2011;29:D7-D9. doi:10.1016/J.VACCINE.2011.06.080
5. Diven DG. An overview of poxviruses. *J Am Acad Dermatol*. 2001;44(1):1-16. doi:10.1067/mjd.2001.109302
6. Potts KG, Irwin CR, Favis NA, et al. Deletion of F4L (ribonucleotide reductase) in vaccinia virus produces a selective oncolytic virus and promotes anti-tumor immunity with superior safety in bladder cancer models. *EMBO Mol Med*. 2017;9(5):638-654. doi:10.15252/emmm.201607296
7. Schmidt FI, Bleck CKE, Mercer J. Poxvirus host cell entry. *Curr Opin Virol*. 2012;2(1):20-27. doi:10.1016/J.COVIRO.2011.11.007
8. Moss B. Poxvirus entry and membrane fusion. *Virology*. 2006;344(1):48-54. doi:10.1016/J.VIROL.2005.09.037
9. Vanderplasschen A, Smith GL. A novel virus binding assay using confocal microscopy: demonstration that the intracellular and extracellular vaccinia virions bind to different cellular receptors. *J Virol*. 1997;71(5):4032-4041. <http://www.ncbi.nlm.nih.gov/pubmed/9094681>. Accessed May 22, 2019.
10. Hsiao JC, Chung CS, Chang W. Vaccinia virus envelope D8L protein binds to cell surface chondroitin sulfate and mediates the adsorption of intracellular mature virions to cells. *J Virol*. 1999;73(10):8750-8761. <http://www.ncbi.nlm.nih.gov/pubmed/10482629>. Accessed May 22, 2019.
11. Hsiao JC, Chung CS, Chang W. Cell surface proteoglycans are necessary for A27L protein-mediated cell fusion: identification of the N-terminal region of A27L protein as the glycosaminoglycan-binding domain. *J Virol*. 1998;72(10):8374-8379. <http://www.ncbi.nlm.nih.gov/pubmed/9733888>. Accessed May 22, 2019.
12. Chung CS, Hsiao JC, Chang YS, Chang W. A27L protein mediates vaccinia virus interaction with cell surface heparan sulfate. *J Virol*. 1998;72(2):1577-1585. <http://www.ncbi.nlm.nih.gov/pubmed/9445060>. Accessed May 22, 2019.
13. Lin CL, Chung CS, Heine HG, Chang W. Vaccinia virus envelope H3L protein

- binds to cell surface heparan sulfate and is important for intracellular mature virion morphogenesis and virus infection in vitro and in vivo. *J Virol.* 2000;74(7):3353-3365. doi:10.1128/jvi.74.7.3353-3365.2000
14. Chiu W-L, Lin C-L, Yang M-H, Tzou D-LM, Chang W. Vaccinia virus 4c (A26L) protein on intracellular mature virus binds to the extracellular cellular matrix laminin. *J Virol.* 2007;81(5):2149-2157. doi:10.1128/JVI.02302-06
  15. Carter GC, Law M, Hollinshead M, Smith GL. Entry of the vaccinia virus intracellular mature virion and its interactions with glycosaminoglycans. *J Gen Virol.* 2005;86(5):1279-1290. doi:10.1099/vir.0.80831-0
  16. Mercer J, Helenius A. Vaccinia Virus Uses Macropinocytosis and Apoptotic Mimicry to Enter Host Cells. *Science (80- ).* 2008;320(5875):531-535. doi:10.1126/science.1155164
  17. Townsley AC, Weisberg AS, Wagenaar TR, Moss B. Vaccinia virus entry into cells via a low-pH-dependent endosomal pathway. *J Virol.* 2006;80(18):8899-8908. doi:10.1128/JVI.01053-06
  18. Bryk P, Brewer MG, Ward BM. Vaccinia Virus Phospholipase Protein F13 Promotes Rapid Entry of Extracellular Virions into Cells. Sandri-Goldin RM, ed. *J Virol.* 2018;92(11). doi:10.1128/JVI.02154-17
  19. Traktman P. 27 Poxvirus DNA Replication. *Cold Spring Harb Monogr Arch.* 1996. [http://dnareplication.cshl.edu/content/free/chapters/27\\_traktman.pdf](http://dnareplication.cshl.edu/content/free/chapters/27_traktman.pdf). Accessed May 22, 2019.
  20. Schramm B, Locker JK. Cytoplasmic Organization of POXvirus DNA Replication. *Traffic.* 2005;6(10):839-846. doi:10.1111/j.1600-0854.2005.00324.x
  21. Broyles SS. Vaccinia virus transcription. *J Gen Virol.* 2003;84(9):2293-2303. doi:10.1099/vir.0.18942-0
  22. Mallardo M, Leithe E, Schleich S, Roos N, Doglio L, Krijnse Locker J. Relationship between vaccinia virus intracellular cores, early mRNAs, and DNA replication sites. *J Virol.* 2002;76(10):5167-5183. doi:10.1128/jvi.76.10.5167-5183.2002
  23. Kates J. and Beeson J. Ribonucleic acid synthesis in vaccinia virus: I. The mechanism of synthesis and release of RNA in vaccinia cores. *J Mol Biol.* 1970;50(1):1-18. doi:10.1016/0022-2836(70)90100-2
  24. Kates JR, McAuslan BR. Messenger RNA synthesis by a "coated" viral genome. *Proc Natl Acad Sci U S A.* 1967;57(2):314-320. doi:10.1073/pnas.57.2.314
  25. Moss B. Poxvirus DNA replication. *Cold Spring Harb Perspect Biol.* 2013;5(9). doi:10.1101/cshperspect.a010199
  26. Cairns J. The initiation of vaccinia infection. *Virology.* 1960;11(3):603-623. doi:10.1016/0042-6822(60)90103-3

27. Katsafanas GC, Moss B. Colocalization of Transcription and Translation within Cytoplasmic Poxvirus Factories Coordinates Viral Expression and Subjugates Host Functions. doi:10.1016/j.chom.2007.08.005
28. Lin Y-CJ, Evans DH. Vaccinia virus particles mix inefficiently, and in a way that would restrict viral recombination, in coinfecting cells. *J Virol.* 2010;84(5):2432-2443. doi:10.1128/JVI.01998-09
29. Tolonen N, Doglio L, Schleich S, Krijnse Locker J. Vaccinia virus DNA replication occurs in endoplasmic reticulum-enclosed cytoplasmic mini-nuclei. *Mol Biol Cell.* 2001;12(7):2031-2046. doi:10.1091/mbc.12.7.2031
30. Geshelin P, Berns KI. Characterization and localization of the naturally occurring cross-links in vaccinia virus DNA. *J Mol Biol.* 1974;88(4):785-796. doi:10.1016/0022-2836(74)90399-4
31. Baroudy BM, Venkatesan S, Moss B. Incompletely base-paired flip-flop terminal loops link the two DNA strands of the vaccinia virus genome into one uninterrupted polynucleotide chain. *Cell.* 1982;28(2):315-324. <http://www.ncbi.nlm.nih.gov/pubmed/7060133>. Accessed May 28, 2019.
32. Pogo BG, Berkowitz EM, Dales S. Investigation of vaccinia virus DNA replication employing a conditional lethal mutant defective in DNA. *Virology.* 1984;132(2):436-444. <http://www.ncbi.nlm.nih.gov/pubmed/6322422>. Accessed May 28, 2019.
33. Moyer RW, Graves RL. The mechanism of cytoplasmic orthopoxvirus DNA replication. *Cell.* 1981;27(2 Pt 1):391-401. <http://www.ncbi.nlm.nih.gov/pubmed/6277506>. Accessed May 28, 2019.
34. Du S, Traktman P. Vaccinia virus DNA replication: two hundred base pairs of telomeric sequence confer optimal replication efficiency on minichromosome templates. *Proc Natl Acad Sci U S A.* 1996;93(18):9693. doi:10.1073/PNAS.93.18.9693
35. Sekiguchi J, Seeman NC, Shuman S. Resolution of Holliday junctions by eukaryotic DNA topoisomerase I. *Proc Natl Acad Sci U S A.* 1996;93(2):785. doi:10.1073/PNAS.93.2.785
36. Garcia AD, Moss B. Repression of Vaccinia Virus Holliday Junction Resolvase Inhibits Processing of Viral DNA into Unit-Length Genomes. *J Virol.* 2001;75(14):6460-6471. doi:10.1128/JVI.75.14.6460-6471.2001
37. Jones E V, Moss B. Mapping of the vaccinia virus DNA polymerase gene by marker rescue and cell-free translation of selected RNA. *J Virol.* 1984;49(1):72-77. <http://www.ncbi.nlm.nih.gov/pubmed/6690722>. Accessed May 28, 2019.
38. Traktman P, Sridhar P, Condit RC, Roberts BE. Transcriptional mapping of the DNA polymerase gene of vaccinia virus. *J Virol.* 1984;49(1):125-131. <http://www.ncbi.nlm.nih.gov/pubmed/6317886>. Accessed May 28, 2019.

39. Earl PL, Jones E V, Moss B. Homology between DNA polymerases of poxviruses, herpesviruses, and adenoviruses: nucleotide sequence of the vaccinia virus DNA polymerase gene. *Proc Natl Acad Sci U S A*. 1986;83(11):3659-3663. doi:10.1073/pnas.83.11.3659
40. Challberg MD, Englund PT. Purification and properties of the deoxyribonucleic acid polymerase induced by vaccinia virus. *J Biol Chem*. 1979;254(16):7812-7819. <http://www.ncbi.nlm.nih.gov/pubmed/468791>. Accessed May 28, 2019.
41. Gammon DB, Evans DH. The 3'-to-5' Exonuclease Activity of Vaccinia Virus DNA Polymerase Is Essential and Plays a Role in Promoting Virus Genetic Recombination. *J Virol*. 2009;83(9):4236-4250. doi:10.1128/JVI.02255-08
42. Willer DO, Mann MJ, Zhang W, Evans DH. Vaccinia Virus DNA Polymerase Promotes DNA Pairing and Strand-Transfer Reactions. *Virology*. 1999;257(2):511-523. doi:10.1006/viro.1999.9705
43. Willer DO, Yao X-D, Mann MJ, Evans DH. In Vitro Concatemer Formation Catalyzed by Vaccinia Virus DNA Polymerase. *Virology*. 2000;278(2):562-569. doi:10.1006/viro.2000.0686
44. Hamilton MD, Nuara AA, Gammon DB, Buller RM, Evans DH. Duplex strand joining reactions catalyzed by vaccinia virus DNA polymerase. *Nucleic Acids Res*. 2006;35(1):143-151. doi:10.1093/nar/gkl1015
45. Evans E, Klemperer N, Ghosh R, Traktman P. The vaccinia virus D5 protein, which is required for DNA replication, is a nucleic acid-independent nucleoside triphosphatase. *J Virol*. 1995;69(9):5353. <https://www.ncbi.nlm.nih.gov/pmc/articles/PMC189376/>. Accessed May 29, 2019.
46. De Silva FS, Lewis W, Berglund P, Koonin E V., Moss B. Poxvirus DNA primase. *Proc Natl Acad Sci*. 2007;104(47):18724-18729. doi:10.1073/pnas.0709276104
47. De Silva FS, Paran N, Moss B. Products and substrate/template usage of vaccinia virus DNA primase. *Virology*. 2009;383(1):136-141. doi:10.1016/j.virol.2008.10.008
48. Paran N, De Silva FS, Senkevich TG, Moss B. Cellular DNA ligase I is recruited to cytoplasmic vaccinia virus factories and masks the role of the vaccinia ligase in viral DNA replication. *Cell Host Microbe*. 2009;6(6):563-569. doi:10.1016/j.chom.2009.11.005
49. Colinas RJ, Goebel SJ, Davis SW, Johnson GP, Norton EK, Paoletti E. A DNA ligase gene in the Copenhagen strain of vaccinia virus is nonessential for viral replication and recombination. *Virology*. 1990;179(1):267-275. <http://www.ncbi.nlm.nih.gov/pubmed/2219723>. Accessed May 29, 2019.
50. Kerr SM, Smith GL. Vaccinia virus DNA ligase is nonessential for virus replication: Recovery of plasmids from virus-infected cells. *Virology*.

1991;180(2):625-632. doi:10.1016/0042-6822(91)90076-N

51. Parks RJ, Winchcombe-Forhan C, DeLange AM, Xing X, Evans DH. DNA ligase gene disruptions can depress viral growth and replication in poxvirus-infected cells. *Virus Res.* 1998;56(2):135-147. <http://www.ncbi.nlm.nih.gov/pubmed/9783462>. Accessed May 29, 2019.
52. Stuart DT, Upton C, Higman MA, Niles EG, McFadden G. A poxvirus-encoded uracil DNA glycosylase is essential for virus viability. *J Virol.* 1993;67(5):2503-2512. <http://www.ncbi.nlm.nih.gov/pubmed/8474156>. Accessed May 29, 2019.
53. Upton C, Stuart DT, McFadden G. Identification of a poxvirus gene encoding a uracil DNA glycosylase. *Proc Natl Acad Sci U S A.* 1993;90(10):4518-4522. doi:10.1073/pnas.90.10.4518
54. Kovacs GR, Moss B. The vaccinia virus H5R gene encodes late gene transcription factor 4: purification, cloning, and overexpression. *J Virol.* 1996;70(10):6796-6802. <http://www.ncbi.nlm.nih.gov/pubmed/8794318>. Accessed May 29, 2019.
55. DeMasi J, Traktman P. Clustered charge-to-alanine mutagenesis of the vaccinia virus H5 gene: isolation of a dominant, temperature-sensitive mutant with a profound defect in morphogenesis. *J Virol.* 2000;74(5):2393-2405. doi:10.1128/jvi.74.5.2393-2405.2000
56. Boyle KA, Greseth MD, Traktman P. Genetic Confirmation that the H5 Protein Is Required for Vaccinia Virus DNA Replication. *J Virol.* 2015;89(12):6312-6327. doi:10.1128/JVI.00445-15
57. Stanitsa ES, Arps L, Traktman P. Vaccinia Virus Uracil DNA Glycosylase Interacts with the A20 Protein to Form a Heterodimeric Processivity Factor for the Viral DNA Polymerase. *J Biol Chem.* 2006;281(6):3439-3451. doi:10.1074/jbc.M511239200
58. Ishii K, Moss B. Mapping Interaction Sites of the A20R Protein Component of the Vaccinia Virus DNA Replication Complex. *Virology.* 2002;303(2):232-239. doi:10.1006/VIRO.2002.1721
59. Beaud G, Beaud R, Leader DP. Vaccinia virus gene H5R encodes a protein that is phosphorylated by the multisubstrate vaccinia virus B1R protein kinase. *J Virol.* 1995;69(3):1819-1826. <http://www.ncbi.nlm.nih.gov/pubmed/7853522>. Accessed June 4, 2019.
60. Welsch S, Doglio L, Schleich S, Locker JK. The Vaccinia Virus I3L Gene Product Is Localized to a Complex Endoplasmic Reticulum-Associated Structure That Contains the Viral Parental DNA. *J Virol.* 2003;77(10):6014-6028. doi:10.1128/JVI.77.10.6014-6028.2003
61. Domi A, Beaud G. The punctate sites of accumulation of vaccinia virus early

- proteins are precursors of sites of viral DNA synthesis. *J Gen Virol.* 2000;81(5):1231-1235. doi:10.1099/0022-1317-81-5-1231
62. Rochester SC, Traktman P. Characterization of the single-stranded DNA binding protein encoded by the vaccinia virus I3 gene. *J Virol.* 1998;72(4):2917-2926. <http://www.ncbi.nlm.nih.gov/pubmed/9525612>. Accessed June 4, 2019.
  63. Greseth MD, Czarnecki MW, Bluma MS, Traktman P. Isolation and Characterization of vΔI3 Confirm that Vaccinia Virus SSB Plays an Essential Role in Viral Replication. *J Virol.* 2018;92(2). doi:10.1128/JVI.01719-17
  64. Doglio L, De Marco A, Schleich S, Roos N, Krijnse Locker J, Locker JK. The Vaccinia virus E8R gene product: a viral membrane protein that is made early in infection and packaged into the virions' core. *J Virol.* 2002;76(19):9773-9786. doi:10.1128/jvi.76.19.9773-9786.2002
  65. Kato SEM, Condit RC, Moussatché N. The vaccinia virus E8R gene product is required for formation of transcriptionally active virions. *Virology.* 2007;367(2):398-412. doi:10.1016/j.virol.2007.05.002
  66. Postigo A, Ramsden AE, Howell M, Correspondence MW, Way M. Cytoplasmic ATR Activation Promotes Vaccinia Virus Genome Replication Article  
Cytoplasmic ATR Activation Promotes Vaccinia Virus Genome Replication. *Cell Rep.* 2017;19. doi:10.1016/j.celrep.2017.04.025
  67. Blackford AN, Jackson SP. ATM, ATR, and DNA-PK: The Trinity at the Heart of the DNA Damage Response. *Mol Cell.* 2017;66(6):801-817. doi:10.1016/j.molcel.2017.05.015
  68. Zou L, Elledge SJ. Sensing DNA damage through ATRIP recognition of RPA-ssDNA complexes. *Science.* 2003;300(5625):1542-1548. doi:10.1126/science.1083430
  69. Strzalka W, Ziemienowicz A. Proliferating cell nuclear antigen (PCNA): a key factor in DNA replication and cell cycle regulation. *Ann Bot.* 2011;107(7):1127-1140. doi:10.1093/aob/mcq243
  70. Tarbouriech N, Ducournau C, Hutin S, et al. The vaccinia virus DNA polymerase structure provides insights into the mode of processivity factor binding. *Nat Commun.* 2017;8(1):1455. doi:10.1038/s41467-017-01542-z
  71. Moss B. Regulation of Vaccinia Virus Transcription. *Annu Rev Biochem.* 1990;59(1):661-688. doi:10.1146/annurev.bi.59.070190.003305
  72. Keck JG, Baldick CJ, Moss B. Role of DNA replication in vaccinia virus gene expression: a naked template is required for transcription of three late transactivator genes. *Cell.* 1990;61(5):801-809. doi:10.1016/0092-8674(90)90190-P
  73. Roberts KL, Smith GL. Vaccinia virus morphogenesis and dissemination. *Trends Microbiol.* 2008;16(10):472-479. doi:10.1016/j.tim.2008.07.009

74. Liu L, Cooper T, Howley PM, Hayball JD. From crescent to mature virion: vaccinia virus assembly and maturation. *Viruses*. 2014;6(10):3787-3808. doi:10.3390/v6103787
75. Dales S, Mosbach EH. Vaccinia as a model for membrane biogenesis. *Virology*. 1968;35(4):564-583. doi:10.1016/0042-6822(68)90286-9
76. Moss B. Origin of the poxviral membrane: A 50-year-old riddle. Condit RC, ed. *PLoS Pathog*. 2018;14(6):e1007002. doi:10.1371/journal.ppat.1007002
77. Maruri-Avidal L, Weisberg AS, Moss B. Direct formation of vaccinia virus membranes from the endoplasmic reticulum in the absence of the newly characterized L2-interacting protein A30.5. *J Virol*. 2013;87(22):12313-12326. doi:10.1128/JVI.02137-13
78. Weisberg AS, Maruri-Avidal L, Bisht H, et al. Enigmatic origin of the poxvirus membrane from the endoplasmic reticulum shown by 3D imaging of vaccinia virus assembly mutants. *Proc Natl Acad Sci U S A*. 2017;114(51):E11001-E11009. doi:10.1073/pnas.1716255114
79. Suárez C, Welsch S, Chlanda P, et al. Open membranes are the precursors for assembly of large DNA viruses. *Cell Microbiol*. 2013;15(11):1883-1895. doi:10.1111/cmi.12156
80. Chlanda P, Carbajal MA, Cyrklaff M, Griffiths G, Krijnse-Locker J. Membrane Rupture Generates Single Open Membrane Sheets during Vaccinia Virus Assembly. *Cell Host Microbe*. 2009;6(1):81-90. doi:10.1016/j.chom.2009.05.021
81. Morgan C. The insertion of DNA into vaccinia virus. *Science*. 1976;193(4253):591-592. <http://www.ncbi.nlm.nih.gov/pubmed/959819>. Accessed June 5, 2019.
82. Cepeda V, Esteban M. Novel insights on the progression of intermediate viral forms in the morphogenesis of vaccinia virus. *Virus Res*. 2014;183:23-29. doi:10.1016/j.virusres.2014.01.016
83. Ansarah-Sobrinho C, Moss B. Role of the I7 protein in proteolytic processing of vaccinia virus membrane and core components. *J Virol*. 2004;78(12):6335-6343. doi:10.1128/JVI.78.12.6335-6343.2004
84. Tooze J, Hollinshead M, Reis B, Radsak K, Kern H. Progeny vaccinia and human cytomegalovirus particles utilize early endosomal cisternae for their envelopes. *Eur J Cell Biol*. 1993;60(1):163-178. <http://www.ncbi.nlm.nih.gov/pubmed/8385018>. Accessed June 5, 2019.
85. Schmelz M, Sodeik B, Ericsson M, et al. Assembly of vaccinia virus: the second wrapping cisterna is derived from the trans Golgi network. *J Virol*. 1994;68(1):130-147. <http://www.ncbi.nlm.nih.gov/pubmed/8254722>. Accessed June 2, 2019.

86. Hollinshead M, Rodger G, Van Eijl H, et al. Vaccinia virus utilizes microtubules for movement to the cell surface. *J Cell Biol.* 2001;154(2):389-402. doi:10.1083/jcb.200104124
87. Lorenzo MM, Perdiguero B, Geada MM, Galindo I, Blasco R. Movements of vaccinia virus intracellular enveloped virions with GFP tagged to the F13L envelope protein. *J Gen Virol.* 2001;82(11):2747-2760. doi:10.1099/0022-1317-82-11-2747
88. Wolffe EJ, Isaacs SN, Moss B. Deletion of the vaccinia virus B5R gene encoding a 42-kilodalton membrane glycoprotein inhibits extracellular virus envelope formation and dissemination. *J Virol.* 1993;67(8):4732-4741. <http://www.ncbi.nlm.nih.gov/pubmed/8331727>. Accessed June 5, 2019.
89. Newsome TP, Scaplehorn N, Way M. Src Mediates a Switch from Microtubule- to Actin-Based Motility of Vaccinia Virus. *Science (80- )*. 2004;306(5693):124-129. doi:10.1126/science.1101509
90. Doceul V, Hollinshead M, Breiman A, Laval K, Smith GL. Protein B5 is required on extracellular enveloped vaccinia virus for repulsion of superinfecting virions. *J Gen Virol.* 2012;93(Pt\_9):1876-1886. doi:10.1099/vir.0.043943-0
91. Law M, Carter GC, Roberts KL, Hollinshead M, Smith GL. From the Cover: Ligand-induced and nonfusogenic dissolution of a viral membrane. *Proc Natl Acad Sci U S A.* 2006;103(15):5989. doi:10.1073/PNAS.0601025103
92. Boulter EA, Appleyard G. Differences between extracellular and intracellular forms of poxvirus and their implications. *Prog Med Virol.* 1973;16:86-108. <http://www.ncbi.nlm.nih.gov/pubmed/4356899>. Accessed June 5, 2019.
93. Law M, Smith GL. Antibody Neutralization of the Extracellular Enveloped Form of Vaccinia Virus. *Virology.* 2001;280(1):132-142. doi:10.1006/viro.2000.0750
94. Vanderplasschen A, Mathew E, Hollinshead M, Sim RB, Smith GL. Extracellular enveloped vaccinia virus is resistant to complement because of incorporation of host complement control proteins into its envelope. *Proc Natl Acad Sci.* 1998;95(13):7544-7549. doi:10.1073/pnas.95.13.7544
95. Zhang WH, Wilcock D, Smith GL, et al. Vaccinia virus F12L protein is required for actin tail formation, normal plaque size, and virulence. *J Virol.* 2000;74(24):11654-11662. doi:10.1128/jvi.74.24.11654-11662.2000
96. Smith GL, Rodger G, van Eijl H, Zhang W-H, Hollinshead M. The vaccinia virus F12L protein is associated with intracellular enveloped virus particles and is required for their egress to the cell surface. *J Gen Virol.* 2002;83(1):195-207. doi:10.1099/0022-1317-83-1-195
97. Hakem R. DNA-damage repair; the good, the bad, and the ugly. *EMBO J.* 2008;27(4):589-605. doi:10.1038/emboj.2008.15
98. Li X, Heyer W-D. Homologous recombination in DNA repair and DNA damage

- tolerance. *Cell Res.* 2008;18(1):99-113. doi:10.1038/cr.2008.1
99. Ehrlich SD, Bierne H, d'Alençon E, et al. Mechanisms of illegitimate recombination. *Gene.* 1993;135(1-2):161-166. <http://www.ncbi.nlm.nih.gov/pubmed/8276254>. Accessed June 10, 2019.
  100. Fenner F, Comben BM. Genetic studies with mammalian poxviruses: I. Demonstration of recombination between two strains of vaccinia virus. *Virology.* 1958;5(3):530-548. doi:10.1016/0042-6822(58)90043-6
  101. Bedson HS, Dumbell KR. *Hybrids Derived from the Viruses of Variola Major and Cowpox.* Vol 62.; 1964. <https://www.ncbi.nlm.nih.gov/pmc/articles/PMC2134606/pdf/jhyg00116-0023.pdf>. Accessed May 14, 2019.
  102. Qin L, Upton C, Hazes B, Evans DH. Genomic Analysis of the Vaccinia Virus Strain Variants Found in Dryvax Vaccine. *J Virol.* 2011;85(24):13049-13060. doi:10.1128/JVI.05779-11
  103. Esposito JJ, Sammons SA, Frace AM, et al. Genome Sequence Diversity and Clues to the Evolution of Variola (Smallpox) Virus. *Science (80- ).* 2006;313(5788):807-812. doi:10.1126/science.1125134
  104. Qin L, Evans DH. Genome scale patterns of recombination between coinfecting vaccinia viruses. *J Virol.* 2014;88(10):5277-5286. doi:10.1128/JVI.00022-14
  105. Yao X-D, Evans DH. Effects of DNA Structure and Homology Length on Vaccinia Virus Recombination. *J Virol.* 2001;75(15):6923-6932. doi:10.1128/JVI.75.15.6923-6932.2001
  106. Bhargava R, Onyango DO, Stark JM. Regulation of Single-Strand Annealing and its Role in Genome Maintenance. *Trends Genet.* 2016;32(9):566-575. doi:10.1016/j.tig.2016.06.007
  107. Morrical SW. DNA-Pairing and Annealing Processes in Homologous Recombination and Homology-Directed Repair. *Cold Spring Harb Perspect Biol.* 2015;7(2):a016444. doi:10.1101/cshperspect.a016444
  108. Wright WD, Shah SS, Heyer W-D. Homologous recombination and the repair of DNA double-strand breaks. *J Biol Chem.* 2018;293(27):10524-10535. doi:10.1074/jbc.TM118.000372
  109. Magee WC, Hostetler KY, Evans DH. Mechanism of inhibition of vaccinia virus DNA polymerase by cidofovir diphosphate. *Antimicrob Agents Chemother.* 2005;49(8):3153-3162. doi:10.1128/AAC.49.8.3153-3162.2005
  110. Pestryakov PE, Lavrik OI. Mechanisms of single-stranded DNA-binding protein functioning in cellular DNA metabolism. *Biochem.* 2008;73(13):1388-1404. doi:10.1134/S0006297908130026
  111. West SC. Molecular views of recombination proteins and their control. *Nat Rev*

- Mol Cell Biol.* 2003;4(6):435-445. doi:10.1038/nrm1127
112. Oakley GG, Patrick SM, Yao J, Carty MP, Turchi JJ, Dixon K. RPA Phosphorylation in Mitosis Alters DNA Binding and Protein-Protein Interactions<sup>†</sup>. *Biochemistry.* 2003;42(11):3255-3264. doi:10.1021/bi026377u
  113. Greseth MD, Boyle KA, Bluma MS, et al. Molecular genetic and biochemical characterization of the vaccinia virus I3 protein, the replicative single-stranded DNA binding protein. *J Virol.* 2012;86(11):6197-6209. doi:10.1128/JVI.00206-12
  114. Davis RE, Mathews CK. Acidic C terminus of vaccinia virus DNA-binding protein interacts with ribonucleotide reductase. *Proc Natl Acad Sci U S A.* 1993;90(2):745-749. doi:10.1073/pnas.90.2.745
  115. Zheng L, Jia J, Finger LD, Guo Z, Zer C, Shen B. Functional regulation of FEN1 nuclease and its link to cancer. *Nucleic Acids Res.* 2011;39(3):781-794. doi:10.1093/nar/gkq884
  116. Balakrishnan L, Bambara RA. Flap endonuclease 1. *Annu Rev Biochem.* 2013;82:119-138. doi:10.1146/annurev-biochem-072511-122603
  117. Lieber MR. The FEN-1 family of structure-specific nucleases in eukaryotic dna replication, recombination and repair. *BioEssays.* 1997;19(3):233-240. doi:10.1002/bies.950190309
  118. Kikuchi K, Taniguchi Y, Hatanaka A, et al. Fen-1 facilitates homologous recombination by removing divergent sequences at DNA break ends. *Mol Cell Biol.* 2005;25(16):6948-6955. doi:10.1128/MCB.25.16.6948-6955.2005
  119. Silva M Da, Shen L, Tcherepanov V, Watson C, Upton C. Predicted function of the vaccinia virus G5R protein. *Bioinformatics.* 2006;22(23):2846-2850. doi:10.1093/bioinformatics/btl506
  120. da Fonseca FG, Weisberg AS, Caeiro MF, Moss B. Vaccinia Virus Mutants with Alanine Substitutions in the Conserved G5R Gene Fail To Initiate Morphogenesis at the Nonpermissive Temperature. *J Virol.* 2004;78(19):10238-10248. doi:10.1128/JVI.78.19.10238-10248.2004
  121. Senkevich TG, Koonin E V, Moss B. Predicted poxvirus FEN1-like nuclease required for homologous recombination, double-strand break repair and full-size genome formation. *Proc Natl Acad Sci U S A.* 2009;106(42):17921-17926. doi:10.1073/pnas.0909529106
  122. Paszkowski P, Noyce RS, Evans DH. Live-Cell Imaging of Vaccinia Virus Recombination. Elde NC, ed. *PLOS Pathog.* 2016;12(8):e1005824. doi:10.1371/journal.ppat.1005824
  123. Dales S, SIMINOVITCH L. THE DEVELOPMENT OF VACCINIA VIRUS IN EARLE'S L STRAIN CELLS AS EXAMINED BY ELECTRON MICROSCOPY. *J Cell Biol.* 1961;10(4):475-503. doi:10.1083/jcb.10.4.475

124. Schindelin J, Arganda-Carreras I, Frise E, et al. Fiji: an open-source platform for biological-image analysis. *Nat Methods*. 2012;9(7):676-682. doi:10.1038/nmeth.2019
125. Kremer JR, Mastronarde DN, McIntosh JR. Computer Visualization of Three-Dimensional Image Data Using IMOD. *J Struct Biol*. 1996;116(1):71-76. doi:10.1006/JSBI.1996.0013
126. Wegel E, Göhler A, Lagerholm BC, et al. Imaging cellular structures in super-resolution with SIM, STED and Localisation Microscopy: A practical comparison. *Sci Rep*. 2016;6(1):27290. doi:10.1038/srep27290
127. Klemperer N, Ward J, Evans E, Traktman P. The vaccinia virus I1 protein is essential for the assembly of mature virions. *J Virol*. 1997;71(12):9285-9294. <http://www.ncbi.nlm.nih.gov/pubmed/9371587>. Accessed August 18, 2019.
128. Yang Z, Bruno DP, Martens CA, Porcella SF, Moss B. Simultaneous high-resolution analysis of vaccinia virus and host cell transcriptomes by deep RNA sequencing. *Proc Natl Acad Sci U S A*. 2010;107(25):11513-11518. doi:10.1073/pnas.1006594107
129. Williams O, Wolffe EJ, Weisberg AS, Merchlinsky M. Vaccinia virus WR gene A5L is required for morphogenesis of mature virions. *J Virol*. 1999;73(6):4590-4599. <http://www.ncbi.nlm.nih.gov/pubmed/10233918>. Accessed June 5, 2019.
130. Garriga D, Headey S, Accurso C, Gunzburg M, Scanlon M, Coulibaly F. Structural basis for the inhibition of poxvirus assembly by the antibiotic rifampicin. *Proc Natl Acad Sci U S A*. 2018;115(33):8424-8429. doi:10.1073/pnas.1810398115
131. Sodeik B, Griffiths G, Ericsson M, Moss B, Doms RW. Assembly of vaccinia virus: effects of rifampin on the intracellular distribution of viral protein p65. *J Virol*. 1994;68(2):1103-1114. <http://www.ncbi.nlm.nih.gov/pubmed/8289340>. Accessed August 19, 2019.
132. Tolonen N, Doglio L, Schleich S, Locker JK. Vaccinia Virus DNA Replication Occurs in Endoplasmic Reticulum-enclosed Cytoplasmic Mini-Nuclei. *Mol Biol Cell*. 2001;12(July):2031-2046. doi:10.1091/mbc.12.7.2031
133. Joklik WK, Becker Y. The replication and coating of vaccinia DNA. *J Mol Biol*. 1964;10(3):452-474. doi:10.1016/S0022-2836(64)80066-8
134. De Silva FS, Moss B. Origin-independent plasmid replication occurs in vaccinia virus cytoplasmic factories and requires all five known poxvirus replication factors. *Virology*. 2005;2(1):23. doi:10.1186/1743-422X-2-23
135. Weisberg AS, Maruri-Avidal L, Bisht H, et al. Enigmatic origin of the poxvirus membrane from the endoplasmic reticulum shown by 3D imaging of vaccinia virus assembly mutants. *Proc Natl Acad Sci*. 2017;114(51):E11001-E11009.

doi:10.1073/pnas.1716255114

136. Moss B, Ward BM. High-speed mass transit for poxviruses on microtubules. *Nat Cell Biol.* 2001;3(11):E245-E246. doi:10.1038/ncb1101-e245
137. Carter GC, Rodger G, Murphy BJ, et al. Vaccinia virus cores are transported on microtubules. *J Gen Virol.* 2003;84(9):2443-2458. doi:10.1099/vir.0.19271-0
138. Smith GL, Vanderplasschen A, Law M. The formation and function of extracellular enveloped vaccinia virus. *J Gen Virol.* 2002;83(12):2915-2931. doi:10.1099/0022-1317-83-12-2915
139. Ploubidou A, Moreau V, Ashman K, Reckmann I, González C, Way M. Vaccinia virus infection disrupts microtubule organization and centrosome function. *EMBO J.* 2000;19(15):3932-3944. doi:10.1093/emboj/19.15.3932
140. Gammon DB, Duraffour S, Rozelle DK, et al. A single vertebrate DNA virus protein disarms invertebrate immunity to RNA virus infection. *Elife.* 2014;3. doi:10.7554/eLife.02910
141. Schramm B, de Haan CAM, Young J, et al. Vaccinia-Virus-Induced Cellular Contractility Facilitates the Subcellular Localization of the Viral Replication Sites. *Traffic.* 2006;7(10):1352-1367. doi:10.1111/j.1600-0854.2006.00470.x
142. Arakawa Y, Cordeiro J V., Way M. F11L-Mediated Inhibition of RhoA-mDia Signaling Stimulates Microtubule Dynamics during Vaccinia Virus Infection. *Cell Host Microbe.* 2007;1(3):213-226. doi:10.1016/j.chom.2007.04.007
143. Zwilling J, Sliva K, Schwantes A, Schnierle B, Sutter G. Functional F11L and K1L genes in modified vaccinia virus Ankara restore virus-induced cell motility but not growth in human and murine cells. *Virology.* 2010;404(2):231-239. doi:10.1016/J.VIROL.2010.05.008
144. Gammon DB, Gowrishankar B, Duraffour S, Andrei G, Upton C, Evans DH. Vaccinia Virus–Encoded Ribonucleotide Reductase Subunits Are Differentially Required for Replication and Pathogenesis. *PLoS Pathog.* 2010;6(7):e1000984. doi:10.1371/JOURNAL.PPAT.1000984